A cost-effective bacteria-based self-healing cementitious composite for low-temperature marine applications

Palin, Damian

DOI

10.4233/uuid:43dd673d-e80c-4e52-b8eb-f9a20df79646

Citation (APA)
Palin, D. (2017). *A cost-effective bacteria-based self-healing cementitious composite for low-temperature marine applications*. [Dissertation (TU Delft), Delft University of Technology]. https://doi.org/10.4233/uuid:43dd673d-e80c-4e52-b8eb-f9a20df79646

Important note
To cite this publication, please use the final published version (if applicable).
Please check the document version above.

A cost-effective bacteria-based self-healing cementitious composite for low-temperature marine applications

Damian PALIN

A cost-effective bacteria-based self-healing cementitious composite for low-temperature marine applications

Proefschrift

ter verkrijging van de graad van doctor
aan de Techniche Universiteit Delft,
op gezag van de Rector Magnificus prof. Ir. K.C.A.M. Luyben,
voorzitter van het College voor Promoties,
in het openbaar te verdedigen op woensdag 6 september 2017 om 12:30 uur

door

Damian PALIN

Master of Science en Innovation Design Engineering,
Imperial College London, Londen, Engeland,
geboren te Liverpool, Engeland.

Dit proefschrift is goedgekeurd door de
   Promotor: Prof. dr. ir. K. van Breugel
   Copromotor: Dr. H. M. Jonkers

Samenstelling promotiecommissie:
   Rector Magnificus   voorzitter
   Prof. dr. ir. K. van Breugel   Technische Universiteit Delft
   Dr. H. M. Jonkers   Technische Universiteit Delft

Onafhankelijke leden:
   Prof. dr. ir. S. Van der Zwaag   Technische Universiteit Delft
   Prof. dr. ir. M. C. M. Van Loosdrecht   Technische Universiteit Delft
   Dr. ir. V. Michaud   École Polytechnique Fédérale de Lausanne
   Prof. Dr. ir. K. Van Tittelboom   Universiteit Gent

Overige leden:
   Dr. V. Wiktor   Cugla BV

To my parents, thank you.

Contents

Summary

Bacteria-based self-healing concrete is an innovative self-healing materials approach, whereby bacteria embedded in concrete can form a crack healing mineral precipitate. Structures made from self-healing concrete promise longer service lives, with associated economic benefits [1]. Despite concretes susceptibility to marine-based degradation phenomena [2], and much of the world's marine infrastructure being located in cool with freezing climatic zones (annual average temperature < 10°C and average summer temperature generally < 20 °C) [3], research on the development of bacteria-based self-healing concrete has been largely restricted to room temperature freshwater studies [4-14]. The objective of the current project was, therefore, to develop a cost-effective bacteria-based self-healing cementitious composite for application in low-temperature marine environments. The current thesis charts the development of this composite.

In Chapter 2 the autogenous healing capacities of ordinary Portland cement (OPC) and blast-furnace slag (BFS) cement mortar specimens submerged in fresh and seawater, are visually quantified and characterised. The BFS cement specimens healed all crack widths up to 104 μm, and OPC specimens healed all crack widths up to 592 μm, after 56 days in seawater. BFS cement specimens healed all crack widths up to 408 μm, and OPC specimens healed all crack widths up to 168 μm, after 56 days in freshwater. OPC specimens in seawater displaying the higher crack healing capacity also demonstrated considerable losses in compressive strength. Differences in performance are attributable to the amount of calcium hydroxide in these mortars and specific ions present in seawater.

Chapter 3 reports on the crack healing capacity of seawater submerged mortar specimens with the aid of a crack permeability test. Cracks of defined widths were created in BFS cement specimens allowing reference crack permeability values to be generated for unhealed-specimens against which healed-specimens were quantified. Specimens with 0.2 mm wide cracks demonstrated no water flow after 28 days submersion. Specimens with 0.4 mm cracks demonstrated decreases in water flow of 66% after 28 days submersion and 50 to 53% after 56 days submersion.

Chapter 4 presents a modified permeability test for generating crack permeability data for cementitious materials. To gauge for any improvement both the modified and

unmodified tests were tested and compared. Cracks were generated in mortar specimens using both tests, the accuracy of these cracks was analysed through stereomicroscopy and computer tomography (CT), and the water flow through the cracks determined. Reduction factors and crack flow models were generated, and the accuracy and reliability of the predictions assessed. All of the models had high predictive accuracies (r^2 = 0.97-0.98), while the reliability of these predictions was higher for the models generated with the crack width analysis through stereomicroscopy. The cracks generated by the modified test were more accurate (within 20 µm of the desired crack widths) than those of the unmodified test. The modified test was 30% quicker (10 hours for twenty-one specimens) than the unmodified test at generating the crack permeability data. Further, crack width analysis through stereomicroscopy is currently/generally quicker than analysis through CT.

Chapter 5 presents a bacterial isolate and organic mineral precursor compound, as part of a cost-effective healing agent for low-temperature marine concrete applications. Organic compounds were screened based on their cost and concrete compatibility, and bacterial isolates based on their ability to metabolise concrete compatible organic compound and to function in a low-temperature marine concrete crack. Magnesium acetate was the cheapest organic compound screened, and when incorporated (1% of cement weight) in mortar specimens had one of the lowest impacts on compressive strength. Bacterial isolate designated psychrophile (PSY) 5 demonstrated very good growth under saline (3%), high pH (9.2), low-temperature (8ºC) conditions, with sodium lactate as an organic carbon source; and good growth at room temperature using magnesium acetate as an organic carbon source. Further, PSY 5 also demonstrated good spore production when grown on monosodium glutamate at room temperature.

Chapter 6 presents a bacteria-based bead for realising self-healing concrete in low-temperature marine environments. The bead, consisting of calcium alginate encapsulating bacterial spores and mineral precursor compounds, was assessed for: oxygen consumption, swelling, and its ability to form an organic-inorganic composite in a simulative marine concrete crack solution (SMCCS) at 8ºC. After six days in the SMCCS, the bacteria-based beads formed a calcite crust on their surface and calcite inclusions in their network, resulting in a calcite-alginate organic-inorganic composite. The beads swell by 300% to a maximum diameter of 3 mm, while theoretical calculations estimate that 0.1 g of the beads are able to produce ~1 mm^3 of calcite after 14 days submersion. Swelling and the formation of bacteria induced mineral precipitation providing the bead with considerable crack healing potential. It is estimated, based on the bacteria-based beads costing roughly 0.7 €.kg^{-1}, that bacteria-based self-healing concrete made using these beads would cost 135 €.m^{-3}.

Chapter 7 presents a bacteria-based self-healing cementitious composite for application in low-temperature marine environments. The composite was tested for its crack healing capacity with the water permeability test presented in Chapter 4, and for its strength development through compression testing. The composite displayed an

excellent crack healing capacity, reducing the permeability of cracks 0.4 mm wide by 95%, and cracks 0.6 mm wide by 93%, following 56 days submersion in artificial seawater at 8ºC.

Some conclusions were drawn based on the results obtained during the development of the bacteria-based self-healing cementitious composite:

- Visual crack closure is not a measurement for the regain of functional properties such as strength. Visual crack closure, therefore, should only be conducted as a complementary method when measuring the regain of such a property.

- The capacity of a cementitious material to heal a crack depends on the width of the crack, thermodynamic considerations, the presence of water and the amount of ions available in the crack. Autogenous crack healing for seawater submerged cementitious materials is principally attributable to the precipitation of aragonite and brucite in the cracks.

- The crack healing capacity of a bacteria-based cementitious composite is directly related to the amount of organic carbon available to the bacteria, and so the cheaper the organic mineral precursor compound, the cheaper the bacteria-based self-healing technology in general. Further, the compound must not have an adverse effect on concrete properties when included and must be readily metabolised by the bacteria as part of the healing agent. Magnesium acetate, in the current study, best balanced these criteria making it a good candidate as the organic mineral precursor compound for the healing agent.

- A large number of specimen replicates ($\geq$ 7) are required to generate reliable crack permeability data, and hence to quantify the crack healing capacity of cementitious materials through their functional water tightness.

- The bacteria-based self-healing cementitious composite displayed an excellent crack healing capacity, reducing the permeability of cracks 0.4 mm wide by 95% and cracks 0.6 mm wide by 93%, following 56 days submersion in artificial seawater at 8ºC. This crack healing capacity was attributable to: mineral precipitation as a result of chemical interactions between the cement paste and seawater; bead swelling; magnesium-based precipitates as a result of chemical interactions between the magnesium of the beads and hydroxide ions of the cement paste; and bacteria-induced mineral precipitation.

- The 28-day compressive strength of mortar specimens incorporated with beads was 55% of plain mortar specimens. Reducing the amount of bacteria-based beads will likely increase the compressive strength of the bacteria-based self-healing cementitious composite. Such a reduction, given the swellability of the beads, may have relatively little impact on the healing capacity of the composite.

- The bacteria-based self-healing cementitious composite shows great potential for realising self-healing concrete in low-temperature marine environments, while the organic-inorganic healing material formed by the composite represents an exciting avenue for self-healing concrete research.

I hope that the work presented herein provide a valuable reference for those interested in bacteria-based self-healing concrete, particularly for application in marine environments, and more generally for those interested in the wider field of self-healing materials research.

Samenvatting

Zelfhelend bacteriebeton is een innovatief zelfhelend materiaal waarin de aan het betonmengsel toegevoegde bacteriën in staat zijn scheurherstellende mineralen te vormen. Constructies gemaakt van dit beton hebben in potentie een langere levensduur, wat economische voordelen met zich meebrengt [1]. Ondanks het feit dat beton gevoelig is voor aantasting in het mariene milieu [2], en veel van de mariene infrastructuur in de wereld zich in koude klimaatzones bevindt (met een gemiddelde jaarlijkse temperatuur van < 10°C en gemiddelde zomerse temperatuur van < 20 °C) [3], heeft het onderzoek naar de ontwikkeling van zelfhelend bacteriebeton zich beperkt tot zoetwaterstudies bij kamertemperatuur [4-14]. Het doel van de huidige studie was daarom een kosteneffectief zelfhelend bacteriebeton te ontwikkelen voor toepassing in koude mariene milieus. Het huidige proefschrift beschrijft de ontwikkeling van dit hybride bacterie-cementgebonden composietmateriaal.

   In hoofdstuk 2 wordt de autogene zelfhelende capaciteit van op Portland cement (PC)- en Hoogovencement (HC) gebaseerde mortel proefstukken, ondergedompeld in zoet- en zeewater, visueel gekwantificeerd en gekarakteriseerd. Scheuren in HC- en PC proefstukken met een respectievelijke wijdte tot 104 μm en tot 592 μm toonden volledig herstel na 56 dagen onderdompeling in zeewater. Voor proefstukken ondergedompeld in zoetwater was dit respectievelijk 408 μm en 168 μm. Hoewel PC proefstukken ondergedompeld in zeewater een hogere autogene scheurherstellende capaciteit vertoonden ging dit wel gepaard met een aanzienlijk verlies in druksterkte. De oorzaak van de waargenomen verschillen in zelfherstel worden toegeschreven aan de specifieke hoeveelheden calcium hydroxide aanwezig in deze mortels en de specifieke ionensamenstelling van zeewater.

   Hoofdstuk 3 rapporteert over het scheurherstellend vermogen van HC gebaseerde mortelproefstukken ondergedompeld in zeewater, waarin scheurherstel functioneel gekwantificeerd wordt aan de hand van een scheurpermeabiliteitstest. In proefstukken werden scheuren van gedefinieerde wijdte gemaakt. Dit maakt het mogelijk permeabiliteitswaarden van verschillende sets proefstukken voor- en na een periode van zelfherstel te kwantificeren. Proefstukken met 0.2 mm-wijde scheuren bleken niet meer waterdoorlatend na 28 dagen onderdompeling in zeewater. Daarentegen vertoonden proefstukken met 0.4 mm-wijde scheuren een afname in waterflow

(waterdoorlatendheid) van 66% na 28 dagen onderdompeling en van 50 tot 53% na 56 dagen onderdompeling.

Hoofdstuk 4 presenteert een aangepast permeabiliteits- (waterdoorlatendheids-) protocol voor het genereren van scheurpermeabiliteitsdata voor cementgebonden materialen. Dit aangepaste protocol werd vergeleken met een eerder ontwikkeld protocol om vast te stellen of de aangepaste versie betere resultaten oplevert. Scheuren in proefstukken werden gemaakt volgens het specifieke voorschrift van beide protocollen en de nauwkeurigheid van de gemaakte scheuren ten aanzien van de voorgenomen scheurwijdten werd vastgesteld middels stereomicroscopie, computertomografie (CT) en waterdoorlatendheid van de proefstukken. Vervolgens werden reductiefactoren bepaald en waterdoorlatendheidsmodellen ontwikkeld waarvan de nauwkeurigheid en betrouwbaarheid van voorspellende waarde werd vastgesteld. Alle modellen hadden een hoge voorspellende nauwkeurigheid (r^2 = 0.97-0.98) terwijl de betrouwbaarheid van de voorspellingen het beste was voor de modellen die ontwikkeld waren op basis van de scheurwijdte-analyse middels stereomicroscopie. De scheuren gemaakt volgens het aangepaste protocol bleken nauwkeuriger (minder dan 20 μm afwijking van de beoogde scheurwijdte) dan die gemaakt volgens het eerder ontwikkelde protocol. Bovendien bleek werken volgens het aangepaste protocol 30% tijdswinst in het genereren van scheurpermeabiliteitsdata (10 uur voor 21 proefstukken) op te leveren. Ook bleek het kwantificeren van gemaakte scheurwijdten met behulp van stereomicroscopie tien keer sneller dan aan de hand van computertomografie.

Hoofdstuk 5 presenteert de karakterisering van een geïsoleerde bacteriestam en van een organische verbinding die door deze bacterie metabolisch omgezet kan worden tot een minerale verbinding. Beiden (bacterie en organische verbinding) maken onderdeel uit van kosteneffectief herstelmiddel ('healing agent') voor lage temperatuur- en mariene toepassingen van zelfhelend beton. Een aantal organische verbindingen werden gescreend op prijs en compatibiliteit met beton, en een aantal bacteriële isolaten op basis van hun vermogen om beton-compatibele organische verbindingen metabolisch om te zetten, en te functioneren in scheuren van beton in een lage-temperatuur mariene milieu. Magnesiumacetaat, de goedkoopste van de gescreende organische verbindingen had, wanneer verwerkt in een hoeveelheid van 1% van het cementgewicht, de laagste negatieve invloed op de ontwikkeling in druksterkte van de proefstukken. Het psychrofiele (koude-minnende) bacteriële isolaat 'PSY 5' vertoonde zeer goede groei in zoute (3%), alkalische (pH 9.2), lage temperatuur (8°C) geïncubeerde groeimedia met natriumlactaat als organische koolstofbron en tevens bij incubatie bij kamertemperatuur met magnesiumacetaat als organische koolstofbron. Verder vertoonde isolaat PSY 5 goede productie van sporen wanneer gekweekt bij kamertemperatuur met mononatriumglutamaat als organische koolstofbron.

Hoofdstuk 6 presenteert de ontwikkeling van een bacteriën-bevattend bolvormig deeltje voor toepassing in zelfhelend beton bij lage temperaturen in het mariene milieu. Het deeltje, bestaande uit in calciumalginaat ingekapselde bacteriesporen en organische voedingsstoffen, werd gekarakteriseerd ten aanzien van zuurstofopnamesnelheid, zwellend vermogen, en het vermogen om een organische-anorganisch composietmateriaal te vormen in kunstmatig beton-poriewater-oplossing (KBPW) bij

8°C. Na zes dagen incuberen in KBPW vormden de bacteriën-bevattende deeltjes een calciet (calciumcarbonaat) korst op het oppervlak en calciet insluitsels in hun netwerk, zodoende resulterend in een calciet-alginaat organisch-anorganisch composietmateriaal. De deeltjes vertoonden zwelling met 300% tot een maximum diameter van 3 mm, en aan de hand van theoretische berekeningen wordt geschat dat 0,1 g deeltjes ~ 1 mm^3 calciet kunnen produceren tijdens 14 dagen incubatie onder water. Door zwelling en de vorming van bacteriële minerale neerslag hebben de deeltjes een aanzienlijk scheurherstellende potentie in beton. Geschat wordt dat de prijs van zelfhelend beton 135 €.m^{-3} zal bedragen op basis van een kostprijs van 0,7 €.kg^{-1} bacterie-deeltjes.

Hoofdstuk 7 presenteert een zelfhelend bacterie-cement-gebonden composietmateriaal voor toepassing bij lage temperaturen in het mariene milieu. Het materiaal werd gekarakteriseerd ten aanzien van druksterkte-ontwikkeling en scheurherstellend vermogen door gebruik te maken van de waterdoorlatendheidstest ontwikkeld en beschreven in hoofdstuk 4. Het materiaal vertoonde een uitstekend scheurherstellend vermogen: een afname in waterdoorlatendheid van 95% voor scheuren van 0.4 mm breedte en een afname van 93% voor scheuren van 0.6 mm breed na 56 dagen onderdompeling in kunstmatig zeewater van 8°C.

Een aantal conclusies kunnen getrokken worden ten aanzien van het onderzoek gedaan in dit promotieonderzoek naar de ontwikkeling van het zelfhelende bacterie-cement composietmateriaal:

- Het kwantificeren van de scheurherstellende capaciteit van cementgebonden materialen door middel van het visueel vaststellen van dichtgaan van scheuren dient uitgevoerd te worden in combinatie met het kwantificeren van een functionele eigenschap zoals toename in sterkte of waterdichtheid.

- Het scheurherstellend vermogen van een cementgebonden materiaal hangt af van de wijdte van de scheur, thermodynamische omstandigheden, de aanwezigheid van water, en de hoeveelheid ionen aanwezig in de scheur. Het autogene scheurherstellend vermogen van in zeewater ondergedompelde cementgebonden materialen is hoofdzakelijk toe te schrijven aan het neerslaan van aragoniet en bruciet in de scheuren.

- Voor het betrouwbaar kwantificeren van het scheurherstellend vermogen van cementgebonden materialen middels een waterdoorlatenheidstest vereist een groot aan ($\geq$ 7) replicate proefstukken.

- Het ontwikkelde zelfherstellende bacterie-cement composietmateriaal heeft een uitstekend scheurherstellend vermogen bij lage temperatuur (8°C) in mariene milieus. Dit scheurherstellend vermogen is toe te schrijven aan: minerale neerslagvorming als gevolg van chemische interacties tussen de cementpasta en zeewater; zwelling van de bacterie-alginaat deeltjes; magnesium-bevattende minerale neerslagvorming als gevolg van chemische interacties tussen het

magnesium afkomstig uit de bacterie-alginaat deeltjes en hydroxide-ionen van de cementpasta; en door bacteriën veroorzaakte minerale neerslagvorming.

- Mortelproefstukken met bacterie-alginaat deeltjes vertoonden een lagere druksterkte dan conventionele mortelproefstukken. Het is de verwachting dat de druksterkte van zelfhelend bacterie-cement composiet materiaal verbeterd kan worden door het aantal bacterie-alginaat deeltjes te verlagen zonder het zelfherstellend vermogen te verminderen.

- Het ontwikkelde zelfhelende bacterie-cement composietmateriaal toont een groot potentieel voor het realiseren en toepassen van zelfhelend beton bij de lage temperaturen in het mariene milieu, terwijl bovendien het organisch-anorganisch scheurherstellende materiaal gevormd door het composietmateriaal nieuwe wegen opent voor verder onderzoek naar zelfherstellend beton.

Gehoopt wordt dat het werk beschreven in dit proefschrift een waardevolle referentie biedt voor zowel diegenen geïnteresseerd in de ontwikkeling van zelfherstellend bacteriebeton als voor het brede onderzoeksveld zelfhelende materialen.

1

Introduction

The fishermen know that the sea is dangerous and the storm terrible, but they have never found these dangers sufficient reason for remaining ashore.

— Vincent Van Gogh

Research undertaken as part of this thesis is concerned with the development of a cost-effective bacteria-based self-healing cementitious composite for application in low-temperature marine environments. The current chapter sets the scene by introducing the main research themes, objectives and thesis outline.

1.1 Marine concrete

Man and the sea are inextricably linked. Many civilisations have grown up along marine coastal regions, taking advantage of the food, transport and trade routes they provide. This relationship continues to the present with approximately 44% of the world's estimated 7.3 billion people living within 150 km of the sea [15]. These people rely heavily on marine infrastructure for shelter, transport, water, sanitation and energy. The demand on existing, and for new, marine infrastructure is set to grow with the global population estimated to reach 9.5 billion by 2050 [16]. Marine infrastructure is principally made from concrete. Reasons for this include concrete's cost-effectiveness, mechanical and durability performance, and the ease with which structural elements can be formed. Recent major marine infrastructural projects include the Channel Tunnel between the British Isles and mainland Europe, the great belt link between eastern and western Denmark; man-made islands such as the ones constructed for the new Denver airport in the United States of America (USA) and the Chep Lak Kok airport in Hong Kong; and the Oosterscheldekering storm surge barrier in the Netherlands. Based on the growing number of these major marine infrastructural projects, it seems that marine concrete construction is set to become an increasingly prominent feature of the twenty-first century.

1.2 Marine concrete deterioration

Many physical and chemical phenomena are usually interdependent and mutually reinforcing in the deterioration of marine concrete. Cracks allow aggressive agents present in seawater to penetrate deep into the concrete, leading to weakening of the cement matrix. Cracks may form in marine concrete due to wave forces, cycles of wetting and drying, thermal stresses and corrosion of steel reinforcement. Cracks as a result of steel reinforcement corrosion are particularly destructive. Steel reinforcement develops a passive layer in concrete, which, while intact protects it from corrosion. Chloride ions present in seawater can destroy this passive layer allowing reinforcing steel to oxidise. As the steel oxidises, or rusts, it expands creating internal pressure, which may cause the surrounding concrete to crack. Seawater may also interact deleteriously with cement paste [17]. Magnesium sulphate, magnesium chloride, and carbon dioxide, present in seawater are known to attack the calcium hydroxide, calcium monosulfoaluminate hydrate and calcium silicate hydrate, of hydrated Portland cement. Magnesium sulphate reacts with calcium hydroxide forming brucite ($Mg(OH)_2$) and gypsum ($CaSO_4 \cdot 2H_2O$), and with calcium hydroxide and calcium monosulfoaluminate hydrate forming ettringite ($CaAl_6(SO_4)_3(OH)_{12} \cdot 26H_2O$) [2]. Magnesium chloride reacts

2

with calcium hydroxide forming brucite and calcium chloride. Dissolved carbon dioxide reacts with calcium hydroxide forming aragonite ($CaCO_3$), calcium bicarbonate upon reaction with aragonite, and tetracalcium aluminum carbonate hydrate and gypsum upon reaction with calcium hydroxide and calcium monosulfoaluminate hydrate. Gypsum, calcium chloride and calcium bicarbonate are soluble in seawater, and so can be easily leached from concrete. This leaching can result in increased porosity and possible weakening of cementitious materials [18, 19]. Brucite formation continues until the calcium hydroxide of hydrated Portland cement is sufficiently depleted. Following this depletion, magnesium sulphate is able to decalcify calcium silicate hydrate (the binding material of the cement) transforming it to magnesium silicate hydrate a non-cementitious material. Conversion of calcium silicate hydrate to magnesium silicate hydrate is known to result in weakening of the cement matrix [19, 20].

Cement production is responsible for 7% of global anthropogenic carbon dioxide emissions [21]. If we were able to extend the service life of concrete infrastructure, then the demand for new infrastructure could be lessened, resulting in lower raw material usage, energy consumption and decreases in related carbon dioxide emissions. Blast-furnace slag (BFS), a product of the steel industry, reduces concrete porosity leading to less permeable, and hence more durable concrete construction. Hydrated BFS cement paste contains less calcium hydroxide than pure ordinary Portland cement (OPC)-based pastes, making the resultant concrete less vulnerable to ionic leaching and subsequent weakening [22]. Marine concrete structures made from BFS cements can still deteriorate, meaning that these structures still need to be inspected and maintained. Such inspection and maintenance can be problematic in the marine environment given that parts of a structure can be submerged or subject to wave action and the tide. It has been estimated that € 5 billion is spent annually on the maintenance and repair of concrete structures in Western Europe [23]. Comprehensive life-cycle analyses (LCA) has indicated that the indirect costs due to traffic jams and associated losses in productivity can be more than ten times the direct cost of maintenance and repair [24]. Spending more money on higher quality concrete should extend the maintenance-free period of concrete construction (Figure 1.1(A and B)). In an ideal world, concrete would be able to repair itself saving on the direct and indirect costs of maintenance and repair (Figure 1.1(C and D)) [1].
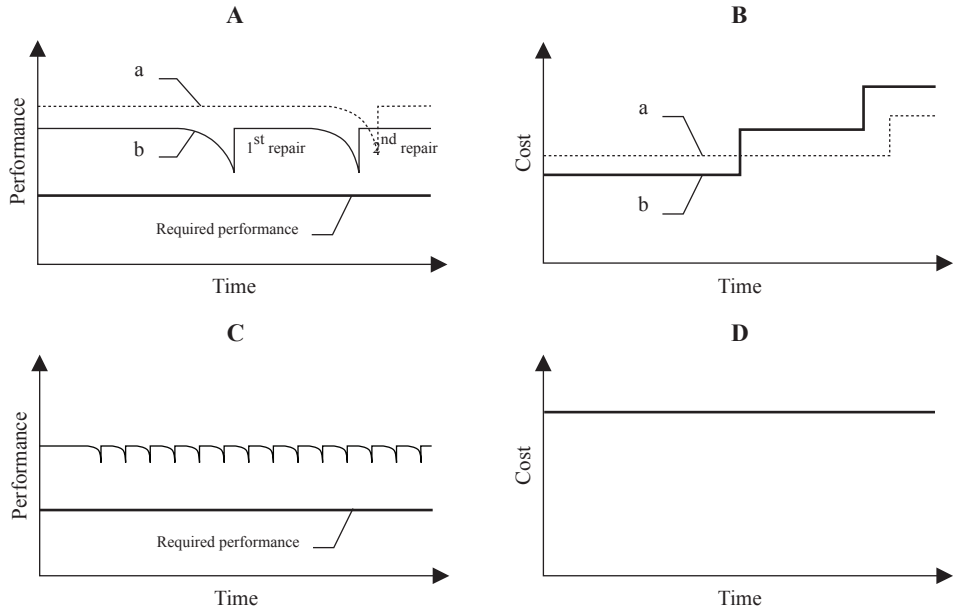
Figure 1.1 The performance (A) and cost (B) over time of high quality (a) and normal (b) structures. The performance (C) and cost (D) over time of a structure made with self-healing concrete. Interest and inflation are not considered in graphs (B and D). This figure is reproduced, with permission, from van Breugel [1].

1.3 Autogenous healing

Concrete has an autogenous ability to heal cracks maintaining functional water tightness, and contributing to the durability of concrete structures. First reported by the French Academy of Science in 1836, autogenous healing is principally attributed to the hydration of unhydrated cement particles and the carbonation of dissolved calcium hydroxide [25]. Numerous studies have recognised the autogenous healing ability of cementitious materials [26-29], however, studies quantifying this phenomenon are somewhat scarce [27, 29-32]. Edvardsen [29] examined the autogenous healing ability of cracked concrete specimens in freshwater through visual observation and permeability measurements. She found that about 50 percent of the specimens with cracks 200 μm wide healed completely over a seven weeks exposure period. She also noted that the majority of this healing occurred within the first 3 to 5 days after submersion. In a later study, Reinhardt and Jooss [27] conducted a permeability test showing the dependencies between the initial crack width, temperature and autogenous healing potential of cementitious materials. This work demonstrated that the flow rate of freshwater through specimens with cracks 50 μm wide incubated at 20, 50 and 80ºC approached zero after

4

14 days, while for cracks 100 µm wide it was ~5% of the initial flow, and those 150 µm wide it was ~15%.

Studies have been conducted on the mineral precipitates formed on marine exposed concrete [33, 34]. These mineral precipitates are markedly different than those formed on the surface of the concrete in fresh water systems. First, a layer of brucite is formed which is later overlaid by aragonite. Conjeaud [33] observed brucite as a layer on the surface of the mortar specimens after two days exposure (earliest test age). Those brucite layers formed on OPC mortar specimens varied in thickness but were on average about 20 to 50 µm thick. Brucite layers formed on Type V (sulphate resistant) cement mortar specimens from the same study were thinner, which was attributed to reduced calcium hydroxide in those specimens. Overlaying these brucite layers was a thicker, but more slowly formed layer of aragonite. Following two years exposure, this aragonite layer reached a thickness of 300 µm for all cement types tested. Maes [32] quantified the autogenous healing capacity of cracked OPC and S50 (50:50 weight % blend of OPC and BFS) mortar specimens, submerged in distilled- and synthetic sea-water through visual observation; and OPC specimens exposed to wet-dry cycles of distilled and a sodium chloride solution through chloride ingress. He found that OPC specimens with cracks 300 µm wide submerged in distilled water visually healed by 70% and in synthetic seawater healed by 85%, and that S50 specimens in distilled water healed by 60% and in synthetic seawater healed by 75%.

Research quantifying the autogenous healing capacity of cementitious materials has been largely restricted to freshwater studies, while what is meant by healing is not always clear.

1.4 Bacteria-based self-healing concrete

An innovative self-healing materials approach is one whereby bacteria immobilised in concrete are able to form a crack healing mineral precipitate [4-14]. These crack healing mineral precipitates can maintain the materials water tightness, making it less susceptible to water-borne degradation phenomena.

Bacteria induced calcium carbonate precipitation readily occurs in nature as a result of bacterial metabolic activity. The principal metabolic pathways used for the development of bacteria-based self-healing concrete have been aerobic respiration of organic compounds and urea hydrolysis. Aerobic respiration of organic compounds follows the general reaction (Equation (1.1)) [35]:

$$(CH_2O)_n + O_2 \xrightarrow{\text{Bacteria}} CO_2 + H_2O \qquad (1.1)$$
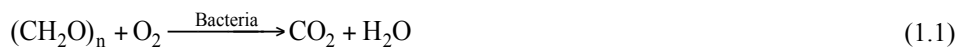
Which results in the production of carbon dioxide and water. Urea hydrolysis follows the general reaction (Equation (1.2)) [36]:

$$CO(NH_2)_2 + H_2O \xrightarrow{\text{Bacteria}} 2NH_3 + CO_2 \qquad (1.2)$$

Which results in the production of carbon dioxide, and ammonia. Carbon dioxide molecules produced by both metabolic pathways in alkaline environments are rapidly chemically converted to carbonate ions, which in the presence of calcium ions precipitate as calcium carbonate (Equation (1.3)):

$$CO_2 + Ca(OH)_2 \longrightarrow CaCO_3 + H_2O \qquad (1.3)$$

These calcium carbonate precipitates have the potential to heal concrete cracks protecting embedded steel reinforcement from external chemical attack (Figure 1.2).
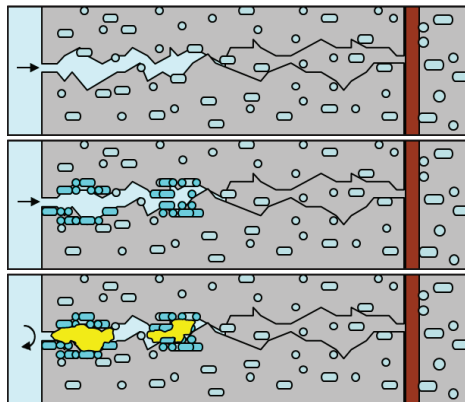
Figure 1.2. A schematic diagram depicting the crack healing mechanism for bacteria-based self-healing concrete. Water ingress activates bacteria in the crack; the bacteria multiply; and induce calcium carbonate precipitation (yellow), sealing the crack. This figure is reproduced, with permission, from Jonkers [4].

Self-healing concrete requires specialised bacteria, which are able to cope with the challenging environment posed by cementitious materials. Such bacteria exist in nature and are part of a group of alkali-resistant spore-formers related to the genus *Bacillus* [6]. Bacterial spores are well suited for concrete incorporation as these hardy cells are able to withstand mechanical and chemical stresses, and can remain viable for 200-300 years in a dry state [37]. Bacterial spores, however, when added directly to concrete during mixing have demonstrated limited viability over time [5]. On account of this, bacteria-based agents (bacterial spores and mineral precursor compounds) have been protected in

6

expanded clay particles [6, 7, 13], and bacterial spores in diatomaceous earth [8], melamine- [9], hydrogel- [10], and alginate-microcapsules [11], before cementitious material inclusion. In fact, all of these strategies have successfully extended the period over which healing could be achieved. Experimental results have shown that bacterial spores and mineral precursor compounds protected in expanded clay particles were able to visually heal cementitious cracks up to 0.46 mm wide after 100 days submersion in freshwater [7]. The same technology, in a later study, was able to reduce the permeability of V-shaped cracks with mouths ~350 μm wide by 98% [13]. Mortar specimens incorporated with diatomaceous earth particles containing bacterial spores, when submerged in a urea calcium media, visually filled the mouths of V-shaped cracks up to 0.17 mm wide [8]. Specimens containing bacterial spores protected in melamine based microcapsules were able to visually heal tensile cracks up to 970 μm wide [9]. Mortar specimens embedded with spores encapsulated in hydrogel microcapsules were able to visually heal cracks ~0.5 mm wide and reduced the permeability of tensile cracks ~220 μm wide by 68% [10]. Despite the growing prominence of marine concrete infrastructure, research on bacteria-based self-healing concrete has been restricted to room temperature freshwater studies [4-14]. If bacteria-based self-healing concrete is to be realised in low-temperature marine environments then bacteria-based agents, and more specifically the bacteria making up part of these agents, will need to function under the same conditions. Development and incorporation of such an agent in cementitious materials should lead to marine concrete infrastructure with longer functional service lives, and associated tremendous economic benefits.

1.5 Objectives

The primary objective of the current project is to develop a cost-effective bacteria-based self-healing cementitious composite for application in low-temperature marine environments. To achieve this objective four sub-objectives were devised: (1) quantify and characterise the autogenous healing capacity of marine exposed cementitious materials; (2) develop a cost-effective bacteria-based healing agent (bacterial spores and mineral precursor compound) for low-temperature marine concrete applications; (3) encapsulate this healing agent; and (4) incorporate the encapsulated agent in a cementitious material, and quantify the healing capacity of the subsequent bacteria-based self-healing cementitious composite.

1.6 Outline of the thesis

This thesis consists of eight chapters (Figure 1.3). Chapter 1 has introduced the key themes pertinent to the research. Research objectives and a thesis outline are also given. Chapters 2-4 present research on the autogenous healing ability of cementitious materials. Chapter 2 reports on the autogenous crack healing capacity of cementitious materials submerged in fresh and seawater through visual crack closure and characterises the healing products. Chapter 3 reports on the functional autogenous healing capacity of cracked cementitious specimens submerged in seawater. A test is then presented for generating crack permeability data for cementitious materials. Chapter 4 presents an improved permeability test for quantifying the functional crack healing capacity of cementitious materials. Chapters 5-7 chart the development of a cost-effective bacteria-based self-healing cementitious composite for application in low-temperature marine environments. Chapter 5 presents a bacteria-based healing agent (bacterial spores and mineral precursor compounds) for low-temperature marine concrete applications. Chapter 6 reports on the encapsulation of the healing agent in calcium alginate forming a smart bacteria-based bead. The functionality of the bacteria-based bead is assessed through oxygen measurements, its ability to swell and to form an organic-inorganic crack healing material in a simulative marine concrete crack solution. Chapter 7 reports on the incorporation of the bacteria-based bead technology in a cementitious material forming a bacteria-based self-healing cementitious composite. The composite is then tested for its autonomous crack healing capacity using the improved permeability test presented in Chapter 4, and for its strength development through compressive strength testing. Chapter 8 draws a number of conclusions and makes recommendations for future research.

The author hopes that the research presented herein provide a valuable reference for those interested in bacteria-based self-healing concrete, and more generally for those interested in the wider field of self-healing materials research.

```
┌─────────────────────────────────────────────┐
│         Chapter 1 – Introduction             │
└─────────────────────────────────────────────┘

┌─────────────────────────────────────────────┐
│  ┌───────────────────────────────────────┐  │
│  │ Chapter 2 – Visual quantification and │  │
│  │ characterization of autogenous healing│  │
│  └───────────────────────────────────────┘  │
│  ┌───────────────────────────────────────┐  │
│  │ Chapter 3 – Functional quantification │  │
│  │      of autogenous healing            │  │
│  └───────────────────────────────────────┘  │
│  ┌───────────────────────────────────────┐  │
│  │ Chapter 4 – An improved test for      │  │
│  │   quantifying functional healing      │  │
│  └───────────────────────────────────────┘  │
└─────────────────────────────────────────────┘

┌─────────────────────────────────────────────┐
│  ┌───────────────────────────────────────┐  │
│  │ Chapter 5 – A cost-effective          │  │
│  │ bacteria-based healing agent for the  │  │
│  │ development of self-healing marine     │  │
│  │            concrete                    │  │
│  └───────────────────────────────────────┘  │
│  ┌───────────────────────────────────────┐  │
│  │ Chapter 6 – A bacteria-based bead for │  │
│  │ self-healing marine concrete applications│
│  └───────────────────────────────────────┘  │
│  ┌───────────────────────────────────────┐  │
│  │ Chapter 7 – A bacteria-based self-healing│
│  │ cementitious composite for application │  │
│  │    in the marine environment           │  │
│  └───────────────────────────────────────┘  │
└─────────────────────────────────────────────┘

┌─────────────────────────────────────────────┐
│      Chapter 8 – Conclusions and outlook     │
└─────────────────────────────────────────────┘
```

Figure 1.3 Thesis outline.

2

Visual quantification and characterization of autogenous healing

He has let loose the two seas meeting together. Between them is a barrier which none of them can transgress.

— Ar-Rahmaan 55:19-20, Qur'an

Concrete can autogenously heal cracks potentially increasing construction durability. Research quantifying this process is limited to freshwater studies making the controlling parameters in seawater unclear. In this chapter, the autogenous crack healing capacities of OPC and BFS cement mortar specimens submerged in fresh and seawater, are visually quantified and characterised. The BFS cement specimens healed all crack widths up to 104 µm, and OPC specimens healed all crack widths up to 592 µm, after 56 days in seawater. BFS cement specimens healed all crack widths up to 408 µm, and OPC specimens healed all crack widths up to 168 µm, after 56 days in freshwater. The OPC specimens submerged in seawater displayed both higher crack healing capacity and losses in compressive strength. Differences in performance are attributable to the amount of calcium hydroxide in these mortars and specific ions present in seawater. Studies quantifying the crack healing capacity of cementitious materials through visual crack closure should be conducted in conjunction with a material functional property such as strength.

2.1 Introduction

Many physical and chemical phenomena are usually interdependent and mutually reinforcing in the deterioration of marine exposed concrete. Concrete durability is intimately related to the transport properties of the material, particularly in aqueous environments. Cracks allow harmful chemicals to penetrate deep into concrete, leading to weakening of the cement matrix and corrosion of the reinforcement. Concrete has a natural or autogenous ability to heal cracks, greatly reducing chemically driven degradation phenomena. First reported by the French Academy of Science in 1836, autogenous healing is principally att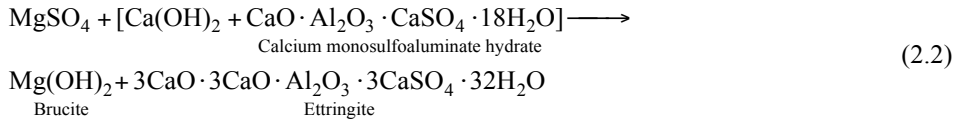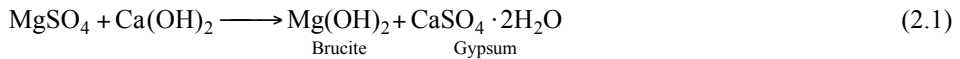ributed to the hydration of unhydrated cement particles and the carbonation of dissolved calcium hydroxide [25]. Numerous studies have recognised this phenomenon [26-29]; however, studies quantifying autogenous healing are scarce [27, 29-31]. Edvardsen [29] examined the autogenous healing ability of cracked concrete specimens in freshwater through visual observation and permeability measurements. She found that about 50% of the specimens with cracks 200 μm wide (mean value) healed completely over a seven-week exposure period. She also noted that the greatest healing occurred within the first 3 to 5 days after submersion. In a later study, Reinhardt and Jooss [27] showed a relationship between temperature and the autogenous healing capacity of cementitious materials. They showed that the flow of water through specimens with cracks 50 μm wide incubated at 20, 50 and 80ºC approached zero after 14 days, while for cracks 100 μm wide at 20ºC it was ~5% of the initial flow, and those 150 μm wide it was ~15% of the initial flow.

   Seawater contains aggressive agents, which may compromise concrete durability. Magnesium sulphate, magnesium chloride, and carbon dioxide are particularly known to attack the calcium hydroxide, calcium monosulfoaluminate hydrate and calcium silicate hydrate, of hydrated Portland cement. Magnesium sulphate reacts with calcium hydroxide forming brucite and gypsum (Equation (2.1)), and with calcium hydroxide and monosulfoaluminate hydrate forming ettringite (calcium sulphoaluminate hydrate)(Equation (2.2)) [2]:

$$MgSO_4 + Ca(OH)_2 \longrightarrow \underset{\text{Brucite}}{Mg(OH)_2} + \underset{\text{Gypsum}}{CaSO_4 \cdot 2H_2O} \tag{2.1}$$

$$MgSO_4 + [Ca(OH)_2 + \underset{\text{Calcium monosulfoaluminate hydrate}}{CaO \cdot Al_2O_3 \cdot CaSO_4 \cdot 18H_2O}] \longrightarrow$$
$$\underset{\text{Brucite}}{Mg(OH)_2} + 3CaO \cdot \underset{\text{Ettringite}}{3CaO \cdot Al_2O_3 \cdot 3CaSO_4 \cdot 32H_2O} \tag{2.2}$$

Magnesium chloride reacts with calcium hydroxide forming brucite and calcium chloride (Equation (2.3)):

$$MgCl_2 + Ca(OH)_2 \longrightarrow \underset{\text{Brucite}}{Mg(OH)_2} + CaCl_2 \qquad (2.3)$$
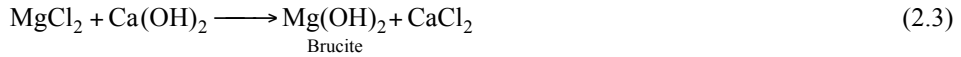
Dissolved carbon dioxide reacts with calcium hydroxide forming aragonite (Equation (2.4)):

$$CO_2 + Ca(OH)_2 \longrightarrow \underset{\text{Calcium carbonate}}{CaCO_3} + H_2O \qquad (2.4)$$
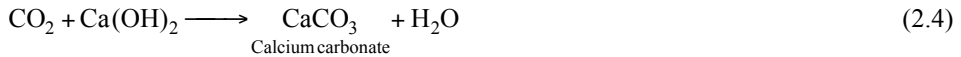
calcium bicarbonate upon reaction with aragonite (Equation (2.5)):

$$CaCO_3 + H_2O + CO_2 \longrightarrow \underset{\text{Calcium bicarbonate}}{Ca(HCO_3)_2} \qquad (2.5)$$

and tetracalcium aluminium carbonate hydrate and gypsum upon reaction with calcium hydroxide and calcium monosulfoaluminate hydrate (Equation (2.6)):

$$CO_2 + \underset{\text{Calcium monosulfoaluminate hydrate}}{[Ca(OH)_2 + CaO \cdot Al_2O_3 \cdot CaSO_4 \cdot 18H_2O]} \longrightarrow$$
$$\underset{\text{Tetracalcium aluminium carbonate hydrate}}{3CaO \cdot Al_2O_3 \cdot CaCO_3 \cdot xH_2O} + \underset{\text{Gypsum}}{CaSO_4 \cdot 2H_2O} \qquad (2.6)$$
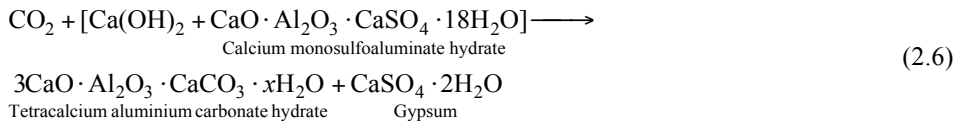
Gypsum, calcium chloride and calcium bicarbonate are soluble in seawater and so are easily leached from concrete, resulting in increased porosity, permeability and possible reductions in mechanical strength [18, 19]. Although the sulphate concentration in seawater is high enough for ettringite formation (Equation (2.2)), the expansive nature of the ettringite formed is reduced by the presence of chloride [19]. In accordance with Equations (2.1-2.3), brucite formation continues until calcium hydroxide is sufficiently depleted. Following this, magnesium sulphate is then able to decalcify the calcium silicate hydrate (the binding material of the cement) transforming it to magnesium silicate hydrate a non-cementitious material. This reaction can be illustrated as follows (Equation (2.7))[38]:
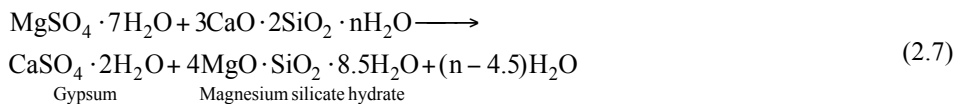
$$MgSO_4 \cdot 7H_2O + 3CaO \cdot 2SiO_2 \cdot nH_2O \longrightarrow$$
$$\underset{\text{Gypsum}}{CaSO_4 \cdot 2H_2O} + \underset{\text{Magnesium silicate hydrate}}{4MgO \cdot SiO_2 \cdot 8.5H_2O} + (n - 4.5)H_2O \qquad (2.7)$$

Conversion of calcium silicate hydrate to magnesium silicate hydrate is known to result in weakening of the cement matrix [19, 20].

The chemical vulnerability of marine exposed concrete may be compounded by

physical stress. Cracks generated through cycles of heating and cooling, wetting and drying, and corrosion of the reinforcing steel greatly increase concrete permeability. Cracks formed in cementitious materials due to corrosion of steel reinforcement are particularly destructive. Steel reinforcement develops a passive layer, which, while intact protects the steel from corrosion. Chloride ions present in seawater, however, may destroy this passive layer allowing reinforcing steel to oxidise in oxygenated areas. Oxidation, or rusting, of the steel reinforcement, can generate expansive pressure within the concrete resulting in cracking and eventual weakening of the concrete matrix [17]. The addition of specific supplementary cementing materials to Portland cement is known to increase the resistance of concrete to marine-based chemical attack [17]. BFS, a product of the steel industry, greatly reduces concrete porosity leading to a less permeable and hence more durable concrete. Hydrated BFS cement paste contains less calcium hydroxide than pure OPC-based cement paste, making the resultant concrete less vulnerable to ionic leaching and subsequent weakening [22].

Studies have been conducted on the surface layers formed on marine exposed concrete [33, 34]. These mineral layers are markedly different than those formed on cementitious materials in freshwater environments. First, a layer brucite is formed (Equations (2.1-2.3)), which is later overlaid by aragonite (Equation (2.4)). Precipitation of aragonite rather than calcite (the more thermodynamically stable of the two calcium carbonate polymorphs) occurs as a result of magnesium ions present in the seawater [39]. Conjeaud [33] in his study observed brucite as a layer on the surface of the mortar specimens after two days exposure (earliest test age). Those brucite layers formed on OPC mortar specimens varied in thickness but were on average about 20 to 50 µm thick. Brucite layers formed on Type V (sulphate resistant) cement mortar specimens from the same study were thinner, which was attributed to reduced calcium hydroxide in those specimens. Overlaying these brucite layers was a thicker, but more slowly formed layer of aragonite. Following two years exposure, the thickness of this aragonite layer reached a value of 300 µm for all cement types tested. Conjeaud concluded that the brucite-aragonite double layer, which formed at the expense of the cement matrix, served as a protective skin suppressing further attack of the mortar matrix. Maes as part of his PhD [32] quantified the autogenous healing capacity of cracked OPC and S50 (50:50 weight % blend of OPC and BFS) mortar specimens, submerged in distilled- and synthetic sea-water through visual observation; and OPC specimens exposed to wet-dry cycles of distilled and a sodium chloride solutions through chloride ingress. He found that OPC specimens with cracks 300 µm wide submerged in distilled water visually healed by 70% and those in synthetic seawater healed by 85%, and that S50 specimens in distilled water healed by 60% and those in synthetic seawater healed by 75%.

Specific ions present in seawater, which on the one hand may afford marine concrete with a certain crack healing potential, on the other, may also be responsible for

reductions in material performance. Quantitative data on the crack healing capacity of marine exposed concrete is still largely missing, while the link between healing and material functional properties such as strength is not clear. The current study aims to quantify autogenous healing capacity of cementitious specimens in relation to material strength. Furthermore, we define: (1) crack closure as the complete visual bridging of a crack at a specific crack width location; (2) crack narrowing as a reduction of a crack width at a specific crack width location; and (3) the crack healing capacity of a material as the maximum crack width for which all analysed crack width locations are 100% healed.

2.2 Experimental program

Four series were set up to characterise and quantify the autogenous healing capacity of submerged mortar specimens: (1) OPC specimens in freshwater; (2) BFS cement specimens in freshwater; (3) OPC specimens in seawater; and (4) BFS cement specimens in seawater. Two specimen geometries were employed, cube specimens to assess compressive strength development and cracked prisms to quantify visual crack closure.

2.2.1 Sample preparation

Cubes (40 × 40 × 40 mm) and prisms (40 × 40 × 160 mm) were cast from OPC (CEM I 42.5 N, ENCI, the Netherlands) and BFS cement (CEM III/B 42.5 N LH, ENCI)(65-80% (w/w)) in accordance with EN 1015-11 [40]. The applied mix design is shown in Table 2.1. Prism specimens were reinforced with a 4 mm threaded steel bar, which was placed in the centre and parallel to the horizontal axis of each prism so that the bar protruded ~30 mm from out the mould. Cubes and prisms were carefully removed from their moulds after 24 hours, sealed in polyethylene plastic bags and kept at room temperature for a total curing period of 28 days. Following curing, prism specimens containing the steel reinforcement were stretched through a displacement-controlled tensile load resulting in the formation of cracks in the prisms up to 1 mm wide.

Table 2.1 Mix-design for mortar specimens.

Constituent	Amount [kg.m^{-3}]	
	CEM I 42.5 N	CEM III/B 42.5 N LH
Cement	507	494
Water	253	247
Sand fraction [mm]:		
1-2	608	608
0.5-1	426	426
0.25-0.5	167	167
0.125-0.25	319	319

2.2.2 Autogenous healing incubation conditions

Two sets of plastic buckets were prepared, the first set containing 4 l of tap water and the second 4 l of artificial seawater (20 ± 2ºC). The artificial seawater was produced from technical grade chemicals (Sigma-Aldrich), the composition of which is shown in Table 2.2. This artificial seawater is based on the major constituents of natural seawater [41]. Tap water and artificial seawater are to be called freshwater and seawater respectively for the remainder of the text. Three cubes were, or one cracked prism was, submerged per bucket (28 days after casting). The water in the buckets was changed once a week for two weeks to mimic in situ conditions and prevent ion depletion. The buckets were kept open to the atmosphere during the experiment to allow for gas diffusion across the water-air interface.

Table 2.2 Artificial seawater composition based on the major constituents of seawater [41].

Compound	Amount [g.l^{-1}]
$NaHCO_3$	0.19
$CaCl_2.2H_2O$	1.47
$MgCl_2.6H_2O$	10.57
$Na_2SO_4.10H_2O$	9.02
KCl	0.75
NaCl	24.08

2.2.3 Precipitate characterisation

Environmental scanning electron microscopy (ESEM)(Philips XL 30 ESEM, Philips) in back-scattered electron (BSE) mode was used to study the surface of the cubes before and after submersion for 56 and 140 days. Prior to analysis, submerged cubes were

removed from the water and air-dried. Cubes submerged for 140 days were also impregnated with epoxy and polished sections prepared for ESEM and energy dispersive spectroscopy (EDS)(Philips EDAX, Philips) analysis. These polished sections were prepared by epoxy impregnating the dry specimens under vacuum. Once the epoxy was hard, the specimens were sawn in two (following the central axis of the cylinders) with a water-cooled diamond saw. The cut surfaces were then ground, impregnated a second time, allowed to harden and polished. The surface composition of the cubes were chemically characterised through Fourier transform infrared spectroscopy (FTIR)(Spectrum 100, Perkin-Elmer Inc.). Samples (< 5 mg) were prepared by scraping the dry surface of the cubes before and after 56 and 140 days submersion. Spectra were the result of 32 scans with a resolution of 4 cm^{-1} in the range of 4000-600 cm^{-1}.

2.2.4 Strength development

The compressive strength of the mortar cubes was determined at a rate of 1 MPa.sec^{-1} with a Servo-Plus compression test machine and Cyber-Plus evolution control unit, 2, 7, 28, 84 and 168 days after casting. Unsubmerged OPC and BFS cement cubes were kept in sealed plastic bags to test for any difference between their compressive strength and the compressive strength of the submerged specimens. The values reported are the average of three specimens.

2.2.5 Quantification of crack healing

Cracks were randomly selected at the side of the prisms. Visual crack closure was assessed through stereomicroscopic observation (Leica MZ6), photographic imaging (Leica application suite 4.0) and measurements made in Photoshop (Adobe Systems Incorporated). The crack healing capacity of the cementitious materials was assessed by removing the prisms from the water (for a total of ~30 min) every two weeks and measuring for any crack width reductions. Crack width measurements were made at the same 1 mm intervals along the length of each crack.

2.3 Results

2.3.1 Microscopy study of surface precipitates

ESEM analysis of precipitates formed on the surface of the specimens revealed a striking difference between those submerged in freshwater (Figure 2.1(A and B)) and those submerged in seawater (Figure 2.1(C and D)), after 56 days. Freshwater submerged

specimens formed a layer of rhombohedral crystals, while specimens in seawater were covered in a billowing layer of needles. Rhombohedral crystals are associated with calcite, and needles with aragonite [42]. Precipitation seemed to have ceased after 56 days submersion.
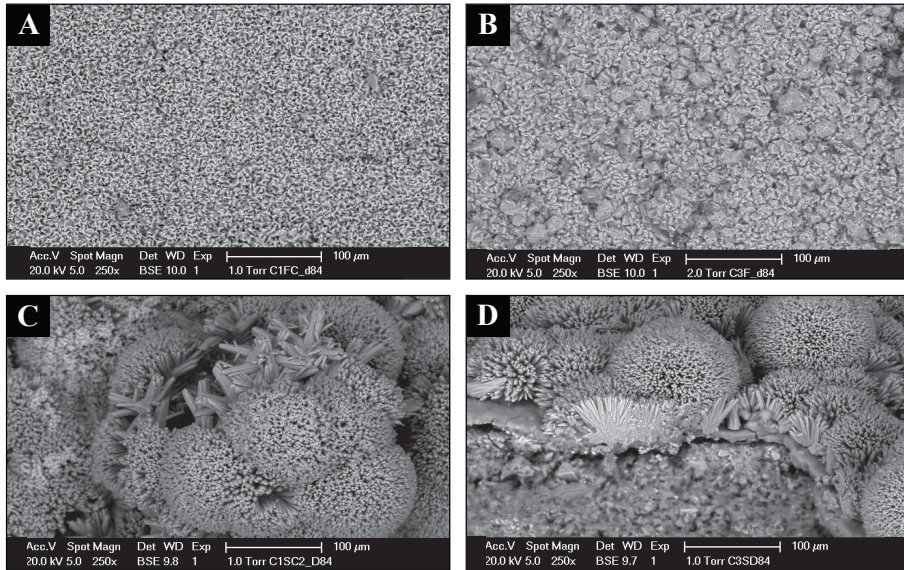
Figure 2.1 ESEM images were taken of: (A) CEM I specimens in freshwater; (B) CEM III/B specimens in freshwater; (C) CEM I specimens in seawater; and (D) CEM III/B specimens in seawater, after 56 days submersion. The images are from the side faces of the specimens as they were submerged in the water.

2.3.2 Analysis of polished sections

ESEM-EDS analysis of the CEM I cube specimens in freshwater displayed a layer ~10 µm thick on their surface (Figure 2.2(A and B)), while CEM III/B specimens formed a layer ~5 µm (Figure 2.2(C and D)). These layers were an association of calcium, oxygen and carbon suggesting them to be calcium carbonate (Equation (2.4)). CEM I and CEM III/B specimens submerged in seawater formed a double skin on their surface. The high magnesium concentrated lower layer, likely brucite (Equations (2.1 and 2.3)), was precipitated on the surface of the specimens and the calcium rich outer layer, likely calcium carbonate (Equation (2.4)), was precipitated on top of that. CEM I specimens formed a lower layer ~50 µm, and upper layer ~150 µm, thick. Below this double skin, the subsurface of the CEM I specimens submerged in seawater appeared visibly porous (Figure 2.2(E and F)). CEM III/B specimens submerged in seawater also formed a lower layer. This layer, however, was far thinner at ~5 µm than those layers formed on the

CEM I specimens, while the outer layer was also thinner at ~100 µm (Figure 2.2(G and H)). Below these surface precipitates, magnesium intrusion could be seen ~100 µm into the CEM III/B mortar matrix (Figure 2H).
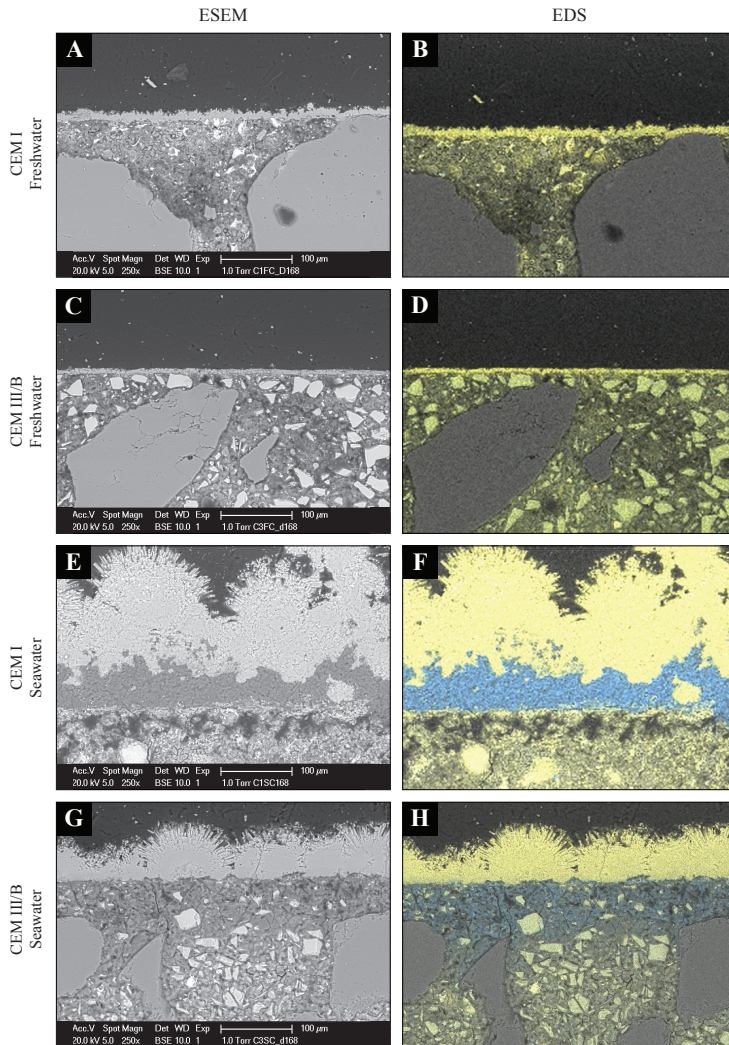
Figure 2.2 ESEM-EDS analysis of polished sections prepared 140 days after submersion. ESEM images showing: (A) CEM I-based specimens after submersion in freshwater; (C) CEM III/B in freshwater; (E) CEM I in seawater and; (G) CEM III/B in seawater. EDS analysis of: (B) CEM I in freshwater; (D) CEM III/B in freshwater; (F) CEM I in seawater; and (H) CEM III/B in seawater. Yellow of the EDS images represents calcium and blue represents magnesium. The surfaces presented in the images are those from the side faces of the specimens as they were submerged in the water.

2.3.3 Chemical characterisation of surface precipitates

The peak positions of the FTIR spectra are tabulated in Table 2.3. Bands at 3642 and 3696 cm^{-1} correspond to the O-H stretching vibration of calcium hydroxide and brucite, respectively [43]. Calcite has characteristic absorption peaks: C-O asymmetric stretching vibration (v_3), C-O out of plane bending (v_2), and C-O planar bending vibration (v_4) centred at 1400, 872 and 712 cm^{-1}, respectively. Aragonite has, in addition, a characteristic peak stretching vibration (v_1) 1083 cm^{-1} and the bending vibration (v_4) centred at 700 and 712 cm^{-1} [44]. Peaks associated with calcium hydroxide and calcite were present on unsubmerged CEM I and CEM III/B specimens. Calcium hydroxide peaks disappeared from both specimen types after 56 days submersion in fresh and seawater. Peaks associated with brucite (Equation (2.1-2.3)) and aragonite (Equation (2.4)) appeared for both specimen types after 56 days submersion in seawater, with the brucite peaks being less pronounced for the CEM III/B specimens.

Table 2.3 FTIR bands of mineral precipitates present on submerged cubes.

CEM I freshwater		CEM III/B freshwater		CEM I seawater		CEM III/B seawater			
Submersion days									
0	56	0	56	0	56	0	56		
Wave number [cm^{-1}]								Mineral	Reference
3643	-	3640	-	3642	-	3642	-	Portlandite [Ca(OH)$_2$]	[21]
-	-	-	-	-	3694	-	3690	Brucite [Mg(OH)$_2$]	[21]
1795	1797	-	1797	-	1786	1794	1787		
1409	1400	1420	1405	1415	1440	1413	1445	Calcite [CaCO$_3$]	[22]
873	872	874	872	-	-	874	-		
713	713	-	713	-	712	712	712		
-	-	-	-	-	1083	-	1083		
-	-	-	-	-	853	-	854	Aragonite [CaCO$_3$]	[22]
-	-	-	-	-	700,712	695,712	700,712		

2.3.4 Visual crack closure

Crack width measurements were made for each series, 0, 14, 28 and 56 days after submersion. Quantification of those results is depicted in Figure 2.3. CEM I specimens submerged in freshwater for 14 days healed all crack widths up to 69 µm and 37% of all monitored crack widths (14 locations out of 38) up to the largest crack width of 536 µm

(Figure 2.3A). After 28 days submersion all cracks up to 168 μm and 82% of cracks up to 557 μm had healed (Figure 2.3B). After 56 days all cracks up to 168 μm and 64% of cracks up to 422 μm remained healed (Figure 2.3C). CEM III/B specimens submerged in freshwater for 14 days healed all crack widths up to 105 μm and 63% of cracks up to 274 μm (Figure 2.3D). After 28 days submersion, all cracks up to 267 μm and 92% of cracks up to 458 μm had healed (Figure 2.3E). After 56 days submersion, all cracks up to 408 μm had healed. CEM I specimens submerged in seawater for 14 days had healed all cracks up to 521 μm and 97% of those cracks up to 601 μm had healed (Figure 2.3A). By day 28 all cracks up to 592 μm and 85% of those up to 734 μm had healed (Figure 2.3B). From day 28 to 56 healing remained unchanged (Figure 2.3C). CEM III/B specimens submerged in seawater for 14 days had healed all crack widths up to 80 μm and 62% up to 431 μm (Figure 2.3D). Healing did not change from day 14 to day 28 (Figure 2.3E). By day 56 all cracks up to 104 μm had healed, while 62% of cracks up to 431 μm remained healed (Figure 2.3F). Figure 2.5 shows a selected crack from each series after 0, 14 and 28 days. Obvious differences can be seen between each series, but most noticeable are the differences in speed of healing between the fresh and seawater submerged specimens. Seawater submerged specimens healed cracks twice as fast as those in freshwater. While CEM I specimens displaying visibly more precipitate than the CEM III/B specimens in both fresh and seawater. Figure 2.4 shows the crack healing capacity of the four series over time. CEM I specimens in seawater displayed the greatest healing capacity, the CEM III/B and CEM I specimens in freshwater displayed considerably less healing, while CEM III/B specimens in seawater displayed the lowest healing.
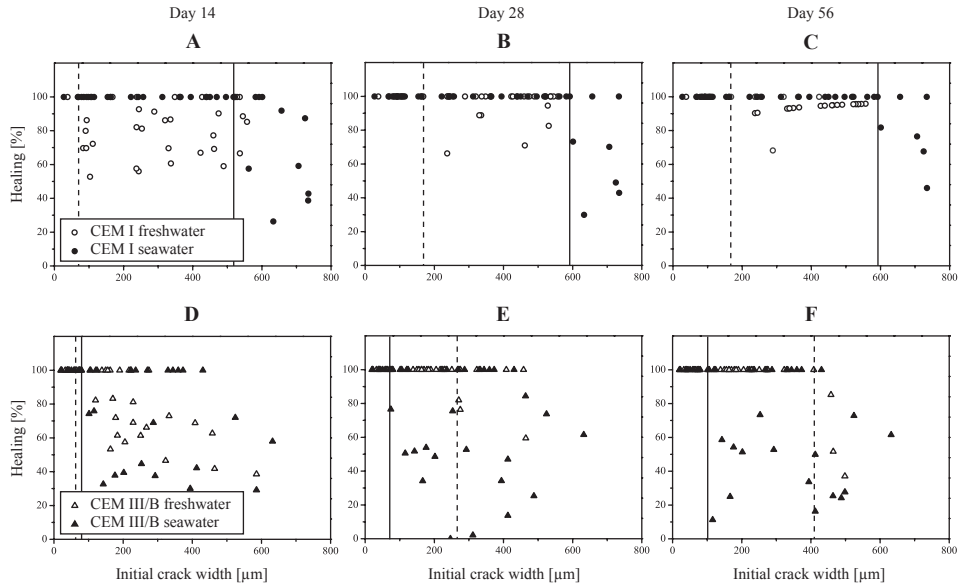
Figure 2.3 Graphs depicting crack healing as a function of the initial crack width for: (A-C) CEM I specimens in fresh and seawater; and (D-F) CEM III/B specimens in fresh and seawater; after (A and D) 14; (B and E) 28; and (C and F) 56 days submersion. Vertical continuous and dashed lines mark the crack healing capacity (i.e. maximum crack width healed for which all crack widths measured were 100% healed) for fresh and seawater submerged specimens, respectively.
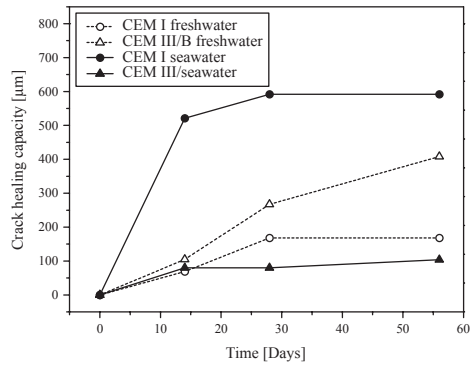
Figure 2.4 Crack healing capacity over time.
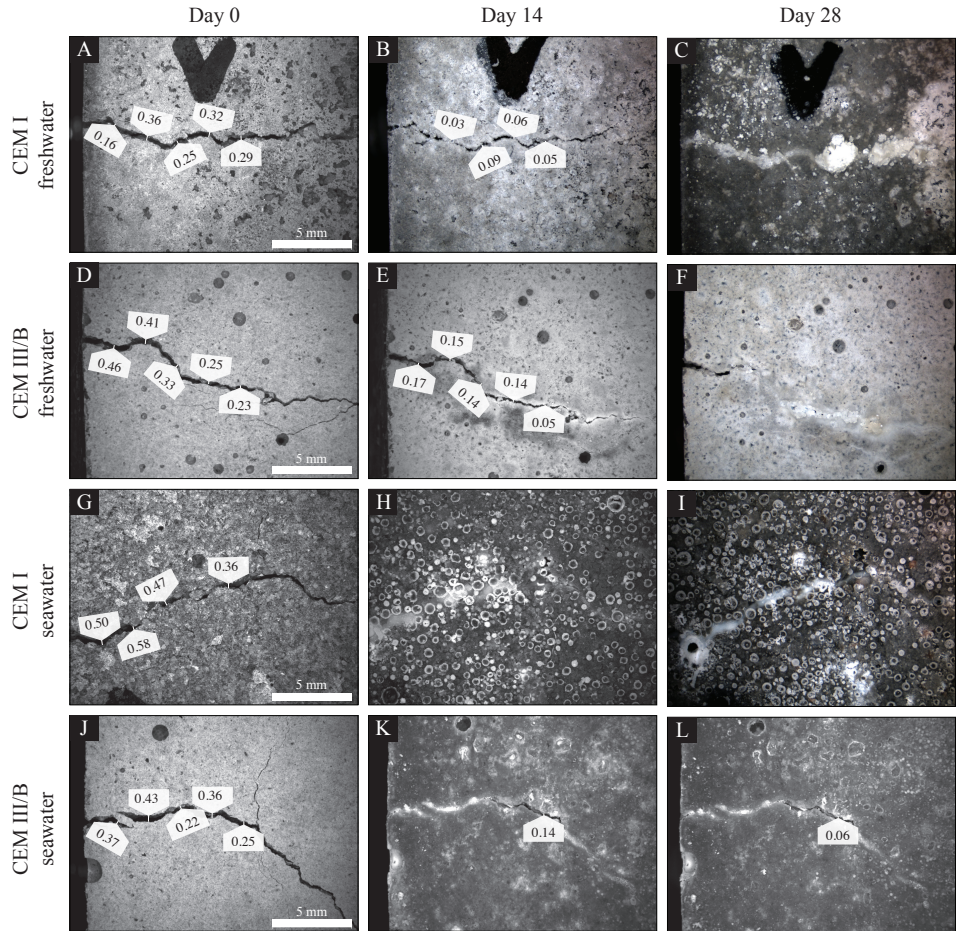
Figure 2.5 Stereomocroscopic images of cracked specimens: (A-C) CEM I specimens in freshwater; (D-F) CEM III/B specimens in freshwater; (G-I) CEM I specimens in seawater and; (J-L) CEM III/B specimens in seawater, (A, D, G and J) 0, (B, E, H and K) 14 and (C, F, I and L) 28 days after submersion. Each crack is one of the cracks from each series presented in Figure 2.3.

2.3.5 Strenght development

Figure 2.6 shows the compressive strength of mortar cubes over time. Before submersion CEM I specimens began with higher compressive strengths than CEM III/B specimens, these roles were reversed by day 28 with CEM III/B specimens having slightly higher compressive strengths than CEM I specimens. 28 days after casting

specimens were submerged in either fresh or seawater. From day 28 to 168 the mean compressive strength of CEM I and CEM III/B specimens submerged in freshwater stabilised at 55-60 MPa, with CEM I specimens having a standard deviation of 22 MPa. Specimens submerged in seawater, however, showed a markedly different tendency. The mean compressive strength of CEM III/B specimens submerged in seawater stabilised much like those in freshwater at ~60 MPa, while the strength of CEM I specimens in seawater decreased from day 28 to 168 from 55 to 45-50 MPa, showing a drop of ~20%. Unsubmerged CEM I specimens maintained a compressive strength of about 55 MPa.
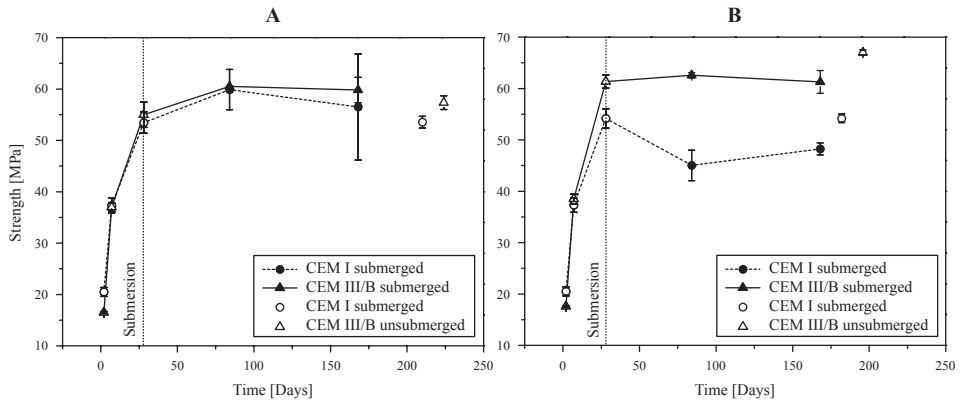
Figure 2.6 Compressive strength development of CEM I- and CEM III/B-mortar cubes cured for 28 days and subsequently submerged in (A) fresh and (B) seawater.

2.4 Discussion

We have investigated the autogenous healing capacity of CEM I and CEM III/B mortar specimens submerged in fresh and seawater. CEM I specimens submerged in seawater displayed the greatest healing capacity, somewhat lower were CEM III/B and CEM I specimens in freshwater and lowest were CEM III/B specimens in seawater.

Differences in healing and degradation phenomena may be attributed to the presence of specific seawater ions and calcium hydroxide concentrations of the mortars tested. Indeed, seawater contains calcium, carbonate, and magnesium ions, which may precipitate as minerals. Mortar specimens submerged in seawater formed a brucite-aragonite layer (Equations (2.1-2,4))(Table 2.3). The seawater provides the carbonate and magnesium ions while the mortar supplies the hydroxide and most of the calcium ions. CEM III/B cement has 65-80% less OPC content than CEM I cement leaving CEM III/B mortar specimens with significantly lower calcium hydroxide and hence healing

capacity. Indeed, after 56 days, CEM III/B mortar specimens in seawater healed all crack width locations up to 104 µm while this value was more than five times higher for CEM I specimens which healed all crack widths up to 592 µm (Figures 2.3 and 2.4). Furthermore, most of the healing for CEM I and CEM II/B specimens submerged in seawater occurred during the first 14 days (Figures 2.2-2.5). Although CEM I specimens submerged in seawater formed the thickest layers (Figure 2.2) and displayed the greatest healing capacity of the series tested (Figures 2.3 and 2.4), they also experienced notable drops in compressive strength (Figures 2.6B). This loss in compressive strength is likely due to the dissolution of calcium hydroxide from the cement matrix, which once depleted also opens up the way for the calcium of the calcium silicate hydrate to be replaced by magnesium forming magnesium silicate hydrate. Porosity and substitution of calcium silicate hydrate for magnesium silicate hydrate are known to reduce the strength of marine exposed concrete [19, 20].

Freshwater, in contrast to seawater, contains low levels of ions. Carbonate ions are present in limited amounts while calcium and magnesium ions are negligible. Submersion of cementitious materials in freshwater increases the amount of calcium ions in the water, resulting in calcite precipitation (Equation (2.4)). Indeed, analysis of mortar specimens submerged in freshwater revealed the formation of a single layer of calcite on their surface (Figure 2.2)(Table 2.3). Carbonate and calcium ions are readily available when the specimens are first submerged in the freshwater. This availability is supported by the crack healing capacities demonstrated by the CEM I and CEM III/B specimens submerged in the freshwater for 14 days, which were quite similar with the CEM I specimens healing all crack width locations up to 69 µm, and the CEM III/B specimens healing all crack width locations up to 105 µm. There was, however, a marked difference in the healing capacities of the two specimen types after 56 days submersion in freshwater, with the CEM III/B mortar specimens healing all crack width locations up to 408 µm, and CEM I specimens healing all crack width locations up to 168 µm (Figures 2.3 and 2.4). The continued healing demonstrated by the CEM III/B specimens likely coming as a result of latent hydraulic reactions. Further, the crack healing capacity of the CEM I mortar specimens submerged in freshwater for 56 days are in good agreement with those presented by Edvardsen [29]. The absence of a dense brucite-aragonite layer on the surface of the freshwater submerged specimens likely allows prolonged leaching of calcium ions over the seawater submerged specimens, and why healing for freshwater specimens was seen beyond day 14. Dissolved calcium hydroxide, which is not precipitated as calcium carbonate likely spreads into the bulk freshwater where it is re-precipitated. Crack healing seemed to stop for CEM I specimens after 28 days, while for CEM III/B specimens it seemed to continue until day 56. This steady increase in visual crack closure by the CEM III/B specimens in freshwater likely results through the steady leaching of ions as a result of the fine pore structure and pozzolanic

reactions associated with BFS cement pastes [45]. In addition to the limited availability of carbonate ions in freshwater, variations in the speed of visual crack closure between fresh and seawater submerged specimens may be attributed to precipitation rates, as calcite in freshwater precipitates slower than aragonite in seawater [46].

CEM I specimens in seawater, displaying the greater healing capacity, also developed considerable losses in compressive strength, while CEM III/B specimens in seawater, and CEM I and CEM III/B specimen in freshwater did not (Figure 6). The reduction in the compressive strength of the CEM I specimens in seawater can be attributed to an increase in the porosity of these specimens due to leaching as a result of aggressive agents in the seawater [18, 19]. Evidence of this porosity could be seen in the subsurface of these specimens (Figure 2.2(E and F)). Previous studies have reported similar reductions in the compressive strength of OPC mortar specimens submerged in seawater [47, 48]. The stable compressive strengths of CEM I and CEM III/B specimens in freshwater can be attributed to the low amount of leaching experienced by these specimens due to the low amount of aggressive agents in freshwater. The stable compressive strength of CEM III/B specimens in seawater can also be attributed to the low amount of leaching experienced by these specimens, this time, however, resulting from the fine pore structure formed by the BFS cement [45].

2.5 Conclusion

The autogenous crack healing capacity of OPC and BFS cement mortar specimens submerged in fresh and seawater were quantified. Of the series tested OPC specimens submerged in seawater displayed the highest healing capacity, OPC and BFS cement specimens in freshwater displayed lower healing capacities, while BFS cement specimens in seawater displayed the lowest healing capacity. OPC specimens submerged in seawater also experienced losses in compressive strength, while the other series did not. Differences in performance between the series are attributable to the amount of calcium hydroxide present in these mortars and specific ions present in seawater. The superior crack healing capacity demonstrated by the OPC specimens over the BFS cement specimens submerged in seawater may give OPC concretes an advantage over BFS concretes in marine environments. Indeed, the superior healing capacity of OPC concretes may be the reason why OPC concrete structures continue to stand for many years in and around our seas. Further, we propose, based on the results presented, that studies quantifying the healing capacity of cementitious materials through visual crack closure do so in conjunction with a material functional property such as strength and/or water tightness. This study represents a valuable reference against which future studies quantifying the healing capacity of cementitious materials can be compared.

3

Functional quantification of autogenous healing

I think the first things that are relevant are the things that should work well; they should function.

— Robin Day

Concrete can autogenously heal cracks contributing to its functional water tightness. In this chapter, we quantify the crack healing capacity of seawater submerged mortar specimens with the aid of a crack permeability test. Cracks of defined widths were created in BFS cement specimens allowing reference crack permeability values to be generated for unhealed-specimens against which healed-specimens were quantified. Specimens with 0.2 mm wide cracks demonstrated no water flow after 28 days submersion. Specimens with 0.4 mm cracks demonstrated decreases in water flow of 66% after 28 days submersion and 50 to 53% after 56 days submersion. The ability of a cementitious material to heal a crack is dependent on the width of the crack, thermodynamic considerations, the presence of water, and the amount of ions available in the crack. Autogenous crack healing for seawater submerged cementitious materials is principally attributable to the precipitation of aragonite and brucite in the cracks. This study represents a valuable reference quantifying the functional autogenous healing capacity of seawater exposed cementitious specimens.

3.1 Introduction

Cracks are a design feature of reinforced concrete. Cracks generally increase concrete permeability, reducing the functionality of water retaining structures and allowing aggressive agents such as those found in seawater to penetrate deep into the material. Penetration of such agents can accelerate concrete deterioration, rendering a concrete structure unfit for use [49]. Concrete has an autogenous ability to heal cracks maintaining the functional water tightness of structures from which they are made. Accurate quantification of concrete permeability may, therefore, provide insights for better service life predictions, particularly for those structures in the marine environment.

Studies are available in the literature quantifying the autogenous healing capacity of cracked cementitious materials through their water permeability [27, 29, 50]. These studies, limited to freshwater, are no doubt built on research quantifying the water permeability of cracked cementitious materials [51-54]. Quantification of crack healing through water permeability measurements presupposes the generation of defined (or at least explicit) crack width geometries. Wang *et al.* in their permeability study [51] introduced a feedback-controlled tensile splitting technique for generating cracks in concrete specimens. This study and subsequent studies employing the same technique [53, 54] did not directly measure the crack width; rather they assumed them to be equal to the lateral displacement of the specimen measured using linear variable differential transformers (LVDTs). This may result in inaccurate measurements due to crack branching and variability along their length. Cracks generated through this technique have also been shown to relax following unloading. Wang *et al.,* [51] noticed that the crack openings after unloading partially closed reducing their widths. Aldea *et al.,* recorded crack reductions of 62-66% for high strength concrete and 56% for normal strength concrete [53] and 32-75% depending on the material type used in a subsequent study [54]. Reinhardt and Jooss [27] in their study included reinforcement in their specimens and were able to form tensile cracks within 0.01 mm of the desired crack width. Though accurate they anticipated that the crack widths, which were measured externally, were not constant over the height of the specimens, demonstrating the difficulty of this method to create defined crack widths. Existing permeability tests also tend to wait for a steady state flow to be achieved, that is, for the crack inflow to equal the crack outflow. This means that the testing periods can last ~14 [27], 20-50 [51], 35-140 [29] and 90-100 days [52]. A long testing period may result in autogenous healing during the test, while the amount of water required to reach a steady state flow may not be practical for many tests. Studies quantifying autogenous healing through water permeability measurements must first know the permeability of an unhealed crack against which a healed crack can be quantified. Reinhardt and Jooss [27] in their study established this initial permeability by flowing water through the cracks at the beginning

of the test. This action, however, has the danger of flushing out the reactive components responsible for healing. Edvardsen [29] in her study was able to negate this flushing out effect by calculating the initial crack flow through Poiseulle's law. Calculations, however, only provide an approximation of the initial permeability. Development of a test that can generate reference crack permeability values for unhealed cracks against which healed cracks of the same geometry could be quantified would, therefore, be of great benefit.

The current chapter aims to quantify the autogenous healing capacity of cracked seawater submerged specimens through their water permeability. Presented is a simple and rapid permeability test. The test includes a novel method for creating defined crack width geometries in cementitious specimens and a simple permeability setup. The test allows cracked specimens to be produced by which reference unhealed permeability values can be defined and healed specimens compared. This study is the first to quantify the functional healing capacity of cracked seawater exposed cementitious specimens through water permeability measurements.

3.2 Experimental program

A permeability test was designed to quantify the autogenous healing capacity of BFS cement mortar specimens following their submersion in seawater. Three series were set up to help quantify healing: (1) to establishes reference permeability values for specimens with cracks 0.2 and 0.4 mm wide; (2) to determine the permeability of specimens with cracks 0.2 and 0.4 mm wide following 28 days submersion in seawater; and (3) to determine the crack permeability of specimens with cracks 0.2 and 0.4 mm wide following 56 days submersion in seawater (Figure 3.1). Crack widths and submersion times are based on the work from Chapter 2.
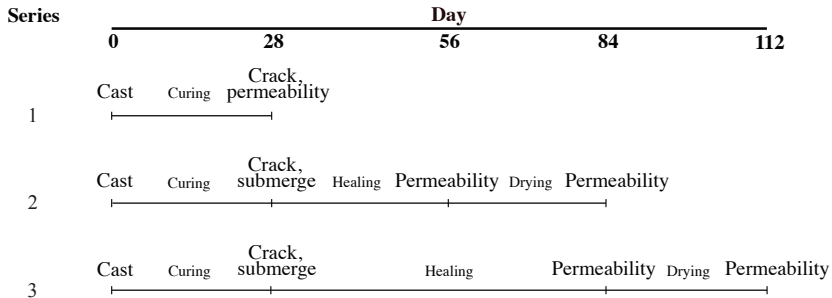

Figure 3.1 Scheme showing the experimental program used to quantify the autogenous healing capacity of cracked BFS cement specimens submerged in seawater. Each series consisting of specimens with cracks 0.2 and 0.4 mm wide and ten specimens each.

3.2.1 Sample preparation

Cylindrical specimens (60 mm long and with a diameter of 33.5 mm) were cast from BFS cement (CEM III/B 42.5 N LH, ENCI) in accordance with EN 1015-11 [40]. BFS cement was chosen to produce the specimens due to the technical benefits it provides marine-based concrete construction (e.g. lower permeability, decreased chloride ion penetration and increased resistance to sulphate attack) [55]. The applied mortar mix design is shown in Table 3.1. The mortar cylinders were designed to fit standard polyvinylchloride pipes (internal diameter 35 mm) and to have two diametrically opposite grooves (2 mm wide and 3 mm deep) running down their side. In order to cast the cylinders, a master pattern was first created in polyvinylchloride. The master pattern was used to cast silicone moulds, which were in turn used to cast the mortar specimens. 24 hours after casting the mortar specimens were carefully removed from their silicone moulds, sealed in polyethylene plastic bags and kept at room temperature for a total curing period of 28 days.

Table 3.1 Mix-design for mortar specimens.

Constituent	Amount [$kg.m^{-3}$]
Cement (CEM III/B 42.5 N LH)	494
Water	247
Sand fraction (mm):	
1-2	608
0.5-1	426
0.25-0.5	167
0.125-0.25	319

3.2.2 Crack calibration

Following curing, specimens were prepared for tensile splitting. Each mortar cylinder was wrapped in polyethylene and steel rods (~80 mm long with a 3 mm diameter) placed at their grooves before being placed between the compression platens of an Instron 8872 servohydraulic testing machine (Instron Corp.). A compressive load was applied at 0.01 $m.s^{-1}$ until the cylinders diametrically split from groove to groove (Figure 2A). The polyethylene wrap served to prevent each specimen falling apart/getting damaged during splitting (Figure 3.1A). The specimens were then carefully unwrapped, separated apart, the groves very lightly brushed with a soft brushed and Perspex spacers 2.2 and 2.4 mm wide placed between their grooves to achieve defined crack widths of 0.2 and 0.4 mm. A two-part adhesive of, Plex 7742 and liquid Pleximon 801 (Evonik Röhm GmbH), was mixed and applied either side of the spacers. Once the glue was dry, the spacers were removed, and the remainder of the grooves (where the spacers had been) were glued.

Specimens were silicone-glued into sections of PVC pipe (60 mm long), the silicone was allowed to cure for 24 hours providing a watertight permeability cell, and a pin fitted at the base of the cell to prevent the specimen "shooting out" from the bottom during testing (Figure 3.1B).
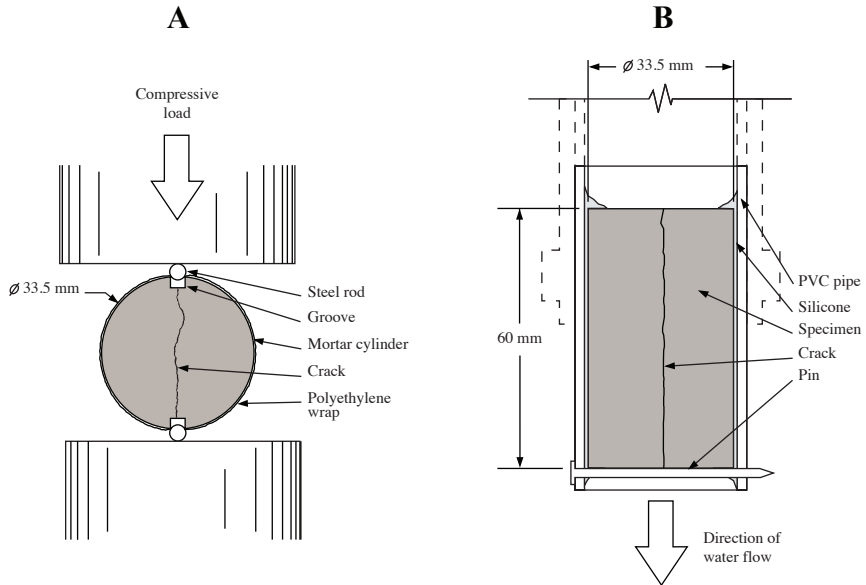
Figure 3.2 Schematic diagrams of: (A) the splitting tension set up used to fracture the cylinders diametrically; and (B) the permeability cell.

3.2.3 Crack evaluation

Cracks at the specimen ends were imaged with a stereomicroscope (Leica MZ6). Crack boundaries were defined by eye, their area measured in Photoshop (Adobe Systems) and the average width calculated.

3.2.4 Permeability setup

Permeability cells from series 1 were first assessed for their permeability. Figure 3.2 shows a schematic of the permeability test setup. Five permeability columns were set up to run in parallel. Each permeability cell was attached via a fitting at the bottom of each

permeability column. Artificial seawater was prepared and poured into reservoirs at the top of each column. The artificial seawater was produced from technical grade chemicals (Sigma-Aldrich), the composition of which can be found in Table 2.2. This artificial seawater, which is to be referred to as seawater for the remainder of the text, is based on the major constituents of natural seawater [41]. Taps in each reservoir were released initiating the permeability test. Water flowing through the cracks was individually collected in catchment buckets and the weight of the water determined at 5, 10 and 30 min. The water level of each column was manually maintained between 1 and 1.05 m giving an almost constant water head of 0.1 bar. Permeability cells of series 2 and 3 were submerged in seawater and vacuumed for 2 hours before submersion to remove any air bubbles trapped in their cracks, which could later hinder healing. Each series, consisting of ten cells, were transferred to plastic buckets containing 4 l of seawater (20 ± 2ºC). Lids were placed on the buckets to prevent evaporation. Cells of series 2 were submerged for 28 days and the cells of series 3 for 56 days. Seawater in the buckets was changed once a week for two weeks to mimic in situ conditions and prevent ion depletion. After submersion, the cells were attached with fittings to the bottom of the permeability columns and the specimens assessed for their permeability. Cells from series 2 and 3 were dried in a drier at 36º C for 28 days and again tested for their permeability to assess the effect of drying on healing.
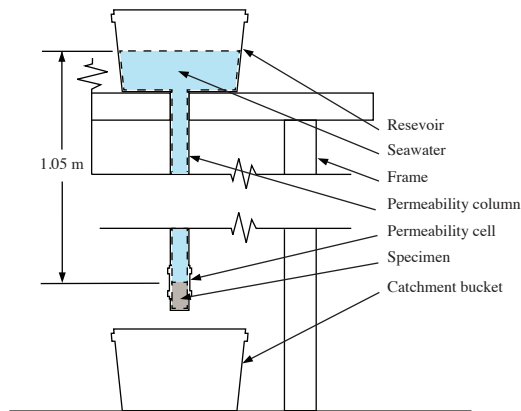
Figure 3.3 Schematic of the permeability setup.

3.2.5 Precipitate characterisation

Mortar specimens having the mean permeability of each series were selected for chemical analysis. These specimens were dried, and precipitates scraped from multiple locations in their cracks (< 5 mg). The precipitates were analysed through FTIR spectroscopy (Spectrum 100, Perkin-Elmer Inc.). Spectra were the result of 32 scans with a resolution of 2 cm^{-1} in the range of 4000-600 cm^{-1}. Polished sections were prepared for ESEM (Philips XL 30 ESEM, Philips) in BSE mode and elemental mapping through EDS (Philips EDAX, Philips). For the preparation of the polished sections refer to the previous chapter. In between preparation and analysis specimens were kept in a desiccator to avoid continued cement hydration. EDS image maps of calcium, magnesium and silica were merged through the apply image tool in Photoshop (Adobe Systems).

3.3 Results

3.3.1 Stereomicroscopy

Stereomicroscopy analysis of cracks intended to be 0.2 mm wide was on average 40 µm less than intended, and those intended to be 0.4 mm wide were on average 50 µm less than intended. Figure 3.3 shows randomly selected specimens from series 1 intended to have 0.2 mm cracks, having cracks: (A) 0.16 mm; (B) 0.17 mm; and (C) 0.16 mm. And crack widths from series 1 intended to have 0.4 mm cracks, having cracks: (D) 0.41 mm; (E) 0.38 mm; and (F) 0.37 mm wide.
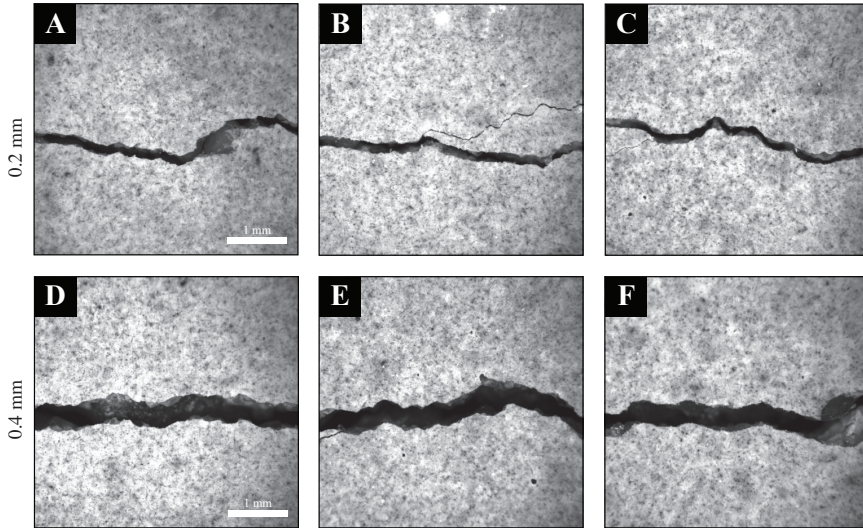
Figure 3.4. Cracks of randomly selected specimens from series 1 intended to have cracks 0.2 (A, B and C) and 0.4 (D, E and F) mm wide.

3.3.2 Water permeability

Figure 3.4 shows a box plot graph depicting: the initial permeability of specimens with cracks 0.2 and 0.4 mm wide; the permeability of specimens with cracks 0.2 and 0.4 mm after 28 and 56 days submersion in seawater; and the permeability of the same specimens after drying. The mean initial permeability for specimens with 0.2 mm wide cracks was 0.6 $cm^3.s^{-1}$ after 5, 10 and 30 min flow. Following 28 days submersion the mean permeability of the 0.2 mm wide cracks was 0 $cm^3.s^{-1}$ after 5, 10 and 30 min flow. The same specimens after drying maintained a mean permeability of 0 $cm^3.s^{-1}$. Specimens with 0.2 mm wide cracks submerged for 56 days also had a mean permeability of 0 $cm^3.s^{-1}$ before and after drying. The initial mean permeability values for specimens with 0.4 mm wide cracks were 3.5 after 5 min flow, and 3 $cm^3.s^{-1}$ after 10 and 30 min flow. The mean permeability of specimens with 0.4 mm wide cracks after 28 days submersion in seawater were 2.4 $cm^3.s^{-1}$ after 5 min flow (a reduction of 33%), and 1 $cm^3.s^{-1}$ after 10 and 30 min flow (a reduction of 66%). Following drying, specimens submerged for 28 days were less permeable, with mean permeability values of 0.6 after 5 min flow, 0.5 after 10 min flow and 0.4 $cm^3.s^{-1}$ after 30 min flow. Specimens following submersion for 56 days had mean permeability values of 1.6 $cm^3.s^{-1}$ after 5 min flow (a reduction of 54%), 1.5 $cm^3.s^{-1}$ after 10 min flow (a reduction of 50%), and 1.4 $cm^3.s^{-1}$ after 30 min flow (a reduction of 53%). Following drying, specimens submerged for 56 days, were also less permeable, with mean permeability values of 1.1 after 5 min flow, 0.9 after 10 min flow and 0.5 $cm^3.s^{-1}$ after 30 min flow.
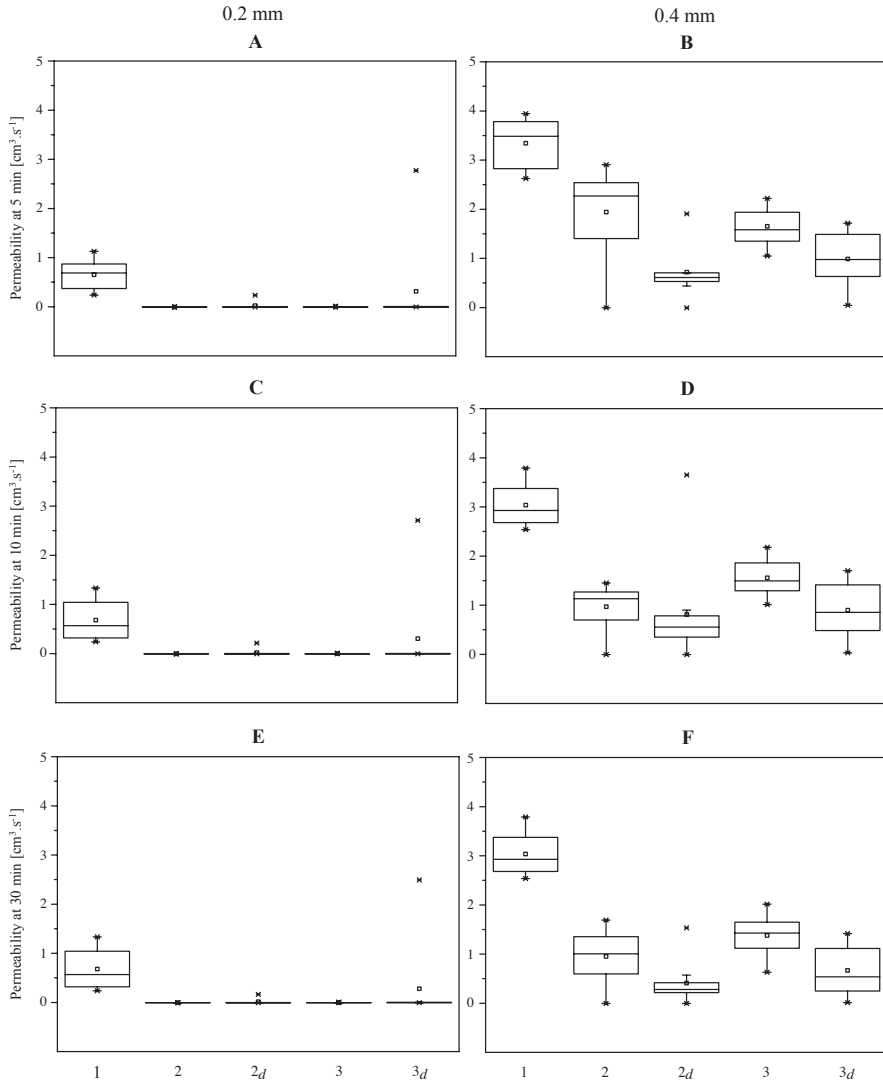
Figure 3.5 6 box plot graphs depicting the crack permeability data for series 1, 2 and 3. Graphs (A, C and E) show the permeability data for the 0.2 mm cracks after: (A) 5; (C) 10; and (E) 30 min flow. Graphs (B, D and F) show the permeability data for the 0.4 mm cracks after: (B) 5; (D) 10; and (F) 30 min flow. The first box plot (1) to the left of the two graph shows the initial permeability, second (2) is the permeability of cracked specimens after 28 days submersion, third (2_d) are the same specimens after drying, fourth (3) is the permeability of cracked specimens after 56 days submersion, and fourth (3_d) the same specimens after drying. Each box represents the permeability of 10 separate specimens. The square symbol of the boxes represents the mean permeability; the whiskers the minimum and maximum permeability values; and the top, middle and bottom lines the 75th, 50th and 25th percentiles ($x_{.75}$, $x_{.5}$ and $x_{.25}$), respectively.

3.3.3 Precipitate characterisation

Figure 3.5 shows both ESEM and EDS images of a selected specimen from each series and crack size. Figure 3.5 (A, B and C) shows ESEM images of a specimen with a 0.2 mm wide crack after 28 days submersion in seawater. The crack was plugged at one end with a dark grey (grey scale binary image) precipitate overlaid by a white precipitate (Figure 3.5A). Dark grey precipitates could be seen in relatively smaller amounts towards the centre of the crack (Figure 3.5B). White and dark grey precipitates could also be seen at the other crack mouth (Figure 3.5C). This white precipitate decreases in quantity from the crack mouth towards the centre of the specimen. Figure 3.5D shows an EDS elemental map corresponding to Figure 3.5A. This map shows the precipitates to be calcium- and magnesium-based, and the intrusion of magnesium ~100 μm into the mortar matrix. Figure 3.5(E, F and G) shows ESEM images of a specimen with a 0.2 mm wide crack after 56 days submersion in seawater. Precipitate formations after 56 days submersion were similar to those after 28 days submersion. ESEM analysis of specimens with 0.4 mm wide cracks submerged for 28 days (Figure 3.5(I, J and K)) and 56 days (Figure 3.5(M, N and O)) were not "plugged", but precipitates could be seen to reduce their crack mouth openings to ~150 μm (I and M). Dark grey precipitates could be seen along the crack walls towards the centre of both cracks (Figure 3.5(J and N)). Dark grey and white precipitates could also be seen at the other end of the crack (Figure 3.5(K and O)). Precipitate formations after 56 days submersion, like the 0.2 mm wide cracks, are much the same as those after 28 days submersion. EDS mapping again showed these precipitates to be calcium and magnesium based (Figure 3.5(L and P)). It is worth pointing that the crack openings facing upwards (as they sat in the water) is where the vast amount of the precipitates were formed. FTIR analysis of precipitates scraped from the cracks revealed bands at 3642 and 3696 cm^{-1} correspond to the O-H stretching vibration of calcium hydroxide and brucite respectively [43]. Calcite has characteristic absorption peaks: C-O asymmetric stretching vibration (v_3), C-O out of plane bending (v_2), and C-O planar bending vibration (v_4) centred at 1400, 872 and 712 cm^{-1}, respectively. While aragonite has, in addition, a characteristic peak stretching vibration (v_1) 1083 cm^{-1} and a bending vibration (v_4) centred at 700 and 712 cm^{-1} [44].
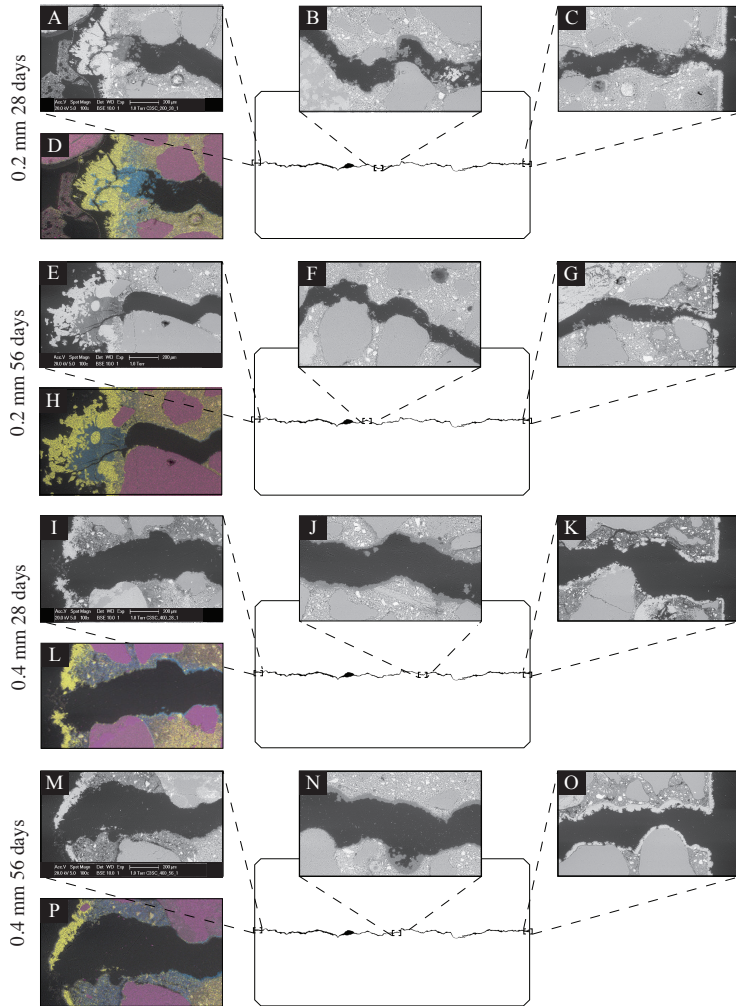
Figure 3.6 ESEM and EDS analysis of polished sections prepared after testing. (A-C) ESEM images of a specimen with 0.2 mm wide crack following 28 days submersion in seawater: (A) shows the crack mouth that was facing upwards when submerged; (B) an area towards the centre of the crack; and (C) the crack mouth at the other end. (D) Is the corresponding EDS image for (A). (E-G) Are ESEM images of a specimen with a 0.2 mm crack following 56 days submersion in seawater: (E) shows the crack mouth facing upwards; (F) an area towards the centre of the crack; and (G) the other crack mouth. (H) Is the EDS image for (E). (I-K) Are ESEM images of a specimen with a 0.4 mm crack following 28 days submersion in seawater: (I) shows the crack mouth that was facing upwards; (J) an area towards the centre; and (K) the other crack mouth. (L) Is the EDS image for (I). (M-O) Are ESEM images of a specimen with a 0.4 mm crack submerged for 56 days in seawater: (M) shows the crack mouth facing upwards; (N) an area towards the centre of the crack; and (O) the other crack mouth. (P) Is the EDS image for (M). Yellow of the EDS images represents calcium, blue magnesium and violet silicate.

3.4 Discussion

The autogenous healing capacity of cracked BFS cement mortar specimens submerged in seawater has been investigated. To do so, a simple and rapid permeability test was developed and implemented. Specimens with 0.2 mm wide cracks were not permeable, and specimens with 0.4 mm wide cracks were less permeable following 28 and 56 days submersion in seawater.

BFS cement is a blend of BFS and ordinary Portland cement. The slag's latent hydraulic properties are activated by calcium hydroxide, which is released from the cement when mixed with water. Cracks in marine concrete allow seawater (pH ≈ 7.5) to come into contact with cement paste of the crack walls (pH ≈ 13). Calcium hydroxide being soluble in seawater (K_{sp} = 4.1 x 10^{-6} [56]) is leached from the cement paste into the crack solution, whereby the hydroxide ions react with magnesium ions in the seawater forming brucite (K_{sp} = 1.2 x 10^{-11} [57])((Equations (3.1-3.3)) [2]:

$$MgSO_4 + Ca(OH)_2 \longrightarrow \underset{\text{Brucite}}{Mg(OH)_2} + \underset{\text{Gypsum}}{CaSO_4 \cdot 2H_2O} \tag{3.1}$$

$$MgSO_4 + [Ca(OH)_2 + \underset{\text{Calcium monosulfoaluminate hydrate}}{CaO \cdot Al_2O_3 \cdot CaSO_4 \cdot 18H_2O}] \longrightarrow$$
$$\underset{\text{Brucite}}{Mg(OH)_2} + \underset{\text{Ettringite}}{3CaO \cdot 3CaO \cdot Al_2O_3 \cdot 3CaSO_4 \cdot 32H_2O} \tag{3.2}$$

$$MgCl_2 + Ca(OH)_2 \longrightarrow \underset{\text{Brucite}}{Mg(OH)_2} + CaCl_2 \tag{3.3}$$
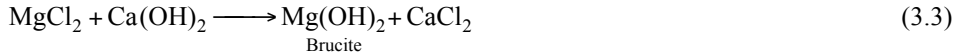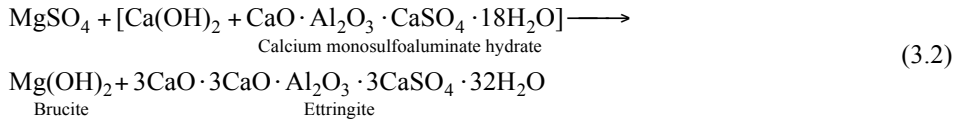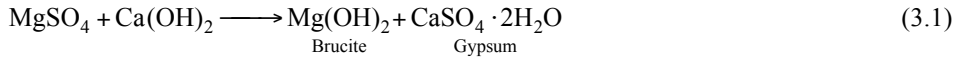
At the same time, alkalis from the cement paste can raise the pH (>8) of the crack water converting bicarbonates to carbonates. These carbonates can then react with calcium from the seawater and mortar matrix forming calcium carbonate (Equation (3.4)):

$$CO_2 + Ca(OH)_2 \longrightarrow \underset{\text{Calcium carbonate}}{CaCO_3} + H_2O \tag{3.4}$$
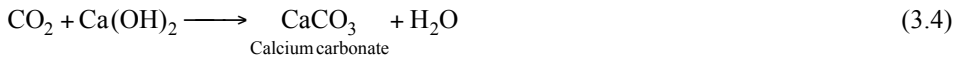
Aragonite (K_{sp} ≈ 6.65 × 10^{-7} [58]) is precipitated in favour of calcite (the more thermodynamically stable of the two calcium carbonate polymorphs) due to magnesium ions binding to nascent calcite crystals inhibiting growth [20].

Carbonate and magnesium ions are quickly depleted in the crack generating a concentration gradient between the crack and bulk water. This gradient causes the calcium and hydroxide ions from the matrix to diffuse along the crack until they meet an

opposing front of magnesium and carbonate ions from the bulk water. This front concentrating at the crack mouths facing upwards where most of the precipitates were formed (Figure 3.6). The crack healing capacity of a cementitious specimen depends on the width of the crack, thermodynamic considerations, the presence of water, and the amount of ions available in the crack. The concrete matrix supplies calcium and hydroxide ions and so the greater the crack surface, the more ions are available for healing. Indeed, relatively similar amounts of precipitate could be seen in the cracks of the specimens, with the 0.2 mm wide cracks and the 0.4 mm wide cracks (Figure 3.5). EDS images show the healing materials to be calcium-, and magnesium-, and not silica-based; healing was, therefore, not as a result of continued hydration. In accordance with Equations (3.1-3.3), brucite formation continues until calcium hydroxide is sufficiently depleted. Following this, magnesium sulphate is then able to decalcify the calcium silicate hydrate (the binding material of the cement) transforming it to magnesium silicate hydrate, a non-cementitious material (Equation (3.5)) [38]:
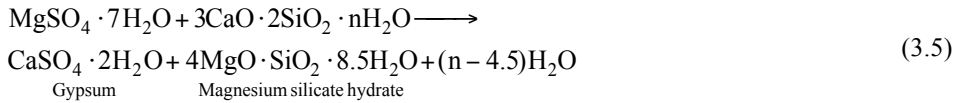
$$MgSO_4 \cdot 7H_2O + 3CaO \cdot 2SiO_2 \cdot nH_2O \longrightarrow$$
$$\underset{\text{Gypsum}}{CaSO_4 \cdot 2H_2O} + \underset{\text{Magnesium silicate hydrate}}{4MgO \cdot SiO_2 \cdot 8.5H_2O} + (n-4.5)H_2O \tag{3.5}$$

Conversion of calcium silicate hydrate to magnesium silicate hydrate is known to result in weakening of the cement matrix [19, 20]. We can see possible evidence of this conversion in Figure 3.5(L and P) with the incursion of magnesium into the cement paste. This incursion is visibly more pronounced for the specimens with 0.4 mm wide cracks, which is likely due to increased ion concentrations of magnesium afforded by the larger cracks, resulting in more leaching and replacement of calcium by magnesium ions (Equation (3.5)).
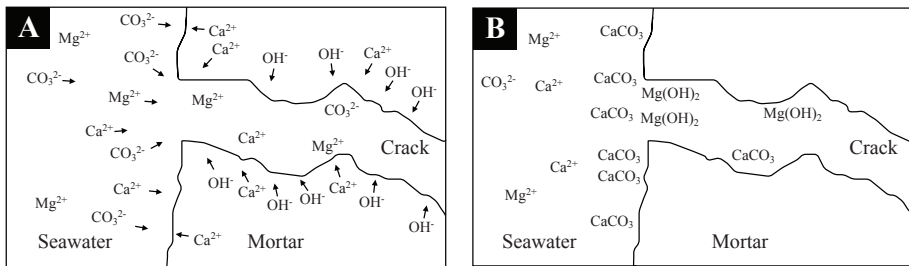

Figure 3.7 Crack schematic depicting a simplified precipitation model of: (A) the main ions, in the paste, crack and bulk water; and (B) the main precipitates, and location of these precipitates in the crack.

Specimens with 0.4 mm wide cracks display differences in the permeability values of specimens submerged for 28 days and those submerged for 56 days (Figure 3.4), with those specimens submerged for 28 days having lower permeabilities than those submerged for 56 days. Statistical analysis revealed this difference to be statistically significant ($P < 0.05$, one-way ANOVA); and may be due to more calcium hydroxide being leached from the cement paste over the longer period. Following drying the dry specimens had lower amounts of water flowing through the cracks (Figure 3.4). These reductions are likely due to capillary water sorption as a result of forces between the solution and the dry specimens [59], and maybe also, due to a reduction in the volume of those cracks due to the formation of precipitates resulting from the drying process.

Calibration of concrete cracks with well-anticipated positions and predictable widths is a difficult venture. Attempts have been made to develop setups, which fulfil these requirements but variability in results within and between studies has been high [51-54]. Stereomicroscopy analysis of cracks generated in this study showed cracks intended to be 0.2 mm wide to be on average 40 µm less than intended and those intended to be 0.4 mm wide to be on average 50 µm less than intended. Cracks were, however, delineated by eye and so include inherent subjectivity. Further, spacers used to define the crack widths were also machined by hand contributing to crack width variances. Using more accurate spacers should allow for more accurate crack widths, and hence more accurate permeability data, to be generated. There was a noticeable difference in flow rate after 5 and 10 min, with the data after 5 min demonstrating considerable scatter. Little difference was seen between crack flow data after 10 and 30 min, indicating the reaching of a steady flow. The reaching of this steady flow is far earlier than the many days reported in the literature [27, 29, 51, 52].

3.5 Conclusion

The functional autogenous healing capacity of seawater exposed cementitious specimens has been quantified through water permeability measurements. A permeability test has been described including a novel method for creating cracks with defined widths in cementitious specimens and a water permeability setup for assessing the water permeability of those cracked specimens. The test allowed multiple replicates to be easily tested, allowing reference crack permeability values to be generated for unhealed-specimens against which healed-specimens were quantified. 0.2 mm cracks fully healed after 28 days submersion in seawater. 0.4 mm cracks healed by 67 % after 28 days submersion and 52 to 50 % after 56 days submersion. This difference between the specimens submerged for 28 and those submerged for 56 days may be due to more calcium hydroxide being leached from the cement paste over the longer period.

Precipitation of aragonite and brucite in the cracks was principally responsible for healing. The width of a crack, thermodynamic considerations and the amount of ions available in the crack determine whether sufficient autogenous healing can be expected to heal a crack.

4

An improved test for generating crack permeability data for cementitious materials

Simplicity is a prerequisite for reliability.

— Edsger Dijkstra

Following on from the previous chapter, a modified test is presented consisting of a cracking method and permeability setup for generating crack permeability data for cementitious materials. Both the unmodified and modified methodologies are tested and compared to gauge for any improvement. Cracks are generated in mortar specimens by both methodologies, the accuracy of the cracks is analysed through stereomicroscopy and computer tomography (CT), and the water flow through those cracks determined. Reduction factors and crack flow models were generated and the reliability of those predictions assessed. Both tests, whose cracks were analysed through stereomicroscopy, produced reliable crack permeability predictions. The modified methodology produced more accurate cracks (within 20 μm of the desired crack widths) than the unmodified methodology and was 30% quicker (10 hours for twenty-one specimens) at generating the crack flow data. Further, crack analysis in the current study through stereomicroscopy was far quicker than through CT. A large number of specimen replicates (≥ 7) are required to generate reliable crack permeability data, and hence for quantifying the crack healing capacity of cementitious materials through their functional water tightness. The modified test can be of great use for generating rapid, accurate and reliable crack permeability data for cementitious materials.

4.1 Introduction

Cracks can allow the ingress of aggressive water-borne agents, having consequences for concrete performance and safety. Water permeability measurements have long been used for assessing the durability [51-54, 60], and more recently for quantifying the healing capacity of cementitious materials [13, 27, 29, 50, 61, 62]. The permeability data presented in these studies, of great value, demonstrate considerable variability, making it difficult to compare data within and between studies. Thus, a permeability test for generating rapid, accurate and reliable crack permeability data would be of great value for studying the healing capacity, and durability, of cementitious materials.

　　Reliable crack permeability data presupposes the generation of cracks with defined geometries. Given the heterogeneous nature of cementitious materials, such geometries are difficult to create in the laboratory. A common method for producing cracks in cementitious specimens is the bending method [13, 63, 64]. Bending cracks are generally generated in reinforced prismatic specimens through three-point or four-point bending. A load is applied to the specimens until bending cracks appear. Though realistic, such cracks have been shown to relax after loading making their final width difficult to control [64]. Another common method for producing cracks in cementitious specimens is the tensile splitting technique [29, 51-54, 60, 61]. Tensile cracks can be generated in cylindrical specimens through diametrical loading. Linear variable displacement transducers (LVDTs) can be fitted to specimens in conjunction with a feedback-controlled machine to control the width of a tensile crack [51-54, 60, 61]. Cracks generated using this technique, like the bending method, have been shown to relax, following unloading, making their final width difficult to control [51-54, 61]. Crack branching also makes it difficult to produce single cracks of defined widths with this method [51, 54]. Further, generating cracks with widths > 0.5 mm wide can result in the specimens becoming too fragile for permeability testing [51, 60]. Reinforcement can be added to the specimens to prevent this "fragility" [54, 65], however, reinforcement has been shown to effect the resultant crack permeability data [54]. Moreover, crack permeability studies quite often have demanding setups and long testing periods. For example, the feedback-controlled tensile splitting method requires a testing machine, computer, LVDTs, etc., making it demanding and expensive to set up [51-54, 60, 61]. All of these setups seem to use glues and/or rubber coatings to seal specimens for testing [27, 29, 51-53, 60, 62]. Such glues and coatings can be time-consuming to apply and may require many hours to dry, while their poor application if unnoticed could result in misleading results. Further, crack permeability studies tend to wait for a steady state flow to be achieved, that is, for the crack inflow to equal the outflow. This means that testing periods can last 90-100 [52, 53, 61] days. Such demanding permeability setups and long testing periods have likely restricted the amount of replicates tested,

exacerbating any variability in the crack permeability data.

Chapter 3 introduced a permeability test for generating crack permeability data for cementitious specimens. The test consisted of a novel method for creating defined crack widths in cementitious specimens and a simple and rapid permeability setup. Mortar cylinders were cast having two diametrically opposite grooves running down their sides. The specimens were split from groove to groove and spacers fitted to create defined parallel crack width geometries. The ease of the test meant that multiple replicates could be easily tested giving statistical power to the resultant crack permeability data. The ability of the cracking method to create cracks with defined widths, coupled with the testing of multiple replicates, meant that reference permeability values for cracked specimens could be generated against which healed cracked specimens could be quantified. Following on from this work it was clear that a number of modifications could be made to improve the speed, accuracy and reliability of the test. The current chapter presents a modified test for generating crack permeability data for cementitious specimens. To gauge for any improvement as a result of the modifications both the unmodified and modified tests are tested and compared.

4.2 Experimental program

Table 4.1 highlights the main differences between the unmodified and the modified permeability tests. In the current study, both tests were tested and compared. Cracks intended to be 0.2, 0.4 and 0.6 mm wide were generated in mortar specimens by both tests. CT and stereomicroscopy were used to assess width of the cracks and water flow to determine their permeability. Based on this information crack flow models were generated and the reliability of those predictions determined.

Table 4.1 Modifications made between the unmodified and modified permeability test.

| | Permeability test | |
Aspect	Unmodified	Modified
Cracking	Instron machine	Vise
Cracked specimens	Separated apart	Kept together
Crack width spacers	Hand machined Perspex	Metal gauges
Permeability cell	Silicone sealant	O-rings and retainer

4.2.1 Specimen preparation

4.2.1.1 Specimen preparation for the unmodified test

Mortar cylinders for the unmodified test were produced/prepared as those in Chapter 3. Cracks were generated in the specimens 0.2, 0.4 and 0.6 mm wide. Images of the cracks were taken at the specimens' ends with a Leica MZ6 (Leica) equipped with LAS v.40 software, with a resolution of 2.2 (1000/447) µm. Crack boundaries were defined by eye, the crack area measured in Photoshop (Adobe Systems), and the average crack width calculated for each specimen. The first two specimens of each series were also subject to crack volume analysis through CT (phoenix|x-ray, GE) with a resolution of 16 µm. Each 360º scan consisting of 1,440 tomographic images taken over ~90 min. Scans were imported and then opened in VG Studio Max 2.0 (Volume Graphics GmbH) to calculate the crack width. A virtual cylinder was drawn within the software program to encompass the crack. The crack volume within the cylinder was isolated by eye with the volume analyser tool and the crack volume known. The width of the crack could then be determined by dividing the crack volume by the height and diameter of the virtual cylinder. Here we define crack width accuracy as the difference between the mean measured and the desired crack width (i.e. measurement A is more accurate than measurement B if the value of A is closer to the desired crack width than B).

4.2.1.2 Specimen preparation for the modified test

A few key differences exist between the modified and unmodified test when preparing the specimens. A vise was used to apply a load to the steel rods and as opposed to the Instron machine. When splitting the specimens, great care was taken to keep the two halves together to prevent material loss. Metal gauges were used to define the crack widths rather than hand machined Perspex spacers.

4.2.2 Permeability setup

4.2.2.1 Permeability setup of the unmodified test

The permeability setup for the unmodified test was the same as that in Chapter 3. This time the test was only run for ten minutes. The duration of water flow was also based on Chapter 3, and how the crack water flow reached a relatively steady flow by ten minutes.

4.2.2.2 Permeability setup of the modified test

The difference between the permeability setups of the unmodified and modified methodologies was the permeability cell used. Machined out polyethylene, the permeability cell of the modified test (60 mm long with internal diameter of 35mm) was designed to house a specimen, and two rubber O-rings located at the upper and lower face of the specimen, such that when a retaining ring was tightened the cell was made watertight (Figure 4.1B).
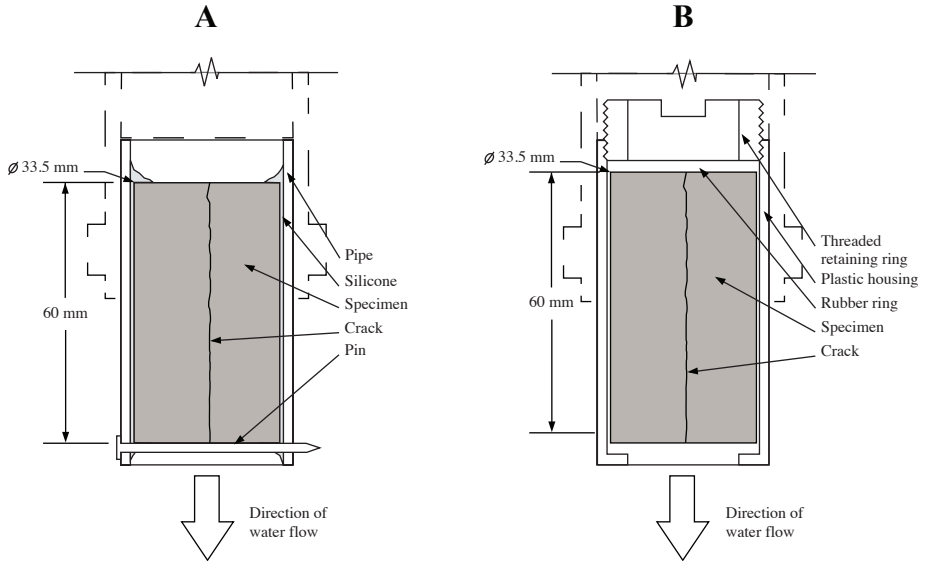
Figure 4.1 Schematic showing the permeability cells of: (A) the unmodified test; and (B) the modified test.

4.2.3. Crack flow model

A common model used to estimate crack water flow is one derived from the laminar flow of incompressible Newtonian fluids between smooth parallel-plates. The model often referred to as Poiseuille's law, can be computed using the following formula (Equation (4.1)) [67]:

$$q_o = \frac{\Delta p \cdot l \cdot w^3}{12 \cdot \eta \cdot d} \tag{4.1}$$

where

q_o = Water flow between smooth parallel plates [$m^3.s^{-1}$]
Δp = Differential water pressure between crack inlet and outlet [$N.m^{-2}$]
l = Crack length (distance across the face of the specimen) [m]
w = Crack width (distance between the crack faces) [m]
d = Crack depth (distance between the faces of the specimen)[m] and
η = Absolute viscosity [$Ns.m^{-2}$]

Smooth parallel crack plates, however, do not occur in cementitious materials. Factors such as roughness and tortuosity reduce the crack water flow, making it less than estimated according to Equation (4.1). To account for roughness and tortuosity Equation (4.1) can be modified to include an empirically derived reduction factor (Equation (4.2)) [29]:

$$q_r = \frac{\xi \cdot \Delta p \cdot l \cdot w^3}{12 \cdot \eta \cdot d} \qquad (4.2)$$

where

q_r = Crack water flow [$m^3.s^{-1}$]
ξ = Reduction factor.

The reduction factor can be estimated if the other parameters are known. In this study, we estimate the reduction factors for the four cases: the unmodified and modified methodologies whose crack widths were measured through CT and stereomicroscopy. The quality of the models will be indicated by: the closeness of the R^2 value to 1; the closeness of the observed values to the predicted value; and the narrowness of the confidence interval (CI) and prediction interval (PI), of the predicted values.

4.3 Results

4.3.1 Crack width analysis

Table 4.4 shows CT and stereomicroscopic crack width analysis for cracks produced by the unmodified and modified method. CT and stereomicroscopoc analysis showed that analysis of the cracks produced by the modified test were within 20 μm of the desired crack width, while those produced by the unmodified test were within 55 μm of the

desired crack width; and that the standard deviation, and hence repeatability, of the crack widths analysed through stereomicroscopy were somewhat similar for both methods.

Table 4.4 Crack width analysis through computer tomography and stereomicroscopy of cracks generated by the unmodified and modified methodologies.

Analysis		Crack widths					
		Unmodified			Modified		
		Desired crack width [μm]			Desired crack width [μm]		
		200	400	600	200	400	600
Computer tomography	$\bar{x}$ [μm]	232	399	495	233	382	601
	D [μm]	32	1	105	33	18	1
Stereomicroscopy	$\bar{x}$ [μm]	160	335	511	222	397	564
	D [μm]	40	65	89	22	3	36
	S [μm]	10	42	25	51	50	35

$\bar{x}$ = Mean of the measured values
D = Difference between mean measured and the desired crack width
S = Estimated standard deviation

4.3.2 Permeability data

Reduction factors were computed for the two methodologies and crack width analysis techniques. The average reduction factor for the unmodified test whose cracks were analysed through CT was 0.15 ± 0.03; for the modified test whose cracks were analysed through CT it was 0.12 ± 0.02; for the unmodified test whose cracks were analysed through stereomicroscopy it was 0.17 ± 0.02; and for the modified test whose cracks were analysed through stereomicroscopy it was 0.15 ± 0.01. Permeability data generated by the two methodologies and crack width analysis techniques were well described by the modified model ($r^2 = 0.97\text{-}0.98$). The cracks produced by the unmodified and modified tests whose cracks were analysed through stereomicroscopy produced similarly narrow CIs and PIs (Figure 4.2(C and D)), and narrower CIs and PIs than those analysed through CT (Figure 4.2(A and B)). The modified test whose cracks were analysed through CT produced narrower CIs and PIs than the unmodified test.
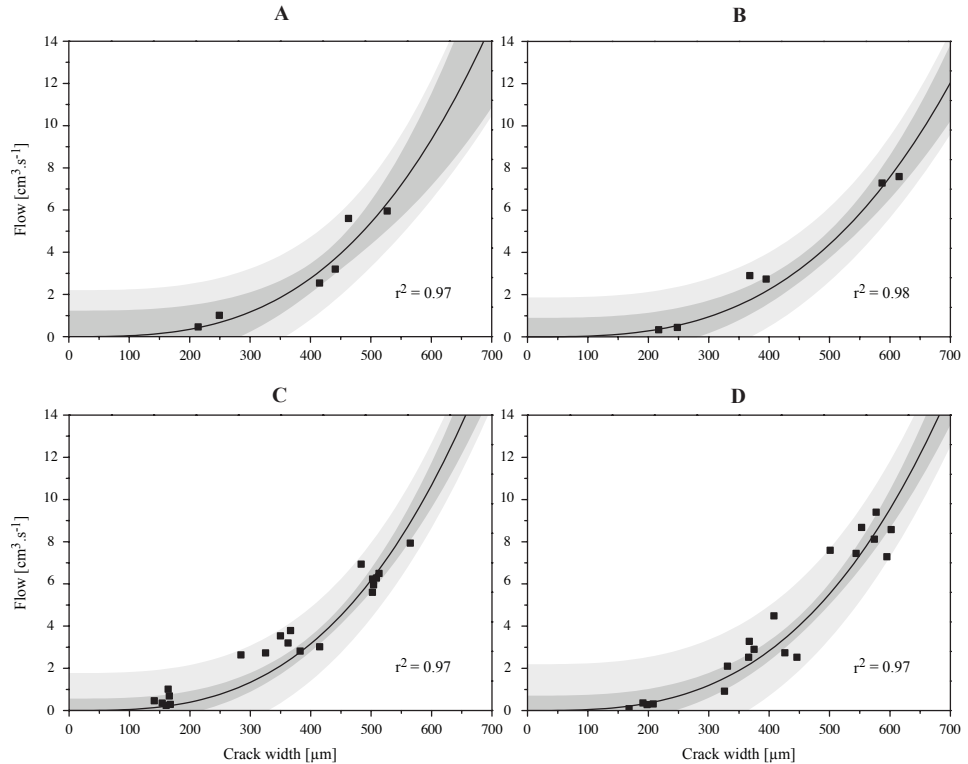
Figure 4.2 Observed values plotted against predicted values for: (A) the unmodified test whose cracks were analysed through CT; (B) the modified test whose cracks were analysed through CT; (C) the unmodified test whose cracks were analysed through stereomicroscopy; and (D) the modified test whose cracks were analysed through stereomicroscopy. Symbols represent the observed values; lines represent the predicted values; the darker shaded areas flanking the lines represent the 95% confidence intervals, and the lighter shaded areas flanking those the 95% prediction intervals. The R-squared (r^2) values for the models are also indicated.

4.3.3 Time taken to produce the permeability data

Table 4.5 gives a breakdown of the main tasks and times taken for both tests to produce the crack flow data for 21 specimens. The modified test was quicker than the unmodified test taking just 8 hours to generate crack flow data for 21 specimens versus 12 hours for the unmodified test. Further, the permeability cell of the unmodified test was quite awkward to prepare, in as far as the silicone used to seal the specimens in the cell took 24 hours to dry and ran the risk of finding its way into the cracks; while the cells of the modified setup could be prepared promptly and easily. Crack analysis through stereomicroscopy was also much quicker than through CT, with stereomicroscopy

analysis taking just 6 hours to image the surface cracks of 21 specimens, and CT taking 32 hours to scan, reconstruct and analyse the cracks of 6 specimens.

Table 4.5 Main tasks and times taken to produce crack permeability data for forty-two specimens.

	Time [h]	
Task	**Unmodified**	**Modified**
Casting	1.5	1.5
Wrapping in polyethylene film	0.75	0.75
Setup for tensile splitting	0.5	0
Splitting	3	1.5
Fitting and gluing of spacers	3.5	3.5
Sealing the permeability cells	3.5	1.5
Permeability test	0.75	0.75
Weighing of the water	0.5	0.5
Total	**14**	**10**

4.4 Discussion

Following on from Chapter 3 a modified test for generating rapid, accurate and reliable crack permeability data for cementitious specimens has been presented. To gauge for any improvement as a result of the modifications both tests were compared in the current study. Cracks of defined widths were generated in mortar specimens by both tests and the flow of water through those cracks determined. Crack flow models were generated and the accuracy and the reliability of those predictions assessed. The accuracy of the four models was very high (r^2 = 0.97-0.98). The reliability of a model is indicated by the narrowness of its CI and PI. The crack flow models generated by the unmodified and modified tests whose cracks were analysed through stereomicroscopy (Figure 4.2(C and D)) produced predicted values with greater reliability than those cracks analysed through CT (Figure 4.2(A and B)). This reliability is attributable to the greater number of replicates that could be easily analysed through stereomicroscopy versus those analysed through CT, and how more sample replicates leads to more reliable estimates [68]. When looking at the predicted values generated by the unmodified and modified tests whose cracks were analysed through CT, we can see that the modified test produced a more reliable predicted value than the unmodified test (Figure 4.2(A and B)). This difference stemming from differences between the crack geometries generated by the two tests, and how the modified test was able to limit factors such as material loss, poor sealing and crack obstruction (e.g., silicone getting in the cracks). The two tests whose cracks were analysed through stereomicroscopy

produced similarly reliable predicted values, demonstrating the value of testing relatively larger sample sets (Figure 4.2(C and D)). Even though the reliability of the predicted values generated by the unmodified and modified methodologies whose cracks were analysed through stereomicroscopy was similar (Figure 4.2(D and E)), cracks generated by the modified test were more accurate than those generated by the unmodified test (Table 4.4). This increased accuracy resulting from the metal gauges being more accurate than the Perspex spaces.

Crack permeability studies often have demanding setups and long testing periods [27, 29, 51-54, 60-62]. Both the unmodified and modified methodologies were relatively quick at producing crack permeability data. The modified test, however, was 30% quicker at producing the permeability data for 21 specimens (Table 4.5). This improved speed coming as a result of not having to use the Instron machine to split the specimens and the ease with which the modified permeability cell could be used. Analysis of the cracks through stereomicroscopy was quicker than through CT, and using crack permeability data generated after 10 minutes water flow is far quicker than the many hours sighted in the literature [52, 53, 61].

4.5 Conclusion

The current chapter has presented a modified permeability test for generating rapid, accurate and reliable crack permeability data for cementitious materials. Both tests were tested and compared to gauge for any improvement. Cracks were generated in mortar specimens by both tests, the accuracy of the cracks was assessed through stereomicroscopy and computer tomography (CT), and the flow of water through the cracks determined. All of the models had high predictive accuracies (r^2 = 0.97-0.98), while the reliability of these predictions was higher for the models generated with the crack width analysis through stereomicroscopy. The modified test produced more accurate cracks than the unmodified test, with the average crack width of the modified test being < 20 μm of the desired crack width, while the cracks of the unmodified test were > 55 μm from the desired crack width. The modified test was 30% quicker at producing the crack flow data than the unmodified test. Further, crack width analysis through stereomicroscopy was far quicker than through CT in the current study. The simplicity/speed of the permeability test means that relatively large numbers of replicates can be easily tested, which is important for generating reliable crack permeability data for cementitious materials. The modified test can, therefore, be of great use for studying the durability and crack healing capacity, of cementitious materials.

5

A cost-effective bacteria-based healing agent for the development of self-healing marine concrete

Any being, if it vary however slightly in any manner profitable to itself, under the complex and sometimes varying conditions of life, will have a better chance of surviving, and thus be naturally selected.

<div align="right">— Charles Darwin, Origin of the Species</div>

The current chapter presents a bacterial isolate and organic mineral precursor compound, as part of a cost-effective agent, for realising self-healing concrete in low-temperature marine environments. Organic compounds were screened based on their cost and concrete compatibility, and bacterial isolates based on their ability to metabolise concrete compatible organic compounds and function in a marine concrete crack. Magnesium acetate was the cheapest organic compound screened and when incorporated (1% of cement weight) in mortar specimens, had one of the lowest impacts on strength (18% lower than the reference specimens). Bacterial isolate designated psychrophile (PSY) 5 demonstrated very good germination/growth at 3% salinity, a pH of 9.2 and 8ºC on sodium lactate; and good growth at room temperature on magnesium acetate. PSY 5 also demonstrated good spore production capability when grown on monosodium glutamate at room temperature. Phylogenetic analysis revealed PSY 5 to be closely related to *Bacillus halmapalus*. Isolation of PSY 5 and identification of magnesium acetate represent significant strides on the way to realising bacteria-based self-healing concrete for application in low-temperature marine environments.

5.1 Introduction

Bacteria-based self-healing concrete is an innovative self-healing materials approach whereby bacteria embedded in concrete can induce a calcium carbonate crack healing mineral precipitate [4-14]. Bacteria do not do this "on purpose", rather, they induce calcium carbonate precipitation as a result of their metabolic activity [69]. Two principle microbial metabolic pathways have been employed for the development of bacteria-based self-healing concrete, namely, aerobic respiration of organic compounds, and urea hydrolysis. Bacterial aerobic respiration of organic compounds results in the production of energy, carbon dioxide and water. Aerobic respiration is the most efficient metabolic pathway for extracting energy from an organic carbon source. Carbon dioxide in alkaline environments (pH > 8) is chemically converted to carbonate, which in the presence of calcium precipitates as calcium carbonate. Calcium carbonate precipitation as a result of bacterial aerobic respiration has been shown to visually heal [6, 7], and seal [13], the cracks of cementitious materials. Bacterial urea hydrolysis results in the production of energy, carbon dioxide and ammonia. Ammonia production causes a pH rise, chemically converting carbon dioxide to carbonate, which in the presence of calcium ions precipitates as calcium carbonate. Calcium carbonate precipitation as a result of urea hydrolysis has also been shown to visually heal [8, 9] and seal [10], the cracks of cementitious material. Ammonia, however, as a by-product of urea hydrolysis carries certain environmental risks [70], and is known to corrode concrete steel reinforcement [71]. Oxygen concentrations can be limited in marine systems [72], and so bacteria fit for the self-healing marine concrete applications should also be able to function under low oxygen conditions. Some bacteria have evolved respiratory systems, which allow them to use oxygen-containing ions, such as nitrate (NO_3^-), rather than free oxygen. Nitrate respiration of organic compounds results in the production of energy, carbon dioxide and either nitrogen gas (N_2) or ammonium (NH_4^+), depending on the metabolic pathway (denitrification or dissimilatory reduction of nitrate to ammonium, respectively). In a recent study Erşan *et al.*, used nitrate respiring bacteria for the development of self-healing concrete [12]. Nitrate respiration is an interesting approach, as the nitrite produced as a result of nitrate reduction is known to inhibit steel reinforcement corrosion [73]. Further, these organisms, with the addition of nitrate to a healing agent, would allow for bacteria-based self-healing under anoxic conditions. The addition of nitrate to a healing agent will, however, increase both the agent's cost and volume. Increasing the cost of the agent is undesirable for obvious reasons, and so too is increasing its volume, as this increase would act as a kind of porosity within the self-healing cementitious material, lowering its strength. Many bacteria are facultative anaerobes, which means that they can respire on oxygen when present, but if it is not, they can switch to an alternative molecule such as nitrate. These facultative anaerobes

may offer the best option for realising bacteria-based self-healing concrete in the marine environment, as these organisms would be able to respire with oxygen when available and switch to nitrate under anoxic condition. This ability to switch would improve the healing efficiency (amount of healing.kg^{-1} of mineral precursor compound), and allow for healing under anoxic conditions.

Concrete is a highly desiccated alkaline environment, and so not all bacteria are suitable for concrete incorporation. There are, however, natural analogues where bacteria thrive. Various species of extremophilic bacteria have been found deep below the earth's surface [74]; and in highly desiccated [75, 76], and alkaline [77, 78], environments. A survival strategy employed by bacteria to deal with these extreme environments is to form spores. Spores are specific, robust bacterial cells, somewhat homologous to the seed of a plant. These robust cells are well suited for concrete incorporation as they are able to withstand mechanical and chemical stresses [79], and can remain viable for 200-300 years in a dry state [37]. Bacterial spores have been shown to survive concrete inclusion [4], and when incorporated in various protective carriers have been shown to improve the crack healing capacity of cementitious materials [5-11, 13]. Despite much of the world's concrete infrastructure being located in low-temperature (annual average temperature < 10ºC, and summer temperature generally < 20ºC) marine environments [3], bacteria-based self-healing concrete has only been shown to work under mild (~21ºC) freshwater conditions [4-13]. If bacteria-based self-healing concrete is to be realised under low-temperature marine conditions, then the bacteria-based healing agent and more specifically the bacteria making up part of this healing agents will need to function under the same conditions.

The current chapter presents a bacterial isolate and organic mineral precursor compound, as part of a cost-effective healing agent, for the development of self-healing marine concrete. Selection of the organic mineral precursor compound is based on its cost and concrete compatibility. Selection of the bacterial isolate is based on its ability to function (i.e. germinate and grow) under low-temperature (8ºC) marine concrete conditions, and to metabolise a cost-effective concrete compatible organic mineral precursor compound. This is the first study to present a bacteria-based healing agent specifically designed for low-temperature marine concrete applications.

5.2 Experimental program

The experimental program consists of four phases. In phase 1 a number of organic compounds — as potential calcium carbonate mineral precursors — are screened based on their cost and mortar compatibility. In phase 2 an enrichment and isolation procedure is undertaken on a microbial mat sample to obtain bacteria fit for self-healing concrete

applications in low-temperature marine environments. In phase 3 the bacterial isolates are characterised regarding their aerobic growth on concrete compatible organic compounds, at different temperatures, and under anaerobic conditions. In phase 4, selected isolates are further characterised concerning their ability to grow at different alkalinities, to produce spores, and their phylogeny.

5.2.1 Organic mineral precursor compounds

Table 5.1 shows potential organic mineral precursor compounds, and their cost, for inclusion as part of a bacteria-based healing agent. The cost for each compound is based on the lowest price quoted per ton from Alibaba.com [80].

Table 5.1 Selected organic compounds, including their cost.

Organic compound	Cost [€.kg^{-1}]
(+)-Magnesium L-ascorbate	1
Carrageenan	2
Chitosan	2
D-(+)-Xylose	1
D-sorbitol	1
Glycerol	1
Gum arabic	1
L-Rhamnose	0.6
Magnesium D-gluconate	0.6
Magnesium L-lactate	1
Magnesium acetate	0.1
Maltodextrin	0.3
Pectin	1
Saccharin sodium	1

5.2.2 Mortar sample preparation

Organics released from a bacteria-based healing agent during mixing could have an adverse effect on concrete properties. Two specimen types were prepared to test this effect: (1) plain mortar specimens, and (2) mortar specimens containing selected organic compounds (Table 5.1). Based on the worst-case scenario compounds were added at 1% of the cement weight to mortar during mixing. The mix-design is shown in Table 5.2. Mortar cubes (40 × 40 × 40 mm) were cast and carefully removed from their moulds after 2 days. Cubes were sealed in polyethylene plastic bags and stored at room temperature until testing. Specimens were tested for their compressive strength 2, 7, 28,

56 and 168 days after casting, at a rate of 1 MPa.sec^{-1}, with a compression test machine and Cyber-Plus evolution control unit. All of the organic compounds used were purchased from Sigma-Aldrich.

Table 5.2 Mix-design for the mortar cubes.

Constituents	Amount [g.l^{-1}]
Cement (CEM III/B 42.5 N LH, ENCI)	494
Water	247
Sand fraction [mm]:	
2-1	608
0.5-1	426
0.25-0.5	167
0.125-0.25	319
Organic mineral precursor	5

5.2.3 Enrichment and isolation

An enrichment and isolation procedure was undertaken on a microbial mat sample from La Salada de Chiprana (a hyper-saline inland lake in the North of Spain), in order to obtain bacteria fit for realising self-healing concrete in low-temperature marine environments. The lake experiences hot summers and cold, dry winters, with a lake-water chemistry dominated by sodium, magnesium, sulphate and chloride ions, and salinities ranging from 35 to 80 g.l^{-1} [81]. Such a microbial mat sample may contain billions of bacteria with high species and metabolic diversity. One gram of the sample was enriched in an alkaline (pH 9.6) saline medium (Table 5.3), with sodium lactate as the organic carbon source; and incubated under low-temperature (10ºC) aerobic conditions. After three weeks the enrichment culture was pasteurised at 80ºC for 30 min to kill the vegetative cells, and leave the viable spores. The enrichment culture was then streaked onto agar plates with the same composition as the enrichment media. Plates were incubated at 10ºC until colony formation. Eight bacterial colonies featuring different colours and morphologies were picked. The eight isolates were designated psychrophile (PSY) 1-8 and streaked onto new plates. Isolated colonies were picked from these plates and stock cultures created.

Table 5.3 Selective media composition.

Component	Amount [mM]
KNO_3	3.75
NH_4Cl	3.75
KH_4PO_4	0.153
$CaCl_2.2H_2O$	1.53
KCl	2.68
$MgCl_2.6H_2O$	1
Carbonate buffer:	
$NaHCO_3$	100
Na_2CO_3	100
Organic carbon source	10

Component	Amount [g.l^{-1}]
Yeast extract	1
NaCl	30
Trace element solution:	
Na_2-EDTA	3
$FeSO_4.7H_2O$	1.1
H_3BO_3	0.3
$CoCl_2.6H_2O$	0.19
$MnCl_2.4H_2O$	0.05
$ZnCl_2$	0.042
$NiCl_2.6H_2O$	0.024
$Na_2MoO_4.2H_2O$	0.018
$CuCl_2.2H_2O$	0.002

5.2.4 First phase of characterisation

Batch tests were conducted to assess the ability of the isolates to grow aerobically on concrete compatible organic compounds at room temperature (21ºC), and at different temperatures using sodium lactate as an organic carbon source. The batch tests were conducted in glass bottles to contain 30 ml of the selective media with a particular organic carbon source (Table 5.3), which were then inoculated with 30 µl of the freshly grown isolates. Bacterial growth was monitored over time through optical density (OD) at 600 nm. The morphology of the isolates was observed through light microscopy using a Zeiss Axioplan 2 microscope. The ability of the isolates to reduce nitrate in the selective media was also tested under anoxic conditions at room temperature. Glass bottles were again prepared containing 30 ml of the selective media with sodium lactate as the carbon source; this time, however, the bottles were sealed with butyl rubber stoppers and the headspace of the bottles were made anoxic through repeated evacuation and flushing with argon gas. The culture media in the bottles were tested after 7 days for nitrite with colourimetric strips (Merck).

5.2.5 Second phase of characterisation

PSY 4, 5 and 6 were selected for further characterisation based on their performance during the first phase of characterisation. The three isolates were tested for growth at different pH's using the selective media with sodium lactate as the organic carbon source. The pH of the media was adjusted by adjusting the bicarbonate to carbonate ratio of the carbonate buffer. PSY 4, 5 and 6 were also tested for their ability to grow on different organic carbon sources at room temperature, and at different temperatures using sodium lactate as an organic carbon source. Following 14 days of growth the cultures were pasteurised and the number of viable spores estimated based on the most probable number (MPN) dilution technique. To do so, the wells (8 × 12) of a sterile microtiter plate were filled with 180 µl of the selective medium with sodium lactate as the organic carbon source. The eight wells of the first row of the microtiter plate were inoculated with 20-µl of the pasteurised cultures and subsequently diluted to extinction in 10 consecutive 10-fold-dilution steps. The last two rows of the plate were left blank as controls to check for contamination. The plates were aseptically stored in polyethylene bags at 8ºC for two weeks.

5.2.6 Phylogenetic characterisation

The partial 16S rRNA gene sequences of PSY 4 and 5 were amplified through polymerase chain reaction (PCR) using bacterial primers 341f (5'-CCTACGGGAGGCAGCAG–3') and 907rM (5'-CCGTCAATTCMTTTGAGTTT'), developed by Muyzer *et al*., [82]. The PCR mixture contained 0.225 µl of each primer (50 µM), 15 µl of *Taq* 2X Master Mix (Qiagen), 13.95 µl of distilled water, and 0.6 µl of the pure cultures. The PCR reaction was performed using a thermal cycler (Biometra) with a program of: 95ºC for 5 min; followed by 35 cycles of 95ºC for 30 sec, 55ºC for 30 sec, 72ºC for 40 sec; and a final extinction at 72ºC for 10 min. The PCR products were loaded on an agarose gel stained with SYBR Safe DNA gel stain (Invitrogen, Thermo Fisher Scientific Inc.). Sequence products were sent for sequencing to BaseClear. Following sequencing, all sequences were checked with CodonCode Aligner v4.2.7 (CodonCode Corp.), and compared with sequences from the genebank of the National Center for Biotechnology Information (NCBI) database using the Basic Local Alignment Search Tool (BLASTn) [83]. A phylogenetic tree was constructed in ARB [84] using the maximum-likelihood algorithm (RAxML) [85].

5.3 Results

5.3.1 Effect of mineral precursor compounds on mortar strength

Figure 5.1 shows the strength development of mortar cubes over time. The 28-day compressive strength of cubes containing magnesium L-lactate was on average 9% lower than the plain mortar specimens. Cubes containing chitin, glycerol and gum Arabic were 12% lower, pectin and sodium saccharin were 16% lower, and magnesium acetate was 18% lower. Cubes containing D-Sorbitol, L-Rhamnose and carrageenan, were > 35% lower, and cubes containing (+)-magnesium L-ascorbate, D-(+)-xylose, maltodextrin and magnesium D-gluconate were > 90% lower than the plain mortar specimens.
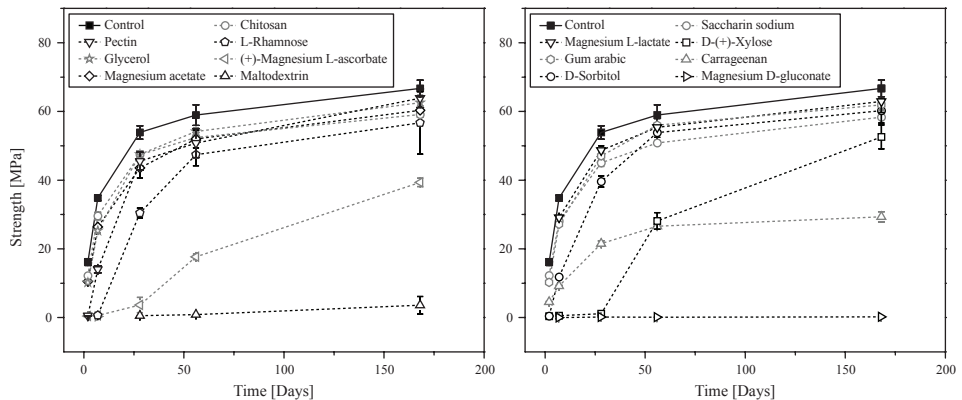
Figure 5.1 Graphs showing the compressive strength development of mortar cubes containing different organic compounds (Table 5.1). Data was split into two figures for greater clarity. Each data point represents five replicate specimens.

5.3.2 Phenotypical characterisation of isolates

Table 5.4 shows some phenotypic characteristics of PSY 1-8. Streaking of the enrichment culture onto agar plates resulted in two distinct rose and beige coloured colonies. Light microscopy revealed all of the isolates to be rod-shaped spore-formers. All of the isolates grew best in the selective media with glucose as the organic carbon source. PSY 3-6 demonstrated good growth with magnesium acetate and magnesium lactate as the organic carbon sources, PSY 1-6 demonstrated good growth on glutamate and PSY 5 and 6 on citrate. All of the isolates demonstrated very good growth at 8ºC. PSY 4 and 6 demonstrating good growth at 4ºC, and PSY 2, 3, 5 and 6 at 15ºC. Plus

symbols in the table are representative of OD, with one plus representing poor growth and an OD < 0.2; two pluses representing good growth and an OD $\geq 0.2 < 0.4$; three pluses representing very good growth and an OD ≥ 0.4. Nitrite was formed in the selective media inoculated with each of the isolates under anoxic conditions; indicating that the bacteria were able to reduce nitrate to nitrite.

Table 5.4 Phynotypical characteristics of the isolated strains.

| | | | | Aerobic growth | | | | | | | | | | | Nitrate reduction |
| | Colony colour | Cell morpholog | Spore former | Organic carbon source | | | | | Temperature [ºC] | | | | | |
Isolate				Acetate	Glucose	Lactate	Glutamate	Cytrate	4	8	15	21	37	
PSY 1	Beige	Rod	Yes	+	+++	+	++	+	++	+++	++	++	+	Yes
PSY 2	Beige	Rod	Yes	+	+++	+	++	+	++	+++	+++	++	+	Yes
PSY 3	Rose	Rod	Yes	++	+++	++	++	+	++	+++	+++	++	++	Yes
PSY 4	Rose	Rod	Yes	++	+++	++	++	+	+++	+++	++	++	++	Yes
PSY 5	Beige	Rod	Yes	++	+++	++	++	++	++	+++	+++	++	++	Yes
PSY 6	Beige	Rod	Yes	++	+++	++	++	++	+++	+++	+++	++	++	Yes
PSY 7	Beige	Rod	Yes	+	+++	+	+	+	++	+++	++	++	+	Yes
PSY 8	Beige	Rod	Yes	+	+++	+	+	+	++	+++	++	++	+	Yes

+ = Poor
++ = Good
+++ = Very good

5.3.3 Further characterisation of selected isolates

Table 5.5 shows further phenotypic characteristics of PSY 4, 5 and 6. PSY 4, 5 and 6 were selected for further characterisation based on their growth under low-temperature (8ºC) saline (30 g.l^{-1} sodium chloride) conditions, using sodium lactate as an organic carbon source, and at room temperature using magnesium acetate as an organic carbon source. PSY 4 and 6 demonstrated good growth and PSY 5 very good growth at a pH of 9.2, and the three demonstrated little to no growth at a pH of 9.7, in selective media with sodium lactate as the organic carbon source. Plus symbols in the table related to aerobic growth represent OD and have the same values as stated in Section 5.3.2. The three isolates grown at room temperature in selective media containing sodium glutamate as the organic carbon source demonstrated good spore production. Plus symbols related to spore production are representative of the amount of spores produced per litre, one plus representing poor spores production (i.e. $< 5 \times 10^5$ bacterial spores.l^{-1}); two pluses representing good spores production (i.e $\geq 5 \times 10^5 < 5 \times 10^8$ bacterial spores.l^{-1}); and three pluses representing very good spores production (i.e. $\geq 5 \times 10^8$ bacterial spores.l^{-1}).

Table 5.5 Further characteristics of PSY 4 and 5.

| Isolate | Aerobic growth | | | | | | | | Sporulation | | | | | | |
| | pH | | | | | Organic carbon source | | | | Temperature [°C] | | | | |
	7	7.4	8.6	9.2	9.7	Glutamate	Citrate	Lactate	Glucose	4	8	15	21	37
PSY 4	-	+	+++	++	-	+++	+	++	+	+	+	+	++	+
PSY 5	-	+++	+++	+++	-	++	+	++	+	+	+	++	++	+
PSY 6	-	+	+++	++	-	++	+	++	+	+	+	++	++	+

- = None
+ = Poor
++ = Good
+++ = Very good

5.3.4 Phylogenetic analysis

Figure 5.2 shows a phylogenetic tree based on the partial 16S rRNA gene sequences of PSY 4 and 5, and their closest relatives. Phylogenetic analysis revealed PSY 4 and 5 to have a 99% sequence coverage with their closest described relative *Bacillus halmapalus* [86, 87].
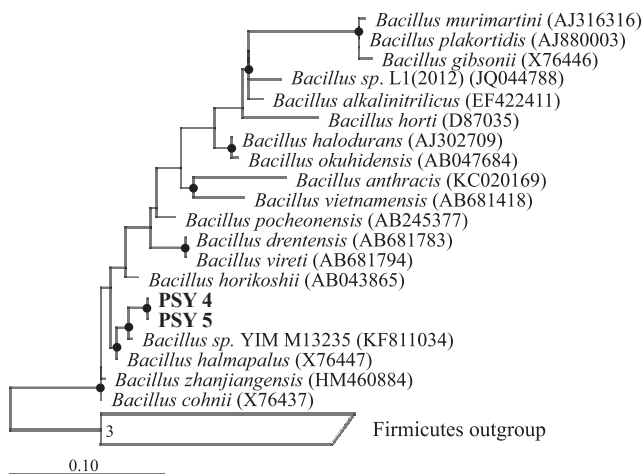
Figure 5.2 Phylogenetic tree based on the 16S rRNA gene sequences of PSY 4 and 5, and their closest relatives. The tree was created in ARB version 5.2 using the maximum-likelihood method and RAxML version 7.04. Relatives were imported from the NCBI database (accession numbers in parenthesis). Isolates were added using the built-in parsimony option. Members of the phylum Firmicutes were used as an out-group to root the tree. The scale bar corresponds to a 10% sequence difference. Bootstrap values are based on 250 replicates, and those greater than 90% are indicated by a dot placed at the node.

5.4 Discussion

The current chapter tested a number of bacterial isolates and organic mineral precursor compounds, for the development of a cost-effective bacteria-based agent, for realising self-healing concrete for application in low-temperature marine environments. In order to isolate suitable bacteria for the development of a bacteria-based healing agent selective pressure was placed on a microbial mat sample from a hypersaline lake in Spain. Eight isolates designated PSY 1-8 were isolated and phenotypically characterised. Of the eight isolates, PSY 4, 5 and 6 demonstrated good growth under low-temperature (8ºC) saline (30 g.l^{-1} sodium chloride) conditions using sodium lactate as an organic carbon source (Table 5.4). The ability of PSY 4, 5 and 6 to grow under low-temperature saline conditions makes these bacteria good candidates for marine concrete applications as the salinity of seawater is about 3%, and much of the worlds marine concrete infrastructure is located in low-temperature environments [3]. PSY 5 grew best at a pH of 9.2 (Table 5.5). Having a bacterium that exhibits very good growth at a pH of 9.2 is important for self-healing concrete applications, as the pH of a concrete crack solution where the bacterium is expected to function will likely have an alkalinity in and around this value. PSY 4, 5 and 6 also demonstrated good growth under room temperature conditions using magnesium acetate as an organic carbon source (Table 5.4). Magnesium acetate was the cheapest organic compound screened (Table 5.1). This makes magnesium acetate a good candidate as the organic mineral precursor compound for the healing agent. It is important to use a low-cost organic mineral precursor compound as the crack healing capacity of a bacteria-based cementitious composite is directly related to the amount of organic carbon available to the bacteria [6], and so the cheaper the organic mineral precursor compound, the cheaper the bacteria-based self-healing technology in general. Further, magnesium acetate when incorporated in mortar specimens had one of the lowest impacts on compressive strength (Figure 5.1). This too is an important factor, as an organic mineral precursor compound as part of a healing agent has the potential to be released during concrete mixing, and so should have minimal effect on concrete properties when incorporated.

The healing capacity of a bacteria-based agent does not need to rely on biological activity alone. Formation of magnesium hydroxide, resulting from a reaction between magnesium in seawater and hydroxide ions from cement paste, has been shown to contribute to the autogenous healing capacity of seawater submerged cementitious specimens [88]. Reaction of magnesium ions from the magnesium acetate with hydroxide ions from cement paste should, therefore, give the healing agent some added "chemical" crack healing potential.

Further, oxygen concentrations can be limited in marine systems [72], and so bacteria fit for marine concrete applications should be capable of functioning under such

conditions. PSY 4, 5 and 6 were capable of using oxygen as an electron acceptor under aerobic conditions, and nitrate under anaerobic conditions. If nitrate were to be added to the healing agent, then these bacterial isolates would be able to respire using "free" oxygen when available and switch to nitrate if this oxygen became limited, allowing for bacteria-based healing under anoxic conditions. Further, nitrite as a by-product of anaerobic nitrate reduction has been shown to inhibit steel reinforcement corrosion [73], which would be particularly desirable for concrete in the marine environment. Optical microscopy of PSY 4, 5 and 6 revealed the presence of spores. Bacterial spores have been shown to survive concrete inclusion [4], and when incorporated in various protective carriers have been shown to improve the crack healing capacity of cementitious materials [5-11, 13]. The ability of the three isolates to grow happily on monosodium glutamate — what is a cheap organic carbon source (0.2 €.kg^{-1} [80]) — at room temperature, increases the cost-effectiveness of healing agents employing these organisms. Of the three isolates, PSY 4 produced the most spores following its growth on monosodium glutamate at room temperature (Table 5.5). It is worth noting that the three isolates lost their sporulation capacity after repeated liquid cultivation, but that recultivation on agar plates retrieved this capacity.

Phylogenetic analysis of PSY 4 and 5 revealed both organisms to have 99% sequence coverage with *Bacillus halmapalus* [85, 86]. Both isolates did, however, demonstrate different phenotypic characteristics to *B. halmapalus*. *B. halmapalus* has been reported to grow within a temperature range of 10-40ºC, while PSY 4 and 5 both grew at lower temperatures with PSY 4 growing better than PSY 5 at 4ºC and both organisms demonstrating very good growth at 8ºC (Table 5.4). Further, *B. halmapalus* does not reduce nitrate, whereas PSY 4 and 5 were both able to reduce nitrate to nitrite under anoxic conditions. These differences make PSY 4 and 5 better bacterial candidates than *B. halmapalus* for the development of a bacteria-based healing agent for low-temperature marine concrete applications.

5.5 Conclusion

The current chapter has screened a number of bacterial isolates, and organic mineral precursor compounds, as part of a cost-effective bacteria-based healing agent, for realising self-healing concrete in low-temperature marine environments. Organic compounds were screened based on their cost and concrete compatibility and bacterial isolates based on their ability to metabolise a concrete compatible organic compound and to function in a marine concrete crack. Based on these tests the bacterial isolate designated PSY 5 and magnesium acetate, represent the best candidates for the development of the healing agent. Magnesium acetate was the cheapest organic

compound screened, and when added to mortar specimens during casting had one of the lowest impacts on compressive strength (reducing the compressive strengths of mortar specimens by 18% as compared to reference specimens). PSY 5 demonstrated very good growth at 3% salinity under low-temperature (8ºC) conditions with sodium lactate as an organic carbon source and good growth at room temperature with magnesium acetate as the organic carbon source. PSY 5 demonstrated good growth, and the best growth of the isolates, at a pH of 9.2. Further, PSY 5 also demonstrated good spore production capability when grown on monosodium glutamate at room temperature. Phylogenetic analysis revealed PSY 5 to have a 99% sequence similarity with *B. halmapalus*. PSY 5, however, demonstrated quite different phenotypic characteristics to *B. halmapalus,* making it a better candidate for realising self-healing concrete in low-temperature marine environments. Isolation of PSY 5 and identification of magnesium acetate, as key components of a bacteria-based healing agent, represent significant strides on the way to developing cost-effective bacteria-based self-healing concrete for application in the marine environment.

6

A bacteria-based bead for self-healing marine concrete applications

The search for differences or fundamental contrasts between the phenomena of organic and inorganic, of animate and inanimate things, has occupied many a men's mind, while the search for community of principle or essential similitude has been pursued by few.
— D'Arcy Wentworth Thompson, On Growth and Form

The current chapter presents a bacteria-based bead for realising self-healing concrete in low-temperature marine environments. The bead, consisting of calcium alginate encapsulating bacterial spores and mineral precursor compounds, was assessed for: oxygen consumption, swelling, and its ability to form an organic-inorganic composite in a simulative marine concrete crack solution (SMCCS) at 8ºC. After 6 days immersion in the SMCCS, the bacteria-based beads formed a calcite crust on their surface and calcite inclusions in their network, resulting in a calcite-alginate organic-inorganic composite. The beads swelled by 300% to a maximum diameter of 3 mm, while theoretical calculations estimate that 0.1 g of the beads were able to produce ~1 mm^3 of calcite after 14 days immersion; providing the bead with considerable crack healing potential. It is estimated based on the bacteria-based beads cost roughly 0.7 €.kg^{-1} that bacteria-based self-healing concrete, made using these beads, would cost 135 €.m^{-3}. The bacteria-based bead shows great potential for realising self-healing concrete in low-temperature marine environments, while the formation of an organic-inorganic composite healing material represents an exciting avenue for self-healing concrete research.

6.1 Introduction

Marine environments are hostile places for concrete infrastructure. There are many physical and chemical phenomena, which are independent and mutually reinforcing in the deterioration of marine concrete structures [19]. A self-healing materials approach is one whereby bacteria immobilised in concrete are able to form a crack healing precipitate [4-14]. Despite much of the world's marine infrastructure being located in cool with freezing climatic zones (annual average temperature < 10ºC, and summer temperature generally < 20ºC)[3], bacteria-based self-healing has exclusively been shown to work at room temperature and under freshwater conditions [4-14]. If bacteria-based self-healing concrete is to be realised under low-temperature saline conditions, then bacteria-based healing agents and more specifically the bacteria making up part of these healing agents will need to function under the same conditions. Bacteria added directly to concrete during the mixing process have been shown to have limited functionality over time [5]. On account of this, a number of strategies have been devised to protect bacteria and bacteria-based agents (bacteria and mineral precursor compounds) before embedment in cementitious materials [6-11, 88]. Protection of bacteria-based agents in clay particles [6, 7], bacteria in diatomaceous earth [8] and melamine-based microcapsules [9] have all extended the period over which functional healing could be achieved. These carriers, however, did not add to the healing capacity of their respective systems. More recently alginate has been proposed as a protective carrier for bacterial spores [11] and as part of a bacteria-based agent [89], for possible self-healing concrete applications. Alginate is a low-cost biopolymer, which swells in the presence of water forming a hydrogel [89]. Alginate hydrogels have been shown to mediate the formation of alginate-mineral composites [91-94]. Synthesis of such organic-inorganic composites is no doubt inspired by the performance of biological composites such as nacre (mother-of-pearl). Nacre with its brick and mortar organic-inorganic composite structure has remarkable strength, hardness and toughness: containing > 95 vol.% of aragonite (a polymorph of calcium carbonate) and 1% (v/v) polymer, is twice as hard and a thousand times tougher than aragonite alone [95-97]. Bergdale *et al.,* engineered a bacteria for the formation of an "organo-mineral biopolymer" (or organic-inorganic composite) for sealing concrete cracks [98]. Though successful, the pathogenicity of the recombinant organism used to produce the composite makes this strategy unsuitable for real-world application. Practical strategies are still needed for the formation of organic-inorganic composite healing materials for self-healing concrete applications.

The current chapter presents a bacteria-based bead for self-healing concrete applications in low-temperature marine environments. The bead consisting of calcium alginate encapsulating bacterial spores and mineral precursor compounds was assessed

for oxygen consumption, swelling, and its ability to form an alginate-calcite organic-inorganic composite in a simulative marine concrete crack solution (SMCCS) at 8ºC.

6.2 Experimental program

6.2.1 Preparation of the bacteria-based beads

A precursor solution was prepared consisting of 1.5% (w/v)) sodium alginate (FMC BioPolymer), 6.4 g.l^{-1} of magnesium acetate (Sigma-Aldrich), 0.4 g.l^{-1} yeast extract and 7×10^8 bacterial spores.l^{-1}. The bacteria, magnesium acetate and yeast extract used in the current chapter are based on Chapter 5. The precursor solution was pumped drop wise through a syringe needle (internal diameter of 0.2 mm) at a height of 5 cm into a gelling solution of calcium acetate (6.4 g.l^{-1})(Sigma-Aldrich)(Figure 6.1), resulting in droplets ~3 mm in diameter. These droplets on entering the calcium acetate solution cross-polymerised forming calcium alginate beads (~3 mm in diameter). The beads produced in batches were removed from the calcium acetate solution after 30 min. Calcium alginate beads containing only mineral precursor compounds (magnesium acetate and yeast extract) and calcium alginate beads were also produced. The calcium alginate beads were cross-polymerised in a calcium chloride gelling solution (6.4 g.l^{-1})(Sigma-Aldrich). Following cross-polymerisation all beads were washed three times in tap water, dried for 24 hours at 36ºC (reducing their diameter to ~0.5 mm) and stored under dry conditions until experimental use.
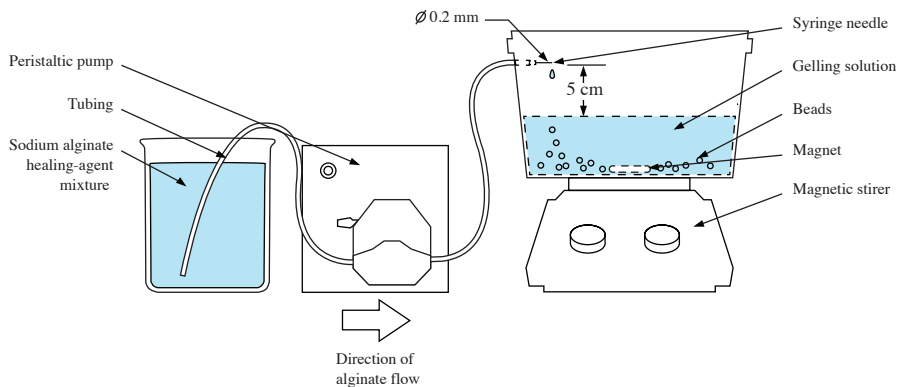

Figure 6.1 Schematic showing the alginate bead production process.

6.2.2 Biogenic mineral formation

The bacteria employed in this study are able to respire using organic carbon following the general reaction (Equation (6.1))[35]:

$$(CH_2O)_n + O_2 \xrightarrow{\text{Bacteria}} CO_2 + H_2O \tag{6.1}$$

Carbon dioxide molecules produced by the bacteria in alkaline environments (such as a concrete crack) are rapidly chemically converted to carbonate ions, which in the presence of calcium ions subsequently precipitate as calcium carbonate (Equation (6.2)) [2]:

$$CO_2 + Ca(OH)_2 \longrightarrow \underset{\text{Calcium carbonate}}{CaCO_3} + H_2O \tag{6.2}$$

Oxygen consumed by the bacteria (Equation (6.1)), provides a valuable indicator as to their activity. Changes in dissolved oxygen concentrations have long been used to assess bacterial activity [99], and more recently for assessing the efficacy of bacteria-based self-healing agents [7, 14].

6.2.3 Oxygen consumption test

Four series were set up for the oxygen consumption test: (1) bacteria-based beads in SMCCS; (2) calcium alginate beads containing mineral precursor compounds in SMCCS; (3) calcium alginate beads in SMCCS; and (4) SMCCS. The SMCCS (whose composition can be seen in Table 6.1) was designed to provide the minerals required by the bacteria for growth, and also to simulate the salinity (3%) and pH (~9.6) of a solution found in a marine concrete crack. The test was conducted in 15 ml glass bottles fitted with oxygen sensors (Planar Oxygen Sensor Spot, PreSens GmbH). 0.1 g of the beads were added to the bottles; the bottles were then filled with SMCCS, sealed having no headspace and placed in a fridge at 8ºC. Dissolved oxygen concentrations were monitored with an oxygen meter (Fibox 3 Oxygen Meter, PreSense GmbH) over a two-week period. We must note that the test was not conducted under aseptic conditions as sterilisation through autoclaving would result in depolymerisation of the alginate [100]. Care was, however, taken to make the test as sterile as possible, by washing the bottles at 80ºC and soaking them in 70% ethanol for one hour before the test. All other aspects of the test were conducted aseptically. The pH of each solution in the bottles was measured before and after the test. Each series was conducted in triplicate.

Table 6.1 Composition of the SMCCS.

Constituent	Compound	Final concentration [mmol.l^{-1}]
Minerals	KH_2PO_4	0.153
	$CaCl_2.2H_2O$	1.53
	KCl	2.68
	$MgCl.6H_2O$	1
Buffer	$NaHCO_3$	100
	Na_2CO_3	100
Constituent	**Compound**	**Final concentration [g.l^{-1}]**
Salinity	NaCl	30

6.2.4 Swelling assessment

Swelling was determined by measuring the diameter of the bacteria-based beads before and after 24 and 48 hours, and 6 days submersion in the SMCCS at 8ºC. The diameter of the beads was measured via a Leica MZ6 optical microscope (Leica Microsystems GmbH) equipped with LAS v.40 software (Leica Microsystems GmbH).

6.2.5 Characterization of the bacteria-based beads

Beads immersed in SMCCS at 8ºC were removed after six days and frozen with liquid nitrogen to preserve their structure. The frozen beads were fractured in half with a scalpel blade and the fractured halves placed on a Peltier stage (-16ºC) within the ESEM chamber (Philips XL 30 ESEM, Philips). The frozen fractured beads were then subjected to ESEM in back scattered electron (BSE) mode and point element analysis through EDS (EDAX, Philips). Beads were also dried at 36ºC for 24 hours, ground into powders and subjected to FTIR spectroscopy (Spectrum 100, Perkin-Elmer Inc.). Spectra were the result of 32 scans in the range of 4000-600 cm^{-1} with a resolution of 2 cm^{-1}. Alginate beads exposed to the same experimental conditions were also analysed.

6.3 Results

6.3.1 Oxygen consumption

Figure 6.2 shows oxygen profiles for: (1) bacteria-based beads in SMCCS; (2) calcium alginate beads containing mineral precursor compounds in SMCCS; (3) calcium alginate beads in SMCCS; and (4) SMCCS. Dissolved oxygen concentrations in bottles containing bacteria-based beads began to drop after one day and continued to drop until depletion. Once depleted oxygen concentrations were replenished by: decanting the SMCCS from each of the bottles into sterile bottles; shaking the sterile bottles vigorously for 5 min; pouring the SMCCS back into the bottles with the beads and continuing the test. Dissolved oxygen concentrations ($\sim$300 μmol.l^{-1}) in bottles containing the bacteria-based beads were depleted five times over a 14-day period. Oxygen concentrations in the bottles containing calcium alginate beads containing mineral precursor compounds also began to drop, but only after eight days. Oxygen concentrations in bottles containing calcium alginate beads, and in bottles with SMCCS, remained constant for the duration of the test. The pH of the SMCCS in bottles containing bacteria-based beads and calcium alginate beads containing mineral precursor compounds dropped from 9.6 to 9.4. The pH of the SMCCS in bottles containing alginate beads and in bottles containing no beads remained unchanged.
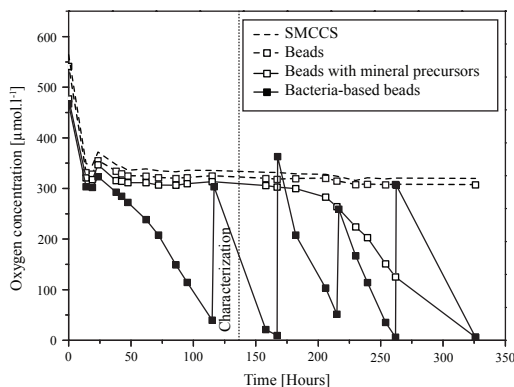

Figure 6.2 Profiles showing the dissolved oxygen concentrations in bottles containing: bacteria-based beads (calcium alginate beads containing bacterial spores, magnesium acetate and yeast extract) in the SMCCS; beads containing mineral precursors (calcium alginate beads containing magnesium acetate and yeast extract) in a SMCCS; alginate beads (calcium alginate beads) in the SMCCS; and the SMCCS, at 8ºC. Each of the triplicates from each series tested displayed very similar phenomena, however, for clarity, only one profile from each series is shown. The vertical dotted line indicates the time when bacteria-based beads and alginate beads were chemically characterised.

6.3.2 Swelling study

Figure 6.3 shows an image of a typical bacteria-based bead before and after immersion in the SMCCS at 8ºC. Beads immersed in the SMCCS typically swelled by 300% reaching their maximum diameter of 3 mm within 24 hours.
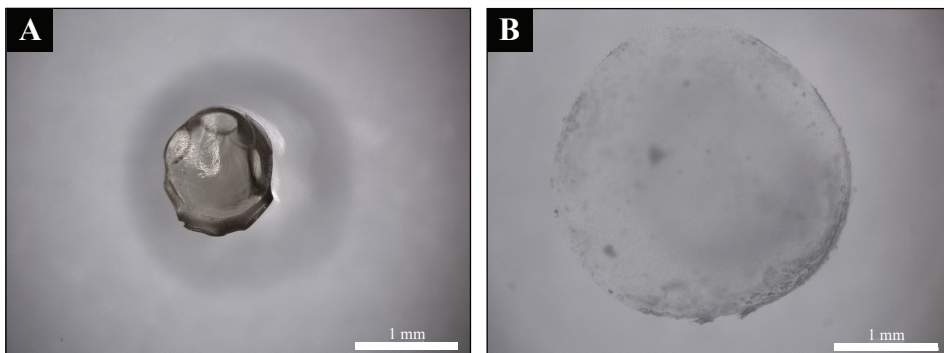

Figure 6.3 Typical bacteria-based bead: (A) before; and (B) after 24 hours submersion in the SMCCS at 8ºC.

6.3.3 Chemical characterisation

ESEM analysis of the frozen bacteria-based beads revealed a crust on their surface (Figure 6.4C), and dumbbell shaped inclusions within their alginate network (Figure 6.4(C and D)). EDS analysis of the crust and dumbbell shaped inclusions showed them to be an association of calcium, oxygen and carbon, suggesting them to be calcium carbonate. FTIR analysis of the beads revealed a broad band centred at 1400 cm^{-1} and a distinct peak at 874 cm^{-1}. Calcite (a polymorph of calcium carbonate) has a C-O asymmetric stretching vibration (v_3) centred at 1400 cm^{-1}, a C-O out of plane bending vibration (v_2) centred at 872 cm^{-1} and a C-O planar bending vibration (v_4) centred at 712 cm^{-1}. Although the bacteria-based beads did not display a distinct peak at 712 cm^{-1}, it is suspected that this peak was obscured by the spectra of the alginate. ESEM (Figure 6.4(A and B)) and FTIR analysis of the alginate beads revealed little or no evidence of mineral precipitation.

A

Bead surface

B/D ESEM image locations

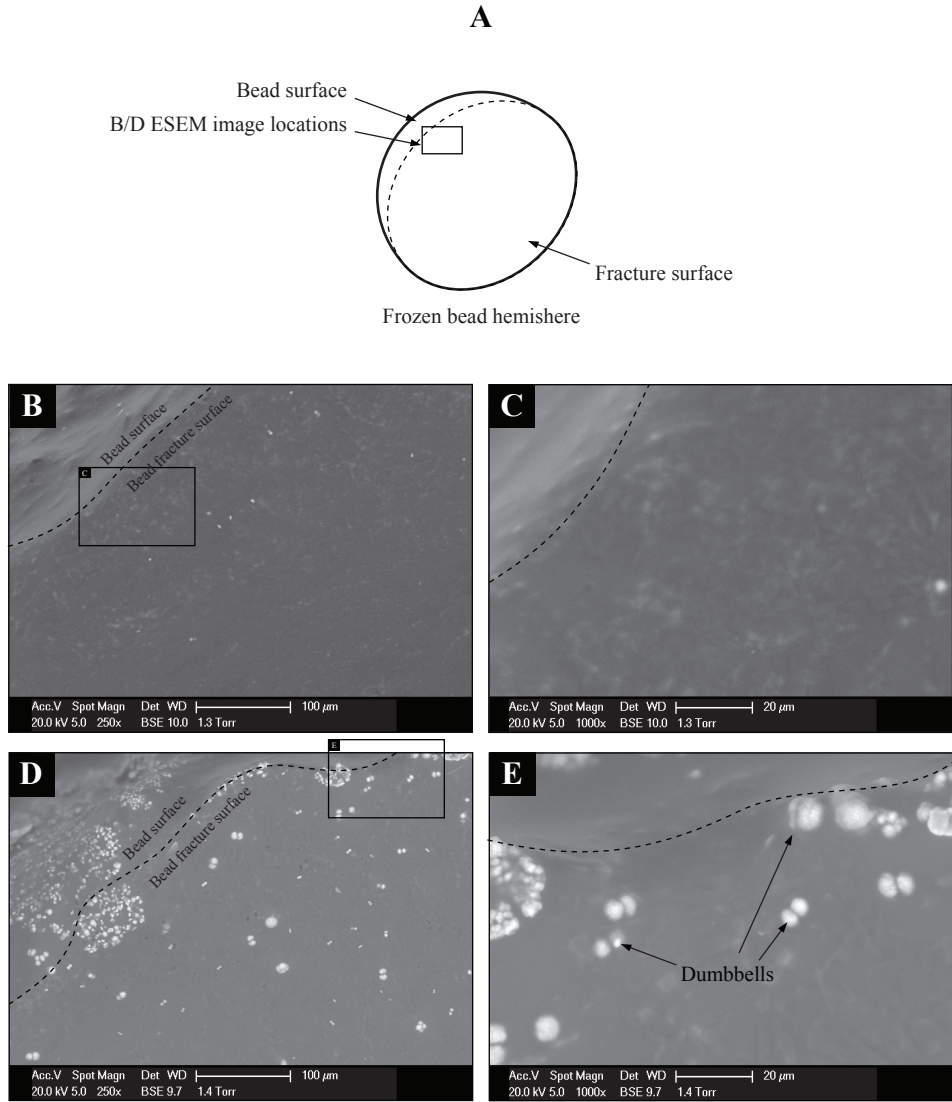Fracture surface

Frozen bead hemishere

Figure 6.4 Schematic (A) of a frozen bead hemispheres; and ESEM images (B and C) showing sections of the frozen cross-sections of a calcium alginate bead, and (D and E) a bacteria-based bead, after six days submersion in SMCCS at 8ºC. The dashed lines depict the edges between the surface and fracture surface of the beads.

6.4 Discussion

A bacteria-based bead for possible self-healing marine concrete applications has been presented. The bacteria-based beads (calcium alginate beads encapsulating bacterial spores and mineral precursor compounds) reduced oxygen concentrations in an SMCCS (3% salinity and pH of 9.6) at 8ºC, forming a calcite-alginate organic-inorganic composite. Beads upon immersion in the SMCSS swelled as a result of interactions between water in the SMCCS and hydrophilic groups of the alginate. The swelling continued due to osmotic forces until the bead reached an equilibrium state. The presence of water makes the mineral precursor compounds within the bead more readily available. This availability triggers the bacteria to switch from their spore to vegetative state, whereupon they begin to metabolise the organic mineral precursor compounds. Carbon dioxide is produced as a result of the bacteria's metabolic activity, which in a high pH environment is converted to carbonate ions (Equation (6.1-6.4)). These carbonate ions then react with calcium ions from the SMCCS forming calcium carbonate (Equation (6.5)). Depletion of the carbonate ions within the bead creates a concentration gradient between the bead and the SMCCS. This gradient causes the carbonate ions to diffuse from inside the bead until they meet an opposing front of calcium ions from the SMCCS. This front was likely concentrated at the surface of the beads and the reason why most of the precipitates were formed at the surface of the beads (Figure 6.4C). Dumbbell shaped calcite inclusions could also be seen within the beads forming an organic-inorganic composite (Figures 6.4(C and D)). As previously mentioned, precipitation of calcium carbonate is dependent on the metabolic activity of the bacteria (Equation (6.1-6.5)). Consequently, the most saturated regions within the bead are expected at the surface of the bacteria. Calcite crystals concentrated at the bacteria's polar ends evolve into dumbbell or cauliflower-like formations. Bacteria have been shown to form cauliflower-like carbonate formations under laboratory conditions [101-104] as well as in natural environments [105].

The bacteria-based beads submerged in the SMCCS swelled by 300% within 24 hours to a final diameter of 3 mm (Figure 6.3). Activated in a concrete crack this swelling has the potential to bridge a crack with a maximum width of 3 mm. Such width is far beyond the autogenous healing capacity of cementitious materials [29, 63], and bacteria based-healing concrete [4-14]. Moreover, the swelling was relatively fast, taking in the order of hours rather than days, and so could provide bacteria-based healing technologies employing this strategy with a relatively fast healing mechanism. Bacteria-induced mineral precipitation also gives the bacteria-based beads a certain crack healing capacity. This capacity can be theoretically calculated based on the amount of oxygen consumed by the bacteria. We can see from Figure 6.2 that ~1500 µmol.l^{-1} of oxygen were consumed within the bottles over 14 days, which equates to 22.5 µmol of oxygen

per 15 ml bottle (or 0.1 g of beads). 22.5 µmol of carbon dioxide has the potential to produce 22.5 µmol of calcium carbonate. The mass of this calcium carbonate can then be calculated using (Equation (6.6))[106]:

$$m = n \times M \tag{6.6}$$

where

m = Mass [g]
n = Number of moles [mol]
M = Molar mass of calcium carbonate [g.mol^{-1}]

resulting in an estimated value of 2.25 mg of calcium carbonate. Taking the density of calcium carbonate to be 2700-2900 kg.m^{-3} [107], we can then calculate the volume using (Equation (6.7)) [108]:

$$V = \frac{m}{\rho} \tag{6.7}$$

where

V = Volume [m^3]
m = Mass [kg]
ρ = Density [kg.m^{-3}]

Meaning that 0.1 g of the bacteria-based beads can induce ~1 mm^3 of calcium carbonate precipitation. This volume gives the beads considerable bacteria-based self-healing potential. What can also be seen in Figure 6.2 is that the beads without bacteria also consumed oxygen. This consumption was likely due to the presence of bacterial "contaminants" present in the bottles and/or in the alginate. And although the beads without bacteria consumed oxygen the bacteria-based beads consumed oxygen far quicker, and hence could provide much faster bacteria-based healing.

It is estimated, based on *bacillus subtilis* spores costing 1 €.kg^{-1}, magnesium acetate costing 0.1 €.kg^{-1}, yeast extract costing 1 €.kg^{-1}, sodium alginate costing 1 €.kg^{-1} and calcium chloride costing 0.2 €.kg^{-1} [80], that the bacteria-based beads cost 0.7 €.kg^{-1}. If 50 kg of the bacteria-based beads were to be added to 1 m^3 of concrete, then the resultant bacteria-based self-healing concrete would cost roughly 115 €.m^{-3} and 35 € more than standard OPC concrete. The bacteria-based beads are > 90% (w/v) alginate, and so by using a lower costing alginate, the overall cost of the beads could be significantly

lowered. Such a low-costing alginate might be one recovered from wastewater [109].
6.5 Conclusion

A bacteria-based bead has been presented for possible self-healing marine concrete applications. The bead consisting of calcium alginate encapsulating bacterial spores and mineral precursor compounds was tested for oxygen consumption, swelling and its ability to form a mineral-polymer composite. Bacteria-based beads were able to reduce the dissolved oxygen concentration within an SMCCS at 8ºC, forming a calcite-alginate organic-inorganic composite. The beads swelled by 300% to a maximum diameter of ~3 mm, while theoretical calculations estimate that 0.1 g of beads (or ~30 beads with a 0.5 mm diameter) are able to produce ~1 mm^3 of calcite over a 14 day period. Both swelling and bacteria induced precipitation afford the bacteria-based beads with considerable crack healing potential. Further, it is estimated, based on the bacteria-based beads costing roughly 0.7 €.kg^{-1}, that bacteria-based self-healing concrete made using these beads would cost about 135 €.m^{-3}. The bead shows great potential for realising self-healing concrete in the low-temperature marine environments, while the formation of organic-inorganic composite healing materials represents an exciting avenue for self-healing concrete research.

7

A bacteria-based self-healing cementitious composite for application in low-temperature marine environments

To the eyes of the man of imagination, nature is imagination itself.

— William Blake

The current chapter presents a bacteria-based self-healing cementitious composite for application in low-temperature marine environments. The composite was tested for its crack healing capacity through water permeability measurements and strength development through compression testing. The composite displayed an excellent crack healing capacity, reducing the permeability of cracks 0.4 mm wide by 95% and cracks 0.6 mm wide by 93%, following 56 days submersion in artificial seawater at 8ºC. This crack healing capacity is attributable to: mineral precipitation as a result of chemical interactions between the cement paste and seawater; bead swelling; magnesium-based precipitates as a result of chemical interactions between the magnesium of the beads and hydroxide ions of the cement paste; and bacteria induced mineral precipitation. Mortar specimens incorporated with beads exhibited lower compressive strengths than the plain mortar specimens. Reducing the amount of beads will likely increase the strength of the composite, and may have a relatively small impact on its healing capacity. This study is the first to demonstrate bacteria-based self-healing of a cementitious material under low-temperature marine conditions, while the formation of organic-inorganic healing materials represents an exciting avenue for self-healing concrete research.

7.1 Introduction

Traditional engineered materials are static and unresponsive. Biological materials, in contrast, have evolved to respond and adapt to environmental and physiological stimuli. Self-healing is an outstanding biological materials response, whereby damage can be autonomously healed restoring functional performance. Bone, for example, is able to form a blood clot around a fracture site. This clot becomes a cartilaginous callus, which later undergoes revascularisation and calcification, and is finally remodelled restoring bone functionality [110]. Biological materials, such as bone, have inspired a revolution in materials design thinking and the development of a new class of smart self-healing materials. These engineered self-healing materials promise longer functional service lives with tremendous associated economic benefits [111].

An innovative self-healing materials approach is one whereby bacteria immobilised in concrete can form a crack healing precipitate [4-14]. Jonkers first introduced a bacteria-based agent — consisting of bacterial spores and an organic mineral precursor compound — for achieving bacteria-based self-healing concrete [4]. The bacterial spores — activated by crack induced water ingress — germinate into active vegetative cells, which are able to convert mineral precursor compounds to calcium carbonate. Calcium carbonate, if precipitated in the cracks can result in the regain of functional water tightness; reducing the concrete's susceptibility to water bore degradation phenomena. Despite much of the world's marine infrastructure being located in cool with freezing climatic zones [3], bacteria-based self-healing concrete has exclusively been shown to work under room temperature freshwater conditions [4-13]. If bacteria-based self-healing concrete is to be realised under low-temperature marine conditions, then the bacteria-based agents used to generate self-healing concrete will need to function under the same conditions. Moreover, bacterial spores added directly to concrete during mixing have demonstrated limited functionality over time [5]. On account of this, bacteria-based agents have been protected in expanded clay particles [6, 7, 13], and bacteria in diatomaceous earth [8] and melamine based microcapsules [9], before being incorporated in cementitious materials. Although these strategies have successfully extended the period over which functional healing could be achieved, they do not actively contribute to the healing capacity of these technologies. More recently alginate has been proposed as a protective carrier for bacterial spores [11] and the formation of a bacteria-based bead [112], for self-healing concrete applications. The bacteria-based bead, of the later study, composed of bacterial spores and mineral precursor compounds (yeast extract and magnesium acetate) encapsulated in calcium alginate, swelled upon submersion in a low-temperature (8ºC) SMCCS forming a bacteria-activated calcite ($CaCO_3$)-alginate composite material. It is envisaged that this bacteria-based bead technology when incorporated in a cementitious material, impart it with a superior crack

healing action. Figure 7.1 shows a schematic of the proposed healing mechanism for a cementitious composite incorporated with the bacteria-based bead technology. In the event of cracking and water ingress (Figure 7.1A), beads along the crack would swell, clogging the crack (Figure 7.1B), which would concomitantly "free up" the bacterial spores, the yeast extract and magnesium acetate. This "freeing up" would then lead to: the magnesium of the magnesium acetate precipitating as magnesium-based minerals, the spores germinating as a result of their exposure to the solubilised yeast extract, and their metabolising of the acetate, inducing calcium-based mineral precipitation in and on the surface of the bacteria-based beads, healing the crack (Figure 7.1C).

In this chapter, the functionality of the bacteria-based bead embedded in cement paste specimens and tested through oxygen consumption measurements in a low-temperature (8ºC) artificial marine concrete crack solution (AMCCS). I then incorporate the bacteria-based beads into mortar specimens forming a bacteria-based self-healing cementitious composite. The bacteria-based self-healing cementitious composite is then assessed for its crack healing capacity and strength development after being submerged in artificial seawater at 8ºC.
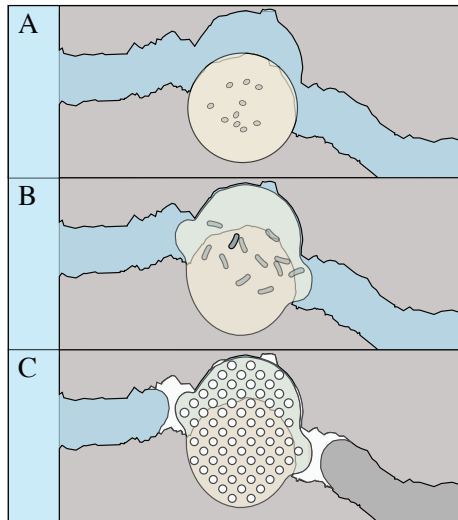
Figure 7.1 Schematic diagram illustrating the proposed healing mechanism: (A) in the event of cracking and water ingress; (B) the bacteria-based beads incorporated in the composite will swell, this swelling will clog the cracks, and concomitantly "free up" the bacteria, yeast extract and magnesium acetate contained in the beads; (C) the magnesium will precipitate as magnesium-based minerals, the spores will germinate as a result of being exposed to the solubilised yeast extract, and metabolise the acetate, inducing calcium-based mineral precipitation (white) in and on the surface of the beads, healing the crack.

7.2 Experimental program

The experimental program for the current study consists of two parts. Part 1 assesses the bio-functionality of the bacteria-based beads from Chapter 6 under low-temperature marine concrete crack conditions. Three series were set up to help assess the bio-functionality of the bead: (1_b) consisting of plain cement paste specimens submerged in an AMCCS at 8ºC; (2_b) consisting of cement paste specimens embedded with beads containing mineral precursor compounds submerged in an AMCCS at 8ºC; and (3_b) consisting of cement paste specimens embedded with bacteria-based beads submerged in an AMCCS at 8ºC. In Part 2 the bacteria-based bead technology is incorporated in mortar forming a bacteria-based self-healing cementitious composite. The bacteria-based self-healing cementitious composite is then assessed for its healing capacity and strength development under low-temperature marine conditions. The healing capacity of the composite is tested using the permeability test presented in Chapter 4. Four series were set up to help quantify the crack healing capacity of the bacteria-based cementitious composite: (1_h) to establish reference permeability values for plain mortar specimens with 0.4 and 0.6 mm wide cracks; (2_h) to determine the autogenous crack healing capacity of plain mortar specimens with 0.4 and 0.6 mm wide cracks following 56 days submersion in artificial seawater at 8ºC, and the same specimens after drying; (3_h) to determine the autonomous crack healing capacity of mortar specimens incorporated with beads containing mineral precursor compounds with 0.4 and 0.6 mm wide cracks following 56 days submersion in artificial seawater at 8ºC, and the same specimens after drying; and (4_h) to determine the crack healing capacity of specimens made from the bacteria-based self-healing cementitious composite with 0.4 and 0.6 mm wide cracks following 56 days submersion in artificial seawater at 8ºC, and the same specimens after drying (Figure 7.2). Strength development of the bacteria-based cementitious composite is assessed through compressive strength testing. Two series were set up to assess the compressive strength development of the composite: (1_c) to establish the compressive strength of plain mortar cubes, and (2_c) to establish the compressive strength of mortar cubes incorporated with beads containing mineral precursor compounds, submerged in artificial seawater at 8ºC.
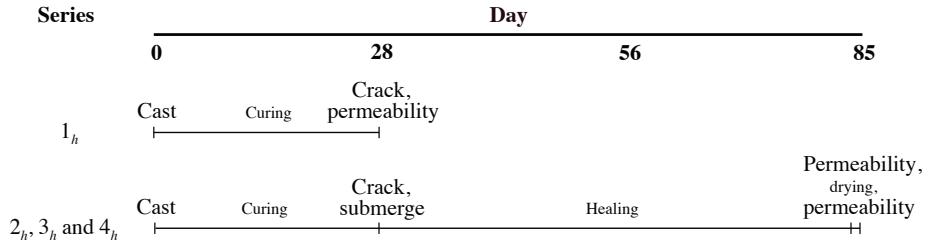
Series	Day			
	0	28	56	85
1_h	Cast	Curing	Crack, permeability	
2_h, 3_h and 4_h	Cast	Curing	Crack, submerge	Healing	Permeability, drying, permeability

Figure 7.2 Scheme showing the experimental program used to quantify the crack healing capacity of the bacteria-based self-healing cementitious composite. The program consisted of four series: (1_h) to establish the initial permeability of unhealed cracked mortar specimens; (2_h) to determine the autogenous healing capacity of cracked mortar specimens after 56 days submersion in seawater at 8ºC, and the same specimens after drying; (3_h) to determine the healing capacity of cracked mortar specimens incorporated with beads containing mineral precursor compounds after 56 days submersion in seawater at 8ºC, and the same specimens after drying; and (4_h) to determine the healing capacity of cracked bacteria-based self-healing cementitious specimens tested after 56 days submersion in seawater at 8ºC, and the same specimens after drying. Each series consisted of specimens with cracks 0.4 and 0.6 mm wide and seven specimens each.

7.2.1 Production of the bacteria-based beads

The same beads and bead production methods were used as in Chapter 6.

7.2.2 Bio-functionality of the bacteria-based bead

The bacteria used in this study consume oxygen as a result of their metabolic activity. Oxygen depletion, therefore, provides a valuable indicator as to the bio-functionality of the bacteria-based beads. In the current study, we were interested as to whether the bacteria-based beads were able to function in a low-temperature (8ºC) marine concrete crack. A specially designed setup was devised to test this, consisting of, an insulated tank, oxygen microsensor, and water cooler (Figure 7.2). The insulated tank further consisted of an experiment chamber filled with an AMCCS, and a cooling chamber filled with freshwater. The AMCCS was produced by adding crushed mortar pieces to artificial seawater (Table 2.2), filtering, and adjusting with artificial seawater to a final pH of 9.6. The artificial seawater used is based on the major constituents of natural seawater [40]. A cooling tube attached to a water cooler was used to cool the water of the cooling chamber, which was in turn used to cool the AMCCS of the experiment chamber to 8ºC. Cement disc specimens (10 mm thick and with a diameter of 33.5 mm) were prepared to test the bio-functionality of the bacteria-based beads. Plain mortar discs were cast for series 1_b, cement discs embedded with beads containing mineral precursor compounds for series 2_b, and cement discs embedded with bacteria-based beads for

series 3$_b$. Discs were cast from BFS cement (CEM III/B 42.5 N LH, ENCI) with a water-to-cement ratio of 0.5. Five beads were embedded in a cluster in the face of freshly cast discs. The disc specimens were carefully removed from their moulds after 24 hours, sealed in polyethylene plastic bags and kept at room temperature for a total curing period of 28 days. Following curing the discs were submerged in the AMCCS of the experiment chamber. Oxygen concentrations were measured in the water column above the specimens with a fibre-optic oxygen microsensor (NTH-PSt1, PreSens GmbH)(Figure 7.4A). The microsensor was mounted to a motorised micromanipulator with a high precision vertical axis (0.1 µm resolution). Oxygen microprofiles were measured in 20 µm steps from 5 mm above the specimens to the surface of the beads. Microsensor measurements were converted to oxygen concentrations via an oxygen meter (Microx TX3, PreSens GmbH). Dissolved oxygen concentrations were monitored over a one-week period. Specimens were tested in duplicate.
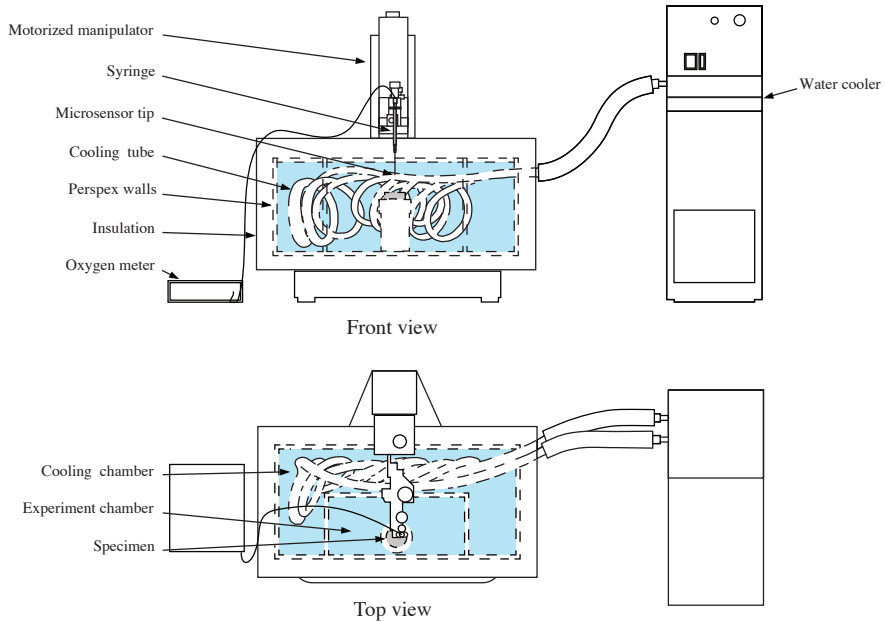

Figure 7.3 Schematic drawing showing the setup used to test the bio-functionality of the bacteria-based beads. The setup consisted of: an insulated tank, oxygen microsensor, and water cooler. The tank was made up of an experiment chamber containing an AMCCS and cooling chamber containing freshwater. A cooling tube attached to a water cooler was used to cool the water of the cooling chamber, which was in turn used to cool the AMCCS of the experiment chamber to 8ºC. Specimens for analysis were submerged in the AMCCS of the experiment chamber, and oxygen measurements were made with a microsensor mounted to a motorised micromanipulator.

7.2.3 Specimen preparation for permeability and compression testing

Two specimen geometries were produced to test the healing capacity and compressive strength development of the bacteria-based self-healing cementitious composite. Cylindrical specimens were produced just like those in Chapter 4 for the permeability test; and cube specimens (40 × 40 × 40 mm) for compressive strength testing. Plain mortar cylinders were cast for series 1_h and 2_h, mortar cylinders containing beads with mineral precursor compounds for series 3_h, and cylinders cast from the bacteria-based self-healing cementitious composite for series 4_h. The applied mix design used to produce the bacteria-based cementitious specimens is shown in Table 7.2. Plain mortar cubes were cast for series 1_c, and mortar cubes incorporated with beads containing mineral precursor compounds were cast for series 2_c. It was decided not to cast mortar cubes containing bacteria-based beads for compressive strength testing as it was thought that the influence of bacteria would be negligible. Following casting, all specimens were sealed in polyethylene plastic bags and kept at room temperature for a total curing period of 28 days. Following curing, the cylinder specimens were again prepared as in Chapter 4.

Table 7.2 Mix-design for the bacteria-based self-healing cementitious composite.

Constituent	Amount [kg.m^{-3}]
Cement (CEM III/B 42.5 N LH)	494
Water	247
Sand fraction [mm]:	
1-2	608
0.5-1	426
0.25-0.5	167
0.125-0.25	319
Bacteria-based beads	50

7.2.4 Crack permeability test

Cylindrical specimens from series 1_h were first assessed for their permeability. Specimens were placed in permeability cells and the permeability cells attached via fittings to the bottom of the permeability columns. Artificial seawater was prepared and poured into reservoirs at the top of each column. Taps in each reservoir were released initiating the permeability test. The permeability test was run for 10 minutes and any water flowing through the cracks was individually collected in catchment buckets and the weight of the water recorded. The water level of each column was manually

maintained between 1 and 1.05 m, giving an almost constant water head of 0.1 bar. Cylinder specimens of series 2_h, 3_h and 4_h, were submerged in artificial seawater and vacuumed for 2 hours to remove any air bubbles trapped in their cracks. Each series was then transferred to a plastic bucket containing 4 l of seawater. Lids were placed on the buckets and the buckets placed in a refrigerator at 8ºC. Seawater in the buckets was changed once a week for a month to mimic in situ conditions and prevent ion depletion. After 56 days submersion the specimens from series 2_h, 3_h and 4_h were assessed for their permeability. Following the permeability testing these specimens were dried in a drier at 36º C for 24 hours and again tested for their permeability. The specimens were dried to evaluate the effect of drying on healing. Each series consisted of seven replicates each.

7.2.5 Characterization of the healing material

Cylindrical specimens with the mean permeability of each series were selected for chemical analysis. These specimens were dried and polished sections prepared. The sections were then analysed through ESEM (Philips XL 30 ESEM, Philips) in BSE mode and elemental mapping through EDS (Philips EDAX, Philips). In between preparation and analysis, specimens were kept in a desiccator to avoid continued cement hydration. EDS image maps of calcium, magnesium and silica were merged through the apply image tool in Photoshop (Adobe, Systems).

7.2.6 Strength development

Cube specimens were placed in buckets in batches of five and submerged in 4l of artificial seawater. Lids were placed on the buckets and the buckets placed in a refrigerator at 8ºC. Artificial seawater in the buckets was changed once a week for a month to mimic in situ conditions and prevent ion depletion. Cube specimens from series 1_c and 2_c were removed from their buckets and tested for their compressive strength 2, 7, 28, 84 and 168 days after casting. Compressive strength testing was conducted with a Servo-Plus compression test machine in conjunction with a Cyber-Plus evolution control unit at a rate of 1 MPa.s^{-1}. Cubes kept in sealed polyethylene plastic bags were also tested 168 days after casting to test for any difference between their compressive strength and the compressive strength of the submerged specimens.

7.3 Results

7.3.1 Bio-functionality of the bacteria-based bead

Specimens embedded with bacteria-based beads showed a decrease in the oxygen

concentration in the diffusive boundary layer (1 mm above the beads) after one day and reached their lowest concentration after two days (Figure 7.4D). In contrast, oxygen concentrations in the water column above the plain cement specimens and specimens embedded with beads containing mineral precursor compounds remained somewhat constant (Figure 7.4(B and C)).
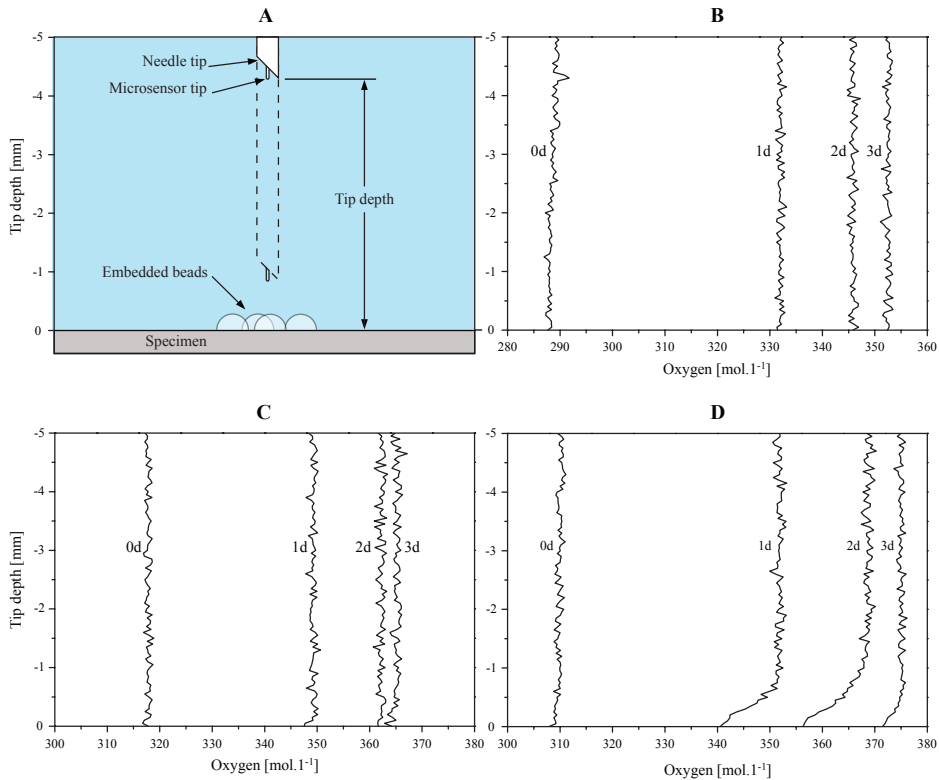

Figure 7.4 (A) a schematic of the water column tested above the specimens; and (B-D) graphs showing the oxygen microprofiles above (B) a cement paste specimen, (C) a cement paste specimen embedded with beads containing mineral precursor compounds, and (D) a cement paste specimen embedded with bacteria-based beads, all submerged in an AMCCS at 8ºC. The height of the schematic diagram corresponds to the height of the water columns in the graphs. 0d, 1d, 2d, 3d represent profiles taken after zero, one, two and three days respectively. For clarity, only one profile is presented in each graph.

7.3.2 Crack healing capacity

Figure 7.5 shows two box plot graphs. Graph (A) on the left shows crack permeability data for specimens with 0.4 mm wide cracks and graph (B) on the right shows crack permeability data for specimens with 0.6 mm wide cracks. The mean initial permeability

of specimens having 0.4 mm wide cracks was 3.0 $cm^3.s^{-1}$. Mortar specimens having 0.4 mm wide cracks had a permeability of 1.0 $cm^3.s^{-1}$ after 56 days submersion (i.e. 33% of the initial permeability). Mortar specimens incorporated with beads containing mineral precursor compounds having cracks 0.4 mm wide had a permeability of 0.5 $cm^3.s^{-1}$ after 56 days submersion (i.e. 18% of the initial permeability). Bacteria-based self-healing cementitious specimens having 0.4 mm wide cracks had the lowest permeability of 0.1 $cm^3.s^{-1}$ after 56 days submersion (i.e. 5% of the initial permeability). Permeability results for the 0.6 mm cracks displayed a similar trend to those of the 0.4 mm cracks. The mean initial permeability of specimens having 0.6 mm wide cracks was 8.2 $cm^3.s^{-1}$. Mortar specimens having 0.6 mm wide cracks had a permeability of 2.6 $cm^3.s^{-1}$ after 56 days submersion (i.e. 32% of the initial permeability). Mortar specimens incorporated with beads containing mineral precursor compounds having cracks 0.6 mm wide had a mean permeability of 1.3 $cm^3.s^{-1}$ after 56 days submersion (i.e. 16% of the initial permeability). Bacteria-based self-healing cementitious specimens having 0.6 mm wide cracks had the lowest permeability of 0.7 $cm^3.s^{-1}$ after 56 days submersion (i.e. 7% of the initial permeability). Specimens containing beads demonstrated slightly lower crack permeabilities following drying, while plain mortar specimens had similar permeabilities before and after drying.
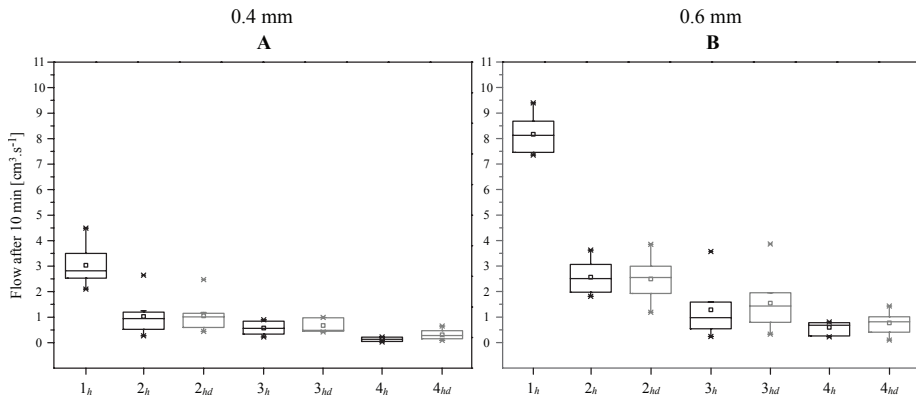

Figure 7.5 Box plot graphs depicting the permeability data for each series. Graph (A) shows the permeability data for specimens with cracks 0.4 mm wide and graph (B) shows the permeability data for specimens with cracks 0.6 mm wide. The first box plot to the left of the two graphs shows the initial permeability for cracked unhealed mortar specimens (1_h); the second box plot from the left shows the permeability of cracked mortar specimens after 56 days submersion in seawater at 8ºC (2_h); the third box plot shows the permeability of the same specimens after drying (2_{hd}); the fourth box plot shows the permeability of cracked mortar specimens with beads containing mineral precursor compounds after 56 days submersion in seawater at 8ºC (3_h); the fifth box plot shows the permeability of the same specimens after drying (3_{hd}); the sixth box plot showing the permeability of cracked bacteria-based self-healing cementitious specimens after 56 days submersion in seawater at 8ºC (4_h); and the final box plot of the same specimens after drying (4_{hd}). Each box plot represents permeability data for seven separate specimens. The square symbol of the boxes represents the mean permeability; the whiskers the minimum and maximum permeability values; and the top, middle and bottom lines the 75th, 50th and 25th percentiles ($x_{.75}$, $x_{.5}$ and $x_{.25}$), respectively.

7.3.3 Healing within the cracks

To assess healing within the cracks, polished sections were prepared from selected specimens. These polished sections were then analysed through ESEM and EDS. Figure 7.7 (A-C) shows ESEM images of a mortar specimen with a 0.4 mm wide crack following 56 days submersion in seawater at 8ºC, and subsequent drying. Dark grey precipitates (binary image) could be seen to have blocked one of the crack mouths (Figure 7.7A), dark grey formations could also be seen towards the centre of the crack (Figure 7.7B). Figure 7.7D shows an elemental map corresponding to Figure 7.7A, revealing the dark precipitates to be magnesium-based. Figure 7.7(E-G) shows ESEM images of a mortar specimen incorporated with beads containing mineral precursor compounds following 56 days submersion in seawater at 8ºC and subsequent drying. Limited precipitation could be seen at the crack mouths (Figure 7.7(E and G)). And dark grey precipitates could be seen along the crack (Figure 7.7F). EDS analysis revealed these precipitates to be magnesium based (Figure 7.7H). Figure 7.7(I-N) shows ESEM images of a specimen made from the bacteria-based self-healing cementitious composite with a 0.4 mm wide crack after 56 days submersion in seawater, and subsequent drying. Again limited precipitation could be seen to have formed at the crack mouths (Figure 7.7(I and K)). Dark grey precipitates could be seen to have formed towards the centre of the crack, and fully bridging the crack (Figure 7.7J). Figure 7.7O shows the EDS elemental map corresponding to Figure 7.7J, again revealing the dark precipitates to be magnesium-based. White precipitates could also be seen in and on the surface of the bacteria-based beads (Figure 7.7(L-N)). EDS elemental mapping revealed these precipitates to be calcium-based.

Similar phenomena could be seen for specimens with 0.6 mm wide cracks. Figure 7.8(A-C) shows ESEM images of a mortar specimen with a 0.6 mm wide crack following 56 days submersion in seawater at 8ºC, and subsequent drying. Limited precipitate formation could be seen at the crack mouths (Figure 7.8(A and C)), and dark grey precipitates could be seen towards the centre of the crack reducing its crack volume (Figure 7.8B). Figure 7.8(E-G) shows ESEM images of a mortar specimen with a 0.6 mm wide crack incorporated with beads containing mineral precursor compounds following 56 days submersion in seawater at 8ºC and subsequent drying. Again limited precipitation could be seen at the crack mouths (Figure 7.8(E and G)), and dark grey precipitates could be seen towards the centre of the crack reducing the crack volume. Some of these precipitates could be seen to form arc shapes, likely forming on the surface of swollen beads (Figure 7.8F). Figure 7.8H shows the elemental map corresponding to Figure 7.8F, again revealing the precipitates to be magnesium-based. Figure 7.8(I-O) shows ESEM images of a bacteria-based self-healing cementitious specimen with a 0.6 mm wide crack following 56 days submersion in seawater at 8ºC,

and subsequent drying. Limited precipitates could be seen at the crack mouths (Figure 7.8(I, J and L)). Dark precipitates were again formed towards the centre of the crack and again in arc-shaped formations (Figure 7.8K). Figure 7.8P shows the elemental map corresponding to Figure 7.8K, which again revealed the dark precipitates to be magnesium-based. White precipitates could also be seen in and on the surface of the bacteria-based beads (Figure 7.8(M-O)). EDS mapping revealed these precipitates to be calcium-based.

7.3.4 Strength development

Figure 7.6 shows the strength development of mortar cubes and mortar cubes incorporated with beads containing mineral precursor compounds. Mortar cubes incorporated with beads containing mineral precursors had lower compressive strengths than the plain mortar specimens. At day 28 the mean compressive strength of the mortar cubes incorporated with the beads was 30.5 MPa (i.e. 55% of the plain mortar cubes). This difference was reduced following 140 days submersion in seawater at 8ºC, as the compressive strength of the mortar cubes incorporated with beads was 35 MPa, (i.e. 77% of the mortar cubes). The compressive strength of the unsubmerged and submerged mortar cubes incorporated with beads were similar, while the compressive strength of the unsubmerged mortar cubes was higher than the submerged cubes, after 168 days.
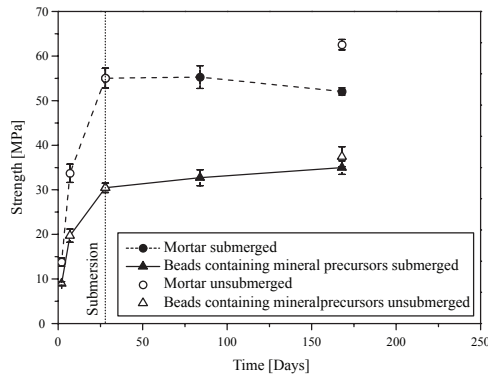

Figure 7.6 Compressive strength development of mortar cubes and mortar cubes incorporated with beads containing mineral precursor compounds, cured for 28 days and subsequently submerged in artificial seawater at 8ºC.
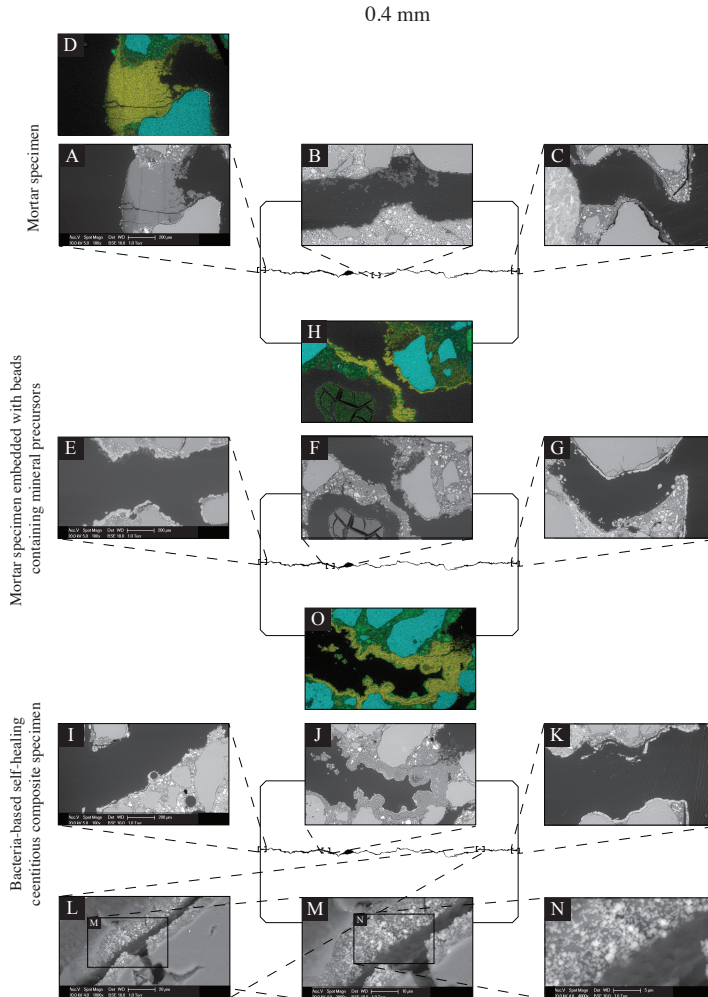
Figure 7.7 ESEM and EDS images of specimens with 0.4 mm wide cracks. (A-C) Are ESEM images of a mortar specimen following 56 days submersion in seawater at 8ºC: (A) shows a crack mouth; (B) an area towards the centre of the crack; and (C) the other crack mouth. (D) Is the EDS map corresponding to (A). (E-G) Are ESEM images of a mortar specimen incorporated with beads containing mineral precursor compounds after 56 days submersion in seawater at 8ºC: (E) shows a crack mouth; (F) an area towards the centre of the crack; and (G) the other crack mouth. (H) Is the EDS map corresponding to (F). (I-N) Are ESEM images of a bacteria-based self-healing cementitious composite specimen following 56 days submersion in seawater at 8ºC: (I) showing a crack mouth; (J) an area towards the centre of the crack; (K) the other crack mouth; (L) a section along the crack of a bacteria-based bead; and (M and N) successive close-ups of the bead. (O) Is the EDS map corresponding to (J). Green in the EDS maps represents calcium, yellow represents magnesium, and blue represents silicate.
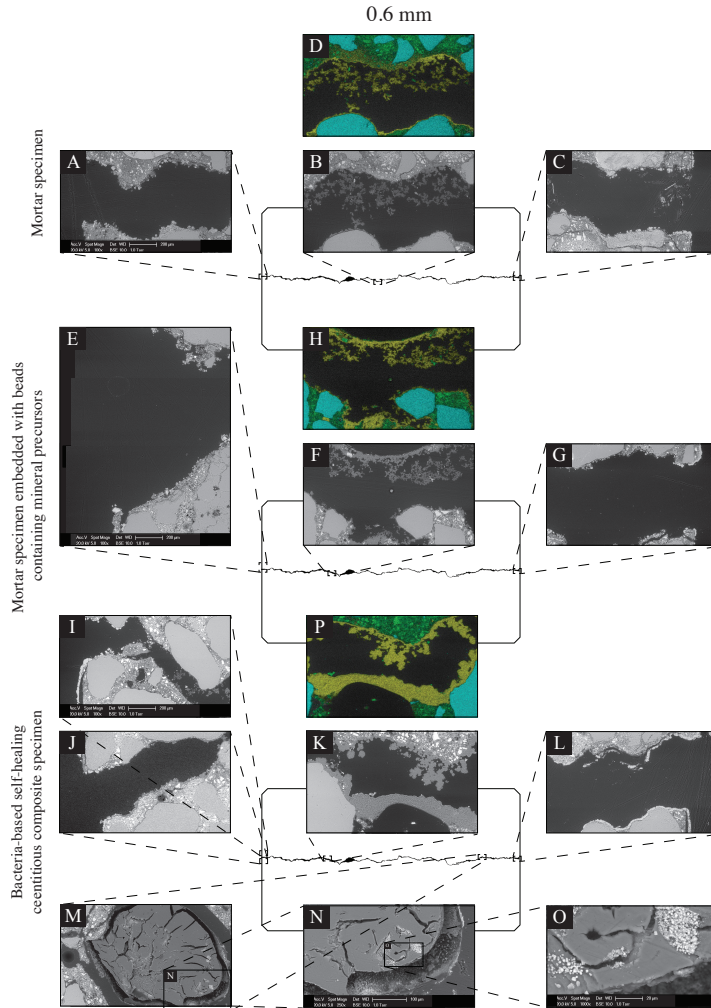
0.6 mm

Figure 7.8 ESEM and EDS images of specimens with 0.6 mm wide cracks. (A-C) Are ESEM images of a mortar specimen following 56 days submersion in seawater at 8ºC: (A) shows a crack mouth; (B) an area towards the centre of the crack; and (C) the other crack mouth. (D) Is the EDS map corresponding to (B). (E-G) Are ESEM images of a mortar specimen incorporated with beads containing mineral precursor compounds after 56 days submersion in seawater at 8ºC: (E) shows a crack mouth; (F) an area towards the centre of the crack; and (G) the other crack mouth. (H) Is the EDS elemental map corresponding to (F). (I-O) Are ESEM images of a bacteria-based self-healing cementitious composite specimen following 56 days submersion in seawater at 8ºC: (I and J) show a crack mouth, which had split into two smaller cracks; (K) an area towards the centre of the crack; (L) the other crack mouth; (M) a section along the crack including a bacteria-based bead; and successive close-ups (N and O) of a bacteria-based bead. (P) Is the EDS elemental map corresponding to (K). Green of the EDS maps represents calcium, yellow represents magnesium and blue represents silicate.

7.4 Discussion

A bacteria-based self-healing cementitious composite has been presented for application in low-temperature marine environments. The composite displayed an excellent crack healing capacity, reducing the permeability of cracks 0.4 mm wide by 95% and cracks 0.6 mm wide by 93%, following 56 days submersion in artificial seawater at 8ºC (Figure 7.5). Healing is attributable to four main mechanisms: mineral precipitation as a result of chemical interactions between the cement paste and seawater; bead swelling; magnesium-based precipitates as a result of chemical interactions between magnesium from the beads and hydroxide ions from the cement paste; and bacteria-based mineral precipitation.

Cementitious materials have an autogenous capacity to heal cracks [27, 29, 50], which is somewhat higher in marine environments [88]. Cracks in cementitious materials allow seawater to come into contact with the cement paste of the crack walls. Calcium hydroxide being soluble in seawater [57] is leached from the crack walls into the crack solution, whereby the hydroxide ions react with magnesium ions in the seawater forming magnesium-based mineral precipitates. At the same time, alkalis from the cement paste raise the pH of the crack solution, converting bicarbonate ions in the seawater to carbonate ions. These carbonate ions then react with calcium ions in the crack solution forming calcium-based mineral precipitates [63, 88]. These mineral precipitates give the bacteria-based self-healing cementitious composite a certain autogenous crack healing capacity. The extent of this capacity can be gauged as the crack healing capacity of the plain mortar specimens submerged in artificial seawater (series 2_h); which were able to reduce the permeability of cracks 0.4 mm wide by 66% and cracks 0.6 mm wide by 68%.

Bead swelling and magnesium from the beads also give the bacteria-based self-healing cementitious composite a certain crack healing capacity. Calcium alginate swells in water meaning that water entering a crack can cause beads along the crack to swell potentially bridging the crack. This swelling likely "frees up" the magnesium acetate in the beads, making more magnesium available for reaction with hydroxide ions leached from the cement paste. This magnesium, like the magnesium from the seawater, will then be able to react with hydroxide ions from the cement paste forming magnesium-based mineral precipitates. These swollen beads also have the potential to provide a support structure upon which mineral precipitates can form. Evidence of bead swelling and the formation mineral precipitates on the surface of swollen beads could be seen in the 0.6 mm wide cracks of specimens incorporated with beads containing mineral precursor compounds (Figures 7.7F), and specimens made from the bacteria-based self-healing cementitious composite (Figure 7.7K). The extent of healing provided by bead swelling and magnesium from the beads can be gauged as the difference in the mean permeability of the plain mortar specimens (series 2_h), and the specimens incorporated

with beads containing mineral precursor compounds (series 3_h), which equates to 16% for the 0.4 mm wide cracks and 15% for the 0.6 mm wide cracks (Figure 7.5).

Bacterial activity also gives the bacteria-based self-healing cementitious composite a certain crack healing capacity. Swelling of the beads likely "frees up" the bacteria and makes the mineral precursor compounds (yeast extract and acetate) more readily available to the bacteria. This availability causes the bacteria to germinate, whereupon they metabolise the compounds producing carbon dioxide. This carbon dioxide then reacts with calcium ions in and at the surface of the beads forming calcium-based precipitates. Evidence of these precipitates could be seen in and on the surface of the bacteria-based beads, forming an organic-inorganic composite healing material (Figure 7.7(L-N) and 7.8(M-O)). The extent of this capacity can be gauged as the difference between the mean crack permeability for mortar specimens incorporated with beads containing mineral precursor compounds (series 3_h) and specimens made from the bacteria-based self-healing cementitious composite (series 4_h), which equates to 13% for the 0.4 mm wide cracks and 10% for the 0.6 mm wide cracks (Figure 7.5). The healing attributable to bacteria-induced mineral precipitation was relatively less as compared to chemical precipitation and bead swelling. The bacteria-induced precipitates were, however, a valuable addition, as the bacteria-based cementitious specimens were less affected by drying than the beads without bacteria. The bacteria-based cementitious specimens also produced permeability data with a lower SD than the other two series, attesting to the technologies reliability (Figure 4). Further, this may not represent the full extent of bacteria-based healing if, for example, the bacteria had not used up all the yeast extract/acetate. The best way to confirm this would be to test an extra set of samples over a longer period, which was not feasible as part of the current study.

What is interesting is that the crack healing capacity was relatively higher for the larger crack width (i.e. that the bacteria-based self-healing cementitious composite was able to reduce the permeability of cracks 0.4 mm wide by 95% and cracks 0.6 mm wide by 93%, following 56 days submersion in artificial seawater at 8ºC). The ability to heal relatively larger crack widths may be due to the beads being able to swell to both crack widths and its corollary of "freeing up" more bacteria and mineral precursor compounds for chemical and bacteria induced mineral precipitation. This being the case, the beads may be able to swell still further allowing the healing of larger crack widths or fewer beads to be used to heal the same size cracks. In fact, in a previous study the bacteria-based beads were shown to swell to ~3 mm [112], and so the beads may be able to heal cracks ~3 mm wide. Drying the bacteria-based self-healing cementitious composite resulted in reductions in its crack permeability (Figure 7.5). These reductions can, in fact, be expected as the swollen beads in the cracks likely contract as a result of drying. This difference was, however, quite small, which might be due to the formation of mineral precipitates in and on the surface of the beads, which are unaffected by drying.

Although the bacteria-based cementitious composite displayed an excellent crack healing capacity, mortar specimens incorporated with beads demonstrated lower

compressive strengths than plain mortar specimens, following 140 days submersion in seawater at 8ºC (Figure 7.6). Despite this, this compressive strength is higher than a bacteria-based self-healing cementitious composite reported in the literature [13] and strong enough to be considered as a reliable construction material. Such reductions in compressive strength can be expected as the beads being much softer than the cement matrix act like a kind of porosity. If we assume that the density of the calcium alginate is 1 kg.m^{-3} [113], then the beads of the bacteria-based cementitious composite would represent 5% of the material's volume. If this 5% volume were air, then we could expect a ~25% reduction in compressive as compared with a specimen containing no air [114], which is somewhat in line with the 45% reduction demonstrated by specimens containing the beads (Figure 7.6). This being the case, then reducing the amount of beads could increase the 28-day compressive strength of the bacteria-based self-healing composite, while, at the same time, due to the swellability of the beads, could have a relatively lesser effect on the healing capacity of the material.

7.5 Conclusion

A bacteria-based self-healing cementitious composite has been presented for low-temperature marine applications. The composite was tested for its crack healing capacity, through water permeability measurements and strength development through compression testing. The composite displayed an excellent crack healing capacity decreasing the water permeability of 0.4 mm wide cracks by 95% and 0.6 mm wide cracks by 93%, following 56 days submersion in artificial seawater at 8ºC. This capacity is attributable to: mineral precipitation as a result of chemical interactions between the cement paste and seawater; bead swelling; magnesium-based precipitates as a result of chemical interactions between the magnesium of the beads and hydroxide ions of the cement paste; and bacteria-based mineral precipitation. Contribution of bacteria-based mineral precipitation to the healing capacity of the self-healing composite was supported by a decrease in oxygen surrounding the bacteria-based beads submerged in the AMCCS at 8ºC. Mortar specimens incorporated with beads, however, exhibited lower compressive strengths than the plain mortar specimens. Such reductions in compressive strength are expected as the beads being much softer than the mortar matrix act as a kind of porosity. Reducing the amount of beads will likely increase the compressive strength of bacteria-based self-healing cementitious composite, and may have a relatively little impact on the materials healing capacity. The bacteria-based self-healing cementitious composite shows great potential for realising cost-effective self-healing concrete in low-temperature marine environments, while the formation of an organic-inorganic composite healing material represents an exciting avenue for self-healing concrete research.

8

Conclusions and outlook

Finally in conclusion let me say just this.

— Peter Sellers

In this final chapter, conclusions are drawn and recommendations made for future research.

8.1 Conclusions

Bacteria-based self-healing concrete is an innovative self-healing materials approach, whereby bacteria embedded in concrete can form a crack healing mineral precipitate. Structures made from self-healing concrete promise longer service lives, with associated economic benefits [1]. Despite growing demands for marine concrete infrastructure, and concretes susceptibility to marine-based degradation phenomena, research on the development of bacteria-based self-healing concrete has been largely restricted to room temperature freshwater studies [4-13]. The current project has presented a cost-effective bacteria-based self-healing cementitious composite for application in low-temperature marine environments. Development of this composite required: understanding and the quantification of the autogenous healing capacity of cementitious materials (Chapters 2 and 3), which included the development of a water permeability test to quantify the functional healing capacity of cementitious materials (Chapters 3 and 4); development of a cost-effective bacteria-based healing agent (bacterial spores and a mineral precursor compound) fit for low-temperature marine applications (Chapter 5); encapsulation of this agent in calcium alginate (Chapter 6); incorporation of the calcium alginate encapsulated agent in a cementitious material, and quantification of the healing capacity of the subsequent bacteria-based self-healing cementitious composite (Chapter 7).

A number of conclusions were drawn based on the results obtained during the development of the composite:

- Visual crack closure is not a measurement for the regain of functional properties such as strength and/or water tightness. Visual crack closure, therefore, should only be conducted as a complementary method when measuring the regain of such properties.

- The capacity of a cementitious material to heal a crack depends on the width of the crack, thermodynamic considerations, the presence of water and the amount of ions available in the crack. Autogenous crack healing for seawater submerged cementitious materials is principally attributable to the precipitation of aragonite and brucite in the cracks.

- The crack healing capacity of a bacteria-based cementitious composite is directly related to the amount of organic carbon available to the bacteria, and so the cheaper the organic mineral precursor compound, the cheaper the bacteria-based self-healing technology in general. The compound must not have an adverse effect on concrete properties when included in cementitous materials and must be readily metabolised by the bacteria of the healing agent. Magnesium acetate, in

the current study, best balanced these criteria making it a good candidate as the organic mineral precursor compound for the healing agent.

- A large number of specimen replicates (≥ 7) are required to generate reliable crack permeability data, and hence to quantify the crack healing capacity of cementitious materials through their functional water tightness.

- The bacteria-based self-healing cementitious composite displayed an excellent crack healing capacity, reducing the permeability of cracks 0.4 mm wide by 95% and cracks 0.6 mm wide by 93%, following 56 days submersion in artificial seawater at 8ºC. This crack healing capacity was attributable to: mineral precipitation as a result of chemical interactions between the cement paste and seawater; bead swelling; magnesium-based precipitates as a result of chemical interactions between the magnesium of the beads and hydroxide ions of the cement paste; and bacteria-induced mineral precipitation.

- The 28-day compressive strength of mortar specimens incorporated with beads was 55% of plain mortar specimens. Reducing the amount of bacteria-based beads will likely increase the compressive strength of the bacteria-based self-healing cementitious composite. Such a reduction, given the swellability of the beads, may have relatively little impact on the healing capacity of the composite.

- The bacteria-based self-healing cementitious composite shows great potential for realising self-healing concrete in low-temperature marine environments, while the organic-inorganic healing material formed by the composite represents an exciting avenue for self-healing concrete research and practical applications.

8.2 Outlook

A cost-effective bacteria-based self-healing cementitious composite has been developed for application in low-temperature marine environments. The material displayed an excellent crack healing capacity when submerged in artificial seawater at 8ºC. Further research is, however, needed before the material can be realised in a working environment. Possible areas for future research could include:

- An investigation to improve the overall strength of the bacteria-based self-healing cementitious composite. The strength of the composite could be improved by reducing the amount of bacteria-based beads incorporated in the composite. It

will, however, be important to see what effect this decrease has on the healing capacity of the composite. Further, it may be possible to improve the overall strength of the composite by using polymers other than alginate to encapsulate the healing agent.

- An investigation to improve the mechanical performance of the healing material formed by the bacteria-based self-healing cementitious composite. Insights on how to improve the mechanical performance of the healing material may be found in the emerging field of bio-inspired organic-inorganic material synthesis. A popular route for synthesising such composite materials is through calcium carbonate precipitation in polymer hydrogels [92, 115-119]. The marriage of such bio-inspired materials synthesis strategies with bacteria-based self-healing concrete technology may allow stronger, harder and tougher crack healing materials to be formed; adding to the overall durability of the bacteria-based self-healing cementitious composite.

- The up scaling of the bacteria-based bead production process. This process should be relatively straightforward given that calcium alginate beads are already industrially produced [120]. It might, however, be interesting to produce the "bead technology" not as beads but as fibres. Using fibres may improve the mechanical performance of the bacteria-based self-healing cementitious composite.

- Installation of the bacteria-based self-healing cementitious composite in a low-temperature marine setting. Such an investigation could see the material included as part of a marine concrete structure (e.g. a small section of a tunnel). The material could then be monitored for its durability performance.

- Conducting a life cycle assessment of the bacteria-based self-healing cementitious composite.

References

[1] K. Van Breugel, Is there a market for self-healing cement-based materials, Proceedings of the first international conference on self-healing materials, 2007.

[2] P.K. Mehta, Durability of Concrete in Marine Environment — A Review, ACI Special Publication, 65 (1980).

[3] P. Fookes, J. Simm, J. Barr, Marine concrete performance in different climatic environments, Proc., Int. Conf. on Concrete in the Marine Environment, The Concrete Society London, 1986.

[4] H.M. Jonkers, Self healing concrete: a biological approach, Self Healing Materials, Springer, 2008, pp. 195-204.

[5] H.M. Jonkers, A. Thijssen, G. Muyzer, O. Copuroglu, E. Schlangen, Application of bacteria as self-healing agent for the development of sustainable concrete, Ecological Engineering, 36 (2010) 230-235.

[6] H. Jonkers, Bacteria-based self-healing concrete, Heron, 56 (2011) 1.

[7] V. Wiktor, H.M. Jonkers, Quantification of crack-healing in novel bacteria-based self-healing concrete, Cement and concrete Composites, 33 (2011) 763-770.

[8] J. Wang, N. De Belie, W. Verstraete, Diatomaceous earth as a protective vehicle for bacteria applied for self-healing concrete, Journal of industrial microbiology & biotechnology, 39 (2012) 567-577.

[9] J. Wang, H. Soens, W. Verstraete, N. De Belie, Self-healing concrete by use of microencapsulated bacterial spores, Cement and Concrete Research, 56 (2014) 139-152.

[10] J. Wang, D. Snoeck, S. Van Vlierberghe, W. Verstraete, N. De Belie, Application of hydrogel encapsulated carbonate precipitating bacteria for approaching a realistic self-healing in concrete, Construction and Building Materials, 68 (2014) 110-119.

[11] J. Wang, A. Mignon, D. Snoeck, V. Wiktor, S. Van Vliergerghe, N. Boon, N. De Belie, Application of modified-alginate encapsulated carbonate producing bacteria in concrete: a promising strategy for crack self-healing, Frontiers in microbiology, 6 (2015).

[12] Y.Ç. Erşan, E. Gruyaert, G. Louis, C. Lors, N. De Belie, N. Boon, Self-protected nitrate reducing culture for intrinsic repair of concrete cracks, Frontiers in microbiology, 6 (2015).

[13] E. Tzviloglou, V. Wiktor, H.M. Jonkers, E. Schlangen, Bacteria-based self-healing concrete to increase liquid tightness of cracks, Construction and Building Materials, 122 (2016) 118-125.

[14] R. Mors, H. Jonkers, Feasibility of lactate derivative based agent as additive for concrete for regain of crack water tightness by bacterial metabolism, Industrial Crops and Products, (2016).

[15] U. Atlas, UN Atlas: 44 Percent of us Live in Coastal Areas, 2010.

[16] U. Nations, World population prospects: The 2012 revision, New York: United Nation, (2013).

[17] A. Neville, Chloride attack of reinforced concrete: an overview, Materials and Structures, 28 (1995) 63-70.

[18] F.P. Glasser, J. Marchand, E. Samson, Durability of concrete — degradation phenomena involving detrimental chemical reactions, Cement and Concrete Research, 38 (2008) 226-246.

[19] P.K. Mehta, Concrete in the marine environment, Taylor & Francis, 2002.

[20] D. Bonen, Composition and Appearance of Magnesium Silicate Hydrate and Its Relation to Deterioration of Cement-Based Materials, Journal of the American Ceramic Society, 75 (1992) 2904-2906.

[21] E. Worrell, L. Price, N. Martin, C. Hendriks, L.O. Meida, Carbon dioxide emissions from the global cement industry 1, Annual Review of Energy and the Environment, 26 (2001) 303-329.

[22] O.E. Gjorv, Long-Time Durablty of Concrete in Seawater, ACI Journal Proceedings, ACI, 1971.

[23] A. Knudsen, F. Jensen, O. Klinghoffer, T. Skovsgaard, Cost-effective enhancement of durability of concrete structures by intelligent use of stainless steel reinforcement, Conference on Corrosion and rehabilitation of reinforced concrete structures, Florida, 1998.

[24] C.L. Freyermuth, Life-Cycle Cost Analysis for Large Bridges, Concrete international, 23 (2001) 89-95.

[25] M. De Rooij, K. Van Tittelboom, N. De Belie, E. Schlangen, Self-Healing Phenomena in Cement-Based Materials, Draft of State-of-the-Art report of RILEM Technical Committee, (2011).

[26] V.C. Li, E.H. Yang, Self healing in concrete materials, Self Healing Materials, Springer, 2008, pp. 161-193.

[27] H.W. Reinhardt, M. Jooss, Permeability and self-healing of cracked concrete as a function of temperature and crack width, Cement and Concrete Research, 33 (2003) 981-985.

[28] A. Neville, Autogenous Healing-A Concrete Miracle?, Concrete international, 24 (2002) 76-82.

[29] C. Edvardsen, Water permeability and autogenous healing of cracks in concrete, ACI Materials Journal-American Concrete Institute, 96 (1999) 448-454.

[30] S. Jacobsen, J. Marchand, H. Hornain, SEM observations of the microstructure of frost deteriorated and self-healed concretes, Cement and Concrete Research, 25 (1995) 1781-1790.

[31] R. Gagné, M. Argouges, A study of the natural self-healing of mortars using air-flow measurements, Materials and Structures, 45 (2012) 1625-1638.
[32] M. Maes, Combined effects of chlorides and sulphates on cracked and self-healing concrete in marine environments, Ghent University, 2015.
[33] M. Conjeaud, Mechanism of sea water attack on cement mortar, ACI Special Publication, 65 (1980).
[34] N. Buenfeld, J. Newman, The development and stability of surface layers on concrete exposed to sea-water, Cement and Concrete Research, 16 (1986) 721-732.
[35] G.M. Gadd, Fungi in biogeochemical cycles, Cambridge University Press, 2006.
[36] W.E. Müller, Molecular biomineralization: aquatic organisms forming extraordinary materials, Springer Science & Business Media, 2011.
[37] H.G. Schlegel, C. Zaborosch, M. Kogut, General microbiology, Cambridge University Press, 1993.
[38] G. Gan, The role of magnesium in concrete deterioration, (1996).
[39] R. Berner, The role of magnesium in the crystal growth of calcite and aragonite from sea water, Geochimica et cosmochimica acta, 39 (1975) 489-504.
[40] B. EN, 1015-11: Methods of test for mortar for masonry, Part 11: Determination of flexural and compressive strength of hardened mortar, European Committee for Standardization, Brussels, (1999).
[41] W. Stumm, J. Morgan, Aquatic chemistry, chemical equilibra and rates in natural waters, Env. Sci. Technol, (1996).
[42] Y. Levi, S. Albeck, S. Weiner, A. Brack, L. Addadi, Control over aragonite crystal nucleation and growth: an in vitro study of biomineralization, Chemistry-A European Journal, 4 (1998) 389-396.
[43] T.L. Hughes, C.M. Methven, T.G. Jones, S.E. Pelham, P. Fletcher, C. Hall, Determining cement composition by Fourier transform infrared spectroscopy, Advanced Cement Based Materials, 2 (1995) 91-104.
[44] F.A. Andersen, L. Brecevic, Infrared spectra of amorphous and crystalline calcium carbonate, Acta Chem. Scand, 45 (1991) 1018-1024.
[45] V.M. Malhotra, P.K. Mehta, Pozzolanic and cementitious materials, Taylor & Francis, 1996.
[46] E.A. Burton, L.M. Walter, Relative precipitation rates of aragonite and Mg calcite from seawater: Temperature or carbonate ion control?, Geology, 15 (1987) 111-114.
[47] M. Santhanam, Studies on sulfate attack: mechanisms, test methods, and modeling, (2001).
[48] M. O'Farrell, S. Wild, B. Sabir, Resistance to chemical attack of ground brick-PC mortar: Part II. Synthetic seawater, Cement and Concrete Research, 30 (2000) 757-765.
[49] M.P. Kumar, J. Monteiro, Concrete: Microstructure, properties, and materials, The Mc Graw Hill Companies Inc, College Custom Series, 1993.
[50] C. Clear, The effects of autogenous healing upon the leakage of water through cracks in concrete, Cement and Concrete Association, 1985.
[51] K. Wang, D.C. Jansen, S.P. Shah, A.F. Karr, Permeability study of cracked concrete, Cement and Concrete Research, 27 (1997) 381-393.

[52] C.-M. Aldea, S.P. Shah, A. Karr, Effect of cracking on water and chloride permeability of concrete, Journal of Materials in Civil Engineering, 11 (1999) 181-187.

[53] C.-M. Aldea, S. Shah, A. Karr, Permeability of cracked concrete, Materials and Structures, 32 (1999) 370-376.

[54] J. Rapoport, C.-M. Aldea, S.P. Shah, B. Ankenman, A. Karr, Permeability of cracked steel fiber-reinforced concrete, Journal of Materials in Civil Engineering, 14 (2002) 355-358.

[55] G. Osborne, Durability of Portland blast-furnace slag cement concrete, Cement and concrete Composites, 21 (1999) 11-21.

[56] K. White, Bridge maintenance inspection and evaluation, CRC Press, 1992.

[57] L. Irving, The precipitation of calcium and magnesium from sea water, Journal of the Marine Biological Association of the United Kingdom (New Series), 14 (1926) 441-446.

[58] J.W. Morse, A. Mucci, F.J. Millero, The solubility of calcite and aragonite in seawater of 35%. salinity at 25º C and atmospheric pressure, Geochimica et cosmochimica acta, 44 (1980) 85-94.

[59] S. Ghosh, Advances in cement technology: critical reviews and case studies on manufacturing, quality control, optimization and use, Elsevier, 2014.

[60] V. Picandet, A. Khelidj, H. Bellegou, Crack effects on gas and water permeability of concretes, Cement and Concrete Research, 39 (2009) 537-547.

[61] C.-M. Aldea, W.-J. Song, J.S. Popovics, S.P. Shah, Extent of healing of cracked normal strength concrete, Journal of Materials in Civil Engineering, 12 (2000) 92-96.

[62] D. Palin, H. Jonkers, V. Wiktor, Autogenous healing of sea-water exposed mortar: Quantification through a simple and rapid permeability test, Cement and Concrete Research, 84 (2016) 1-7.

[63] P. Schießl, M. Raupach, Laboratory studies and calculations on the influence of crack width on chloride-induced corrosion of steel in concrete, ACI Materials Journal, 94 (1997) 56-62.

[64] M. Şahmaran, Effect of flexure induced transverse crack and self-healing on chloride diffusivity of reinforced mortar, Journal of Materials Science, 42 (2007) 9131-9136.

[65] H.-W. Reinhardt, M. Jooss, Permeability and self-healing of cracked concrete as a function of temperature and crack width, Cement and Concrete Research, 33 (2003) 981-985.

[66] W. Stumm, J.J. Morgan, Aquatic chemistry: chemical equilibrium and rates in natural waters, Wiley, New York, (1996).

[67] J. Huitt, Fluid flow in simulated fractures, AIChE Journal, 2 (1956) 259-264.

[68] P. Rowe, Essential statistics for the pharmaceutical sciences, John Wiley & Sons, 2015.

[69] H.L. Ehrlich, D.K. Newman, A. Kappler, Ehrlich's Geomicrobiology, CRC press, 2015.

[70] E.D. Ongley, Control of water pollution from agriculture, Food & Agriculture Org. 1996.

[71] A.M. Neville, Properties of concrete, 1995.

[72] K. Tuutti, Corrosion of steel in concrete, 1982.

[73] Y.Ç. Erşan, H. Verbruggen, I. De Graeve, W. Verstraete, N. De Belie, N. Boon, Nitrate reducing $CaCO_3$ precipitating bacteria survive in mortar and inhibit steel corrosion, Cement and Concrete Research, 83 (2016) 19-30.

[74] B.B. Jørgensen, S. D'Hondt, A starving majority deep beneath the seafloor, Science, 314 (2006) 932-934.

[75] R.I. Dorn, T.M. Oberlander, Microbial origin of desert varnish, Science, 213 (1981) 1245-1247.

[76] R. José, B.M. Goebel, E.I. Friedmann, N.R. Pace, Microbial diversity of cryptoendolithic communities from the McMurdo Dry Valleys, Antarctica, Applied and Environmental Microbiology, 69 (2003) 3858-3867.

[77] K. Pedersen, E. Nilsson, J. Arlinger, L. Hallbeck, A. O'Neill, Distribution, diversity and activity of microorganisms in the hyper-alkaline spring waters of Maqarin in Jordan, Extremophiles, 8 (2004) 151-164.

[78] A.A. Joshi, P.P. Kanekar, A.S. Kelkar, Y.S. Shouche, A.A. Vani, S.B. Borgave, S.S. Sarnaik, Cultivable bacterial diversity of alkaline Lonar Lake, India, Microbial Ecology, 55 (2008) 163-172.

[79] J.-L. Sagripanti, A. Bonifacino, Comparative sporicidal effects of liquid chemical agents, Applied and environmental microbiology, 62 (1996) 545-551.

[80] (2016): http://Alibaba.com.

[81] H.M. Jonkers, R. Ludwig, R. De Wit, O. Pringault, G. Muyzer, H. Niemann, N. Finke, D. De Beer, Structural and functional analysis of a microbial mat ecosystem from a unique permanent hypersaline inland lake:'La Salada de Chiprana'(NE Spain), FEMS Microbiology Ecology, 44 (2003) 175-189.

[82] G. Muyzer, K. Smalla, Application of denaturing gradient gel electrophoresis (DGGE) and temperature gradient gel electrophoresis (TGGE) in microbial ecology, Antonie van Leeuwenhoek, 73 (1998) 127-141.

[83] S.F. Altschul, W. Gish, W. Miller, E.W. Myers, D.J. Lipman, Basic local alignment search tool, Journal of Molecular Biology, 215 (1990) 403-410.

[84] W. Ludwig, O. Strunk, R. Westram, L. Richter, H. Meier, Yadhukumar, A. Buchner, T. Lai, S. Steppi, G. Jobb, W. Förster, I. Brettske, S. Gerber, A.W. Ginhart, O. Gross, S. Grumann, S. Hermann, R. Jost, A. König, T. Liss, R. Lüßmann, M. May, B. Nonhoff, B. Reichel, R. Strehlow, A. Stamatakis, N. Stuckmann, A. Vilbig, M. Lenke, T. Ludwig, A. Bode, K.H. Schleifer, ARB: a software environment for sequence data, Nucleic Acids Research, 32 (2004) 1363-1371.

[85] A. Stamatakis, RAxML-VI-HPC: maximum likelihood-based phylogenetic analyses with thousands of taxa and mixed models, Bioinformatics, 22 (2006) 2688-2690.

[86] P. Nielsen, D. Fritze, F.G. Priest, Phenetic diversity of alkaliphilic Bacillus strains: proposal for nine new species, Microbiology, 141 (1995) 1745-1761.

[87] P. Vos, G. Garrity, D. Jones, N.R. Krieg, W. Ludwig, F.A. Rainey, K.-H. Schleifer, W. Whitman, Bergey's Manual of Systematic Bacteriology: Volume 3: The Firmicutes, Springer Science & Business Media, 2011.

[88] D. Palin, V. Wiktor, H.M. Jonkers, Autogenous healing of marine exposed concrete: Characterization and quantification through visual crack closure, Cement and Concrete Research, 73 (2015) 17-24.

[89] D. Palin, Bacteria-based agent for self-healing marine concrete, Concrete Solutions, (2014) 105-108.

[90] A.S. Hoffman, Hydrogels for biomedical applications, Advanced drug delivery reviews, 64 (2012) 18-23.

[91] A. Alcantara, P. Aranda, M. Darder, E. Ruiz-Hitzky, Bionanocomposites based on alginate–zein/layered double hydroxide materials as drug delivery systems, Journal of Materials Chemistry, 20 (2010) 9495-9504.

[92] M.Ø. Olderøy, M. Xie, B.L. Strand, E.M. Flaten, P. Sikorski, J.-P. Andreassen, Growth and nucleation of calcium carbonate vaterite crystals in presence of alginate, Crystal Growth & Design, 9 (2009) 5176-5183.

[93] S. Abramson, C. Meiller, P. Beaunier, V. Dupuis, L. Perrigaud, A. Bée, V. Cabuil, Highly porous and monodisperse magnetic silica beads prepared by a green templating method, Journal of Materials Chemistry, 20 (2010) 4916-4924.

[94] J.-L. Wu, C.-Q. Wang, R.-X. Zhuo, S.-X. Cheng, Multi-drug delivery system based on alginate/calcium carbonate hybrid nanoparticles for combination chemotherapy, Colloids and Surfaces B: Biointerfaces, 123 (2014) 498-505.

[95] J. Currey, J. Taylor, The mechanical behaviour of some molluscan hard tissues, Journal of Zoology, 173 (1974) 395-406.

[96] U. Wegst, M. Ashby, The mechanical efficiency of natural materials, Philosophical Magazine, 84 (2004) 2167-2186.

[97] A. Jackson, J. Vincent, R. Turner, The mechanical design of nacre, Proceedings of the Royal Society of London B: Biological Sciences, 234 (1988) 415-440.

[98] T.E. Bergdale, R.J. Pinkelman, S.R. Hughes, B. Zambelli, S. Ciurli, S.S. Bang, Engineered biosealant strains producing inorganic and organic biopolymers, Journal of biotechnology, 161 (2012) 181-189.

[99] B.T. Hargrave, Epibenthic algal production and community respiration in the sediments of Marion Lake, Journal of the Fisheries Board of Canada, 26 (1969) 2003-2026.

[100] W.J. Leo, A.J. McLoughlin, D.M. Malone, Effects of sterilization treatments on some properties of alginate solutions and gels, Biotechnology progress, 6 (1990) 51-53.

[101] R. Warthmann, Y. Van Lith, C. Vasconcelos, J.A. McKenzie, A.M. Karpoff, Bacterially induced dolomite precipitation in anoxic culture experiments, Geology, 28 (2000) 1091-1094.

[102] P.H. Monaghan, M.L. Lytle, The origin of calcareous ooliths, Journal of Sedimentary Research, 26 (1956).

[103] C. Buczynski, H.S. Chafetz, Habit of bacterially induced precipitates of calcium carbonate and the influence of medium vicosity on mineralogy, Journal of Sedimentary Research, 61 (1991).

[104] C. Lalou, Studies on bacterial precipitation of carbonates in sea water, Journal of Sedimentary Research, 27 (1957).

[105] H.S. Chafetz, Marine peloids: a product of bacterially induced precipitation of calcite, Journal of Sedimentary Research, 56 (1986).

[106] W. Conover, Chemistry, (Lewis, Rob; Evans, Wynne), Journal of Chemical Education, 79 (2002) 437.

[107] I.J. McColm, L.S. O'Bannon, Dictionary of ceramic science and engineering, Springer1994.

[108] J. Bird, C. Ross, Mechanical engineering principles, Routledge, 2014.

[109] Y. Lin, K. Nierop, E. Girbal-Neuhauser, M. Adriaanse, M. Van Loosdrecht, Sustainable polysaccharide-based biomaterial recovered from waste aerobic granular sludge as a surface coating material, Sustainable Materials and Technologies, 4 (2015) 24-29.

[110] R. Marsell, T.A. Einhorn, The biology of fracture healing, Injury, 42 (2011) 551-555.

[111] N.K. Guimard, K.K. Oehlenschlaeger, J. Zhou, S. Hilf, F.G. Schmidt, C. Barner-Kowollik, Current trends in the field of self-healing materials, Macromolecular Chemistry and Physics, 213 (2012) 131-143.

[112] D. Palin, V. Wiktor, H. Jonkers, A bacteria-based bead for possible self-healing marine concrete applications, Smart Materials and Structures, 25 (2016) 84008-84013.

[113] A.-V. Salac, L. Zhang, J.-M. Gherbezza, Measurement of the mechanical properties of alginate beads using ultrasounds, (2011).

[114] P. Klieger, Landmark Series: Further Studies on the Effect of Entrained Air on Strength and Durability of Concrete with Various Sizes of Aggregates, Concrete International, 25 (2003) 26-45.

[115] H. Li, L.A. Estroff, Calcite Growth in Hydrogels: Assessing the Mechanism of Polymer-Network Incorporation into Single Crystals, Advanced Materials, 21 (2009) 470-473.

[116] M.F. Butler, N. Glaser, A.C. Weaver, M. Kirkland, M. Heppenstall-Butler, Calcium carbonate crystallization in the presence of biopolymers, Crystal growth & design, 6 (2006) 781-794.

[117] N. Wada, M. Okazaki, S. Tachikawa, Effects of calcium-binding polysaccharides from calcareous algae on calcium carbonate polymorphs under conditions of double diffusion, Journal of crystal growth, 132 (1993) 115-121.

[118] N. Wada, K. Yamashita, T. Umegaki, Effects of carboxylic acids on calcite formation in the presence of Mg^{2+} ions, Journal of colloid and interface science, 212 (1999) 357-364.

[119] E. Asenath-Smith, H. Li, E.C. Keene, Z.W. Seh, L.A. Estroff, Crystal growth of calcium carbonate in hydrogels as a model of biomineralization, Advanced Functional Materials, 22 (2012) 2891-2914.

[120] J. Burgain, C. Gaiani, M. Linder, J. Scher, Encapsulation of probiotic living cells: From laboratory scale to industrial applications, Journal of Food Engineering, 104 (2011) 467-483.

Acknowledgements

I first want to thank my two guides on this journey, Henk and Virginie. Thank you, Henk, for inviting me on this adventure. I will forever remember the interview at Schipol and you telling me that I had the position, and this before I made my presentation. Thank you for the time we shared in the lab, your always open door, showing me what good science is, and what it takes to be a great supervisor. Thank you, Virginie, for, showing me the power of organisation, always being there, the red pen and asking me "what do you mean?". I will take parts of you both with me in all I do.

I also want to thank a few people who have allowed this journey to happen. Thank you, Leon, for inviting me to Delft during my masters, and sharing your insights on all things Biogrout, thank you for recommending me to Henk for the PhD position and being as they say in China one of my *gui ren*. Thank you, Erik, for being the man with the idea behind bacteria-based self-healing concrete, for without it, I may never have worked in this area, which I love. Thank you, Anke, for writing the grant, which funded my PhD. Thank you, Sybrand, for building such a vibrant self-healing materials community at Delft. Thank you, Mark, for sharing your lab. Thank you, Nele, for a warm and fruitful stay in Gent. And thank you, Klaas, for helping me over the line.

Thank you, Ger, Arjan, John, Maiko and Ton, for being the "technical oil" which allowed my PhD to happen. Thank you, Ger, for your amasing energy and patience. Thank you, Arjan, for "hoe gaat het met je vrouw?", tractor videos, and of course for the many hours we spent playing with alginate beads, liquid nitrogen and the ESEM. Thank you, Microlabers, Renée, Lupita (and Dennis), Eirini, Balquis, Jacapo, Tim, Neven, Amir, Keiyu, Bahman, Xuliang, Nynke, Mladena and Branko, Farad, Natalie, Bart, Claudia, Jiayi, Stefan (and Bianca), Marija and Patrick, Ma Xu, Hitham, Martin, Oğuzhan, Ye, Janette, Marc and Dessi. And thank you, Rene, my room buddy, I truly enjoyed sharing 6.02 with you. Thank you to the EBTers for always making me feel welcome. And particularly Mitch, thank you for the "dopje" and the "flam", for your patience and help with all things microbial, and for lunch in the gardens at Biotechnology. Thank you sixth floorers, Rafid, Marcello, Luis, Ki and Medhi. And thank you to the cleaning ladies for all those frights!

I want to say a special thank you to the Aikido Stichting Delft, and in particular Charles and Jan, I always cycled home with energy and a smile. And thank, Jure and Pat, thank you for your friendship, the quiet moments, making filo pastry, all the yummy

dinners, and countless coffees. I always felt at home around you. And my friends at home in Ireland, thank for never being distant, despite my many years away, I am so lucky to know you.

Thank you to my parents, thank you for your support over the years. I hope you are as proud of me as I am of you.

And, Mo Yu, my love, thank you for being this yummy, funny, smartness, in my life.

Delft,
February 2017.

Publication list

Journal publications

D. Palin, V. Wiktor, H.M. Jonkers, Autogenous healing of marine exposed concrete: Characterization and quantification through visual crack closure, Cement and Concrete Research, 73 (2015) 17-24.

D. Palin, H.M. Jonkers, V. Wiktor, Autogenous healing of sea-water exposed mortar: Quantification through a simple and rapid permeability test, Cement and Concrete Research, 84 (2016) 1-7.

D. Palin, V. Wiktor, H.M. Jonkers, A bacteria-based bead for possible self-healing marine concrete applications, Smart Materials and Structures, 25 (2016) 84008-84013.

D. Palin, V. Wiktor and H.M. Jonkers, A bacteria-based self-healing cementitious composite for application in low-temperature marine environments, Biomimetics, 3 (2017).

D. Palin, Y. Mo, V. Wiktor and H.M. Jonkers, A modified methodology for producing rapid, accurate and reliable crack permeability data for cementitous materials, *under review*.

D. Palin, M. Geleijnse, B. Abbas, V. Wiktor and H.M. Jonkers, A cost-effective bacteria-based agent for the development of self-healing marine concrete, *submitted*.

Book contributions

H.M. Jonkers, V. Wiktor, M.G. Sierra-Beltran, R.M. Mors, E. Tziviloglou, and **D. Palin**. In Van der Zwaag S. and Brinkman E., ed. Self Healing Materials: Pioneering Research in the Netherlands, IOS Press 2015.

E. Tziviloglou, K. van Tittelboom, **D. Palin**, J. Wang, M.G. Sierra-Beltrán, Y.Ç. Erşan, R. Mors, V. Wiktor, H.M. Jonkers, and E. Schlangen. Bio-Based Self-Healing Concrete: From Research to Field Application. In M.D. Hager, S. van der Zwaag, and U.S. Schubert, ed., Self-healing Materials, 2016.

Conference procedings

D. Palin, V. Wiktor, and H. M. Jonkers, Bacteria-based self-healing concrete for application in the marine environment. Proceedings of the Fourth International Conference on Self-Healing Materials ICSHM2013, (2013).

H. M. Jonkers, **D. Palin**, P. Flink, and A. Thijssen, Microbially mediated carbonation of marine alkaline minerals: Potential for concrete crack healing. Proceedings of the Fourth International Conference on Self-Healing Materials ICSHM2013, (2013).

D. Palin, Y.Ç. Erşan, V. Wiktor, N. De Belie, and H.M. Jonkers. A rapid and repetable method for establishing the water permeability of cracked mortar specimens, fib symposium 2015, (2015).

D. Palin, V. Wiktor, H. Jonkers, Towards cost efficient bacteria based self-healing marine concrete, Concrete Solutions 2014, (2014) 105.

D. Palin, A. Thijssen, V. Wiktor, H. M. Jonkers, and E. Schlangen, ESEM-BSE coupled with rapid nano-scratching for micro-physicochemical analysis of marine exposed concrete. 15th Euroseminar on Microscopy Applied to Building Materials (2015).

D. Palin, V. Wiktor, H.M. Jonkers, Bacteria-based agent for self-healing marine concrete, International Conference in Self-Healing Materials (ICSHM) 2015, (2015).

H. M. Jonkers, R. Mors, M. G. Sierra-Beltran, E. Tziviloglou, **D. Palin**, and V. Wiktor, Self-healing of cracks in concrete via bacterial aerobic metabolic conversion of organic compounds. RILEM Conference on Microorganisms-Cementitious Materials Interactions, (2016).